Technische Universität München
TUM School of Life Sciences

The role of stores in recycling sucrose and supplying respiration of a perennial C_3 grass: on the effects of Last Glacial Maximum to projected end-of-21st-century atmospheric CO_2 concentration

Jianjun Zhu

Vollständiger Abdruck der von der promotionsführenden Einrichtung TUM School of Life Sciences der Technischen Universität München zur Erlangung des akademischen Grades eines

Doktors der Naturwissenschaften
genehmigten Dissertation.

Vorsitz: Prof. Dr. Jürgen Geist

Prüfer*innen der Dissertation:

1. Prof. Dr. Johannes Schnyder
2. Prof. Dr. Gerd Patrick Bienert

Die Dissertation wurde am 05.09.2022 bei der Technischen Universität München eingereicht und durch die promotionsführende Einrichtung TUM School of Life Sciences am 01.03.2023 angenommen.

Contents

Abstract

Aims: Organic carbon stores provide substrate for plant growth and respiration and are mainly formed as carbohydrates (e.g. fructan and sucrose). However, little is known about the effect of past and future carbon dioxide concentration ([CO_2]) on the role of organic carbon stores in the recycling of sucrose and supplying substrate to respiration. This thesis aimed to quantitatively assess the ^{13}C tracer dynamics in the main non-structural carbohydrate fractions at the whole shoot level and in plant respiration at the whole plant level of perennial ryegrass (*Lolium perenne* L.) - a perennial C_3 forage grass - and their responses to [CO_2] during plant growth. Of particular interest was (1) to assess the performance of the $^{13}CO_2/^{12}CO_2$ labelling system used to trace C incorporation, turnover and use in respiration, (2) to determine the effects of [CO_2] on the fluxes in central carbohydrate metabolism (fructan, sucrose, glucose, and fructose) in the shoot, including fructan cycling and sucrose recycling, (3) to investigate the [CO_2] effect on the respiratory substrate supply system at a whole-plant level including the numbers, half-lives, size and importance of kinetically distinct pools, and (4) to explore the potential relationship between carbohydrate fractions and respiratory substrate use.

Materials and Methods: Stands of perennial ryegrass were grown in [CO_2] of 200, 400 or 800 μmol mol^{-1} with a limiting nitrogen fertilizer supply. Well-developed, same-age stands were dynamically labelled with near-natural abundance $^{13}CO_2/^{12}CO_2$ mixtures, followed by measurements of the $^{13}C/^{12}C$ ratio (defined as $\delta^{13}C$) of plant respired CO_2 in the dark period and $\delta^{13}C$ of shoot carbohydrate fractions (sucrose, fructan, glucose, and fructose). Finally, relevant compartmental models were parametrized for the tracer kinetics of respired CO_2 at the whole-plant scale and carbohydrate fractions at the shoot level.

Results and Discussion: The results showed that the $^{13}CO_2/^{12}CO_2$ labelling system was prone to inevitable but minor artefacts (mainly due to opening the growth chambers for system maintenance and plant handling and sampling purposes), so that max. 4% error in source CO_2 occurred through air contamination with extraneous CO_2 across the three [CO_2] levels, and a max. 2.6% inter-contamination when a preparative HPLC system separated different carbohydrates. The work highlights the value of a two-chamber approach with CO_2 sources of distinct $\delta^{13}C_{CO2}$ to determine the isotopic end-members of mixing models for quantitative analysis of the tracer kinetics in respired CO_2, biomass, and carbohydrate fractions. Carbohydrate accumulation was enhanced by increasing [CO_2] from 200 to 800 μmol mol^{-1},

mainly due to a significant increase in fructan mass. A four-pool compartmental model of carbohydrate metabolism indicated that the most significant impact of elevating [CO_2] on central carbohydrate metabolism in the shoot was to increase carbon cycling through the fructan pool. Sucrose re-synthesis from breakdown products of fructan (fructose) accounted for an increasing proportion of total sucrose synthesis and was similar in magnitude to sucrose neo-synthesis at elevated [CO_2]. Independent of the [CO_2] effect, respired C was supplied by a short-term and a long-term pool, and the importance of the long-term pool was substantial (*c.* 58%). Increasing [CO_2] from 200 μmol mol^{-1} to 800 μmol mol^{-1} increased the size of the long-term pool by 197% and its half-life by 148%. Comparing tracer kinetics of respired CO_2 and individual carbohydrates showed that the long-term pool was likely composed of fructan while the short-term pool probably mainly consisted of a mixture of transport and vacuolar sucrose.

Conclusion: This thesis provides, firstly, a methodical assessment of a quantitative $^{13}CO_2/^{12}CO_2$ labelling system and demonstrates that a two-chamber approach is a powerful means to analyze the C tracer kinetics in biomass or carbohydrate fractions. Secondly, the analysis of tracer kinetics and compartmental modelling confirmed a constitutive role of the fructan store in recycling sucrose and supplying substrate to respiration. In addition, it allowed the identification of carbohydrate substrates in the respiratory supply system. Finally, my results demonstrate the [CO_2] effect on carbon fluxes in carbohydrate metabolism at the whole shoot level and in the respiratory substrate at the whole plant scale, providing information on how an important perennial C_3 grass may have responded to past Glacial Maximum low [CO_2] and may respond to future high [CO_2].

Zusammenfassung

Zielsetzung: Organische C Speicher liefern C für Pflanzenwachstum und Respiration v.a in Form von Kohlenhydraten (z.B. Fructane und Saccharose). C-Flüsse in Speichern liefern Informationen über den Kohlenhydrat-Stoffwechsel und das respiratorische Versorgungssystem der Pflanzen, und deren Reaktion auf Umweltbedingungen. Das Ziel dieser Arbeit war die Untersuchung der Rolle von organischen C-Speichern und des respiratorischen Versorgungssystems bei unterschiedlicher atmosphärischer CO_2-Konzentration in Deutsch Weidelgras (*Lolium perenne*, C_3). Von besonderem Interesse war (1) die Beurteilung der Funktionsfähigkeit einer $^{13}CO_2/^{12}CO_2$-Markierungsanlage, (2) die Anwendung von Tracer-Kinetiken zur Untersuchung des Einflusses verschiedener atmosphärischer CO_2-Konzentrationen auf C-Flüsse im zentralen Kohlenhydrat-Stoffwechsel (Fructane, Saccharose, Glukose und Fructose) im Sproß, (3) die Untersuchung von C-Flüssen im respiratorischen Versorgungssystem auf der Ebene ganzer Pflanzen incl. Anzahl, Halbwertszeit, Größe und Bedeutung kinetisch unterschiedlicher Pools, und (4) die Untersuchung des Zusammenhangs zwischen verschiedenen Kohlenhydrat-Fraktionen und dem respiratorischen Substrat.

Materialien und Methoden: Im Markierungsversuch wurden Bestände von Deutsch Weidelgras bei atmosphärischen CO_2-Konzentrationen von 200, 400 oder 800 $\mu mol\ mol^{-1}$ und limitierender N-Versorgung angezogen. Geschlossene Bestände gleichen Alters wurden mit CO_2 aus zwei isotopisch unterschiedlichen, natürlichen Quellen markiert, begleitet von Messungen des $\delta^{13}C$ in der Dunkelperiode respirierten CO_2 sowie des $\delta^{13}C$ der wichtigsten Kohlenhydrat-Fraktionen im Sproß. Mithilfe dieser Daten wurden kompartimentelle Modelle parametrisiert, die die Tracer-Kinetiken im respirierten CO_2 auf der Ganz-Pflanzen-Ebene sowie in den Kohlenhydrat-Fraktionen im Sproß beschreiben.

Ergebnisse und Diskussion: Beim Betrieb der $^{13}CO_2/^{12}CO_2$-Markierungsanalge wurden unvermeidliche aber geringfügige Fehler festgestellt, welche u.a. beim Öffnen der Klimakammern für Wartungs- und Probenahmezwecke auftreten; 4 % des von den Pflanzen aufgenommene C stammte von CO_2 aus der Umgebungsluft (Kontamination) und nicht von den beiden zur Markierung verwendeten CO_2-Quellen. Zudem war die Trennung der verschiedenen Kohlenhydrat-Fraktionen mittels präparativer HPLC mit einem geringen Fehler behaftet (max. 2,6 %). Andererseits konnte die Leistungsfähigkeit des Zwei-Kammer-Ansatzes der $^{13}CO_2/^{12}CO_2$-Markierung demonstriert werden, v.a. für die Bestimmung der beiden

Endglieder des Tracer Mischungsmodels zur Bestimmung der Anteile alten und neuen C in den untersuchten Pools und Flüssen. Die Gehalte der Nicht-Struktur-Kohlenhydrate nahmen mit zunehmender CO_2-Konzentration von 200 auf 800 µmol mol^{-1} zu, v.a. hinsichtlich der Gesamtmasse der Fructane. Ein Vier-Pool-Model des Kohlenhydrat-Stoffwechsels implizierte, dass der stärkste CO_2-Effekt auf der Umsetzung des Fructan-Pools beruhte. Saccharose-Resynthese aus den Abbauprodukten von Fructanen erklärte einen zunehmenden Anteil der gesamten Saccharose-Synthese und war in der erhöhten CO_2-Konzentration von ähnlicher Größenordnung wie die Saccharose-Neusynthese. Unabhängig von der CO_2-Konzentration wurden der Substratkohlenstoff für die Respiration aus einem kurzfristigen und einem Speicherpool bereitgestellt. Die Bedeutung des Speicherpools für die Respiration war beträchtlich (*c.* 58 %). Die Erhöhung der CO_2-Konzentration führte zu einer Vergrößerung des Speicher-Pools um 197 % und zu einer Verlängerung seiner Halbwertszeit um 148 %. Der Vergleich der Tracer-Kinetik von respiratorischem CO_2 und einzelnen Kohlenhydraten zeigte, dass der Speicherpool vermutlich mit Fructan identisch war, während der kurzfristige Pool wahrscheinlich hauptsächlich aus einer Mischung aus Transport- und vakuolärer Saccharose bestand.

Schlussfolgerungen: Diese Arbeit diente der Einschätzung der Funktionalität einer $^{13}CO_2/^{12}CO_2$ Markierungsanlage und demonstrierte die Nützlichkeit eines Zwei-Kammer-Ansatzes mit unterschiedlichen $^{13}CO_2/^{12}CO_2$-Quellen für die Analyse von Tracer-Kinetiken in verschiedenen C-Pools und -Flüssen. Tracer-Kinetiken und kompartimentelle Modellierung demonstrierten die grundlegende Rolle von C-Speichern im Saccharose-Stoffwechsel und als Substrat für die Respiration. Zusätzlich ermöglichten die Ergebnisse die Identifizierung von Kohlenhydrat-Fraktionen als Substrat für die Respiration. Schliesslich zeigten die Untersuchungen zu den Auswirkungen unterschiedlicher CO_2-Konzentrationen auf die C-Flüsse im Kohlenhydrat-Stoffwechsel und Respiration, wie C_3-Gräser auf vergangene, niedrige CO_2-Konzentrationen reagierten und erlauben die Einschätzung wie sie sich an zukünftige, erhöhte CO_2-Konzentration anpassen.

List of Figures

List of Tables

1. Introduction

1.1 Plant responses under varying atmospheric CO_2 concentration

In recent decades, there has been a considerable research interest into the impact of increasing atmospheric CO_2 concentrations ([CO_2]) on various aspects of plant biology, including photosynthesis, growth, nutrition, and morphology (Franks et al., 2012). Studies have explored the effects of [CO_2] across a range of scales, spanning from those present during the Last Glacial Maximum (LGM; 18000–20000 years ago) to projected end-of-21st-century levels (Sage & Coleman, 2001; Lüscher et al., 2004; Ainsworth and Long, 2005).

An early expectation has been that [CO_2] would enhance photosynthetic capacity, which is typically associated with the rate of carboxylation by Rubisco in C_3 plants, such as perennial ryegrass (*Lolium perenne*), the object of this study. In C_3 plants, the Rubisco carboxylation reaction is not saturated at current [CO_2] levels, and an increase in atmospheric [CO_2] was generally expected to lead to a boost in photosynthesis (Drake et al., 1997). Conversely, low [CO_2] levels have been found to strongly limit C_3 photosynthesis (Sage & Coleman, 2001), reducing the capacity of plants to assimilate nutrients (Tissue et al., 1995). Additionally, reductions in carbon (C) availability have been observed to alter biomass allocation patterns, with plants allocating more biomass to their leaves at the expense of their roots (Sage & Cowling, 1999). Furthermore, constrained biomass production caused by low [CO_2] levels may have constrained the ability of plants to complete their life cycle (Dippery et al., 1995). Studies have also shown that short-term elevated [CO_2] can significantly stimulate leaf photosynthesis (Ainsworth et al., 2003), increase leaf concentration of total nonstructural carbohydrates and alter the carbon : nitrogen ratio of litter (Körner, 2000), but long-term stand- and ecosystem-scale responses were generally much smaller and sometimes absent (Long et al., 2006). In particular, the availability of growth resources such as nitrogen (N) and phosphorus (P) were found to strongly influence a plant's response to increasing [CO_2] (Terrer et al., 2016; Terrer et al., 2019). For example, Lüscher et al. (2004) reported that the availability of mineral N in the soil was a main factor limiting the growth response of *L. perenne* to elevated [CO_2].

Organic C stores represent a significant functional component of plant biomass under rising CO_2 (Körner, 2006), but their role and integration in whole plant C metabolism has not been studied in any detail, as I explain below. Therefore, this thesis utilized experimental and

modelling approaches to explore the interplay of organic C stores in sucrose recycling and respiratory substrate supply to improve understanding of how organic carbon store respond to varying [CO_2] levels, as experienced in the past and as projected for the end of this century. In that I used perennial ryegrass as a model C_3 grass, as it has a very high economic value as a forage crop (Chapman et al., 2017) and its physiology has been studied in relative detail also in response to [CO_2] (Lüscher et al., 2004).

1.2 Ecophysiological functions of organic C stores in C_3 grasses

Virtually all CO_2 fixed in photosynthesis is either deposited in plant structural biomass or returned to the atmosphere through (autotrophic) respiration (Trumbore, 2006; Lehmeier et al., 2008). Thus, respiration and deposition in structural biomass represent the terminal fates for fixed carbon (C) within plants. Interestingly, the balance between being respired and used in growth, denoted by the so-called carbon-use efficiency (CUE, defined as CUE = (photosynthesis – respiration) / photosynthesis), tends to be relatively constant in herbaceous plants with a CUE of ~0.6-0.7, meaning that a relatively constant fraction of 0.3-0.4 of photosynthetically fixed C is respired in diverse environmental contexts (Thornley, 2011; Gong et al., 2017).

However, between being fixed and respired or deposited in structural biomass, C compounds may cycle through diverse metabolic pathways in different cellular compartments in multiple tissues and organs (Gebbing et al., 1998; Lehmeier et al., 2008; Schnyder et al., 2012; Verbančič et al., 2018). The temporal delay between being captured in photosynthesis and respired or deposited as structural C can be extended dramatically by temporary storage as reserves (Chapin et al., 1990; Smith & Stitt, 2007). These stores can represent a substantial fraction of total vegetative plant biomass and are thought to serve primarily as buffers that accommodate or balance fluctuating disparities between photosynthetic activity and assimilate demands for growth, defense and maintenance activities (Pollock & Cairns, 1991; Schnyder, 1993; Chapin et al., 1990). In most C_3 and C_4 plant families, vacuolar sucrose in leaf blades and other photosynthetically active tissues is the main diurnal carbohydrate store in both vegetative and reproductive grass (Jenner & Rathjen, 1972; Schnyder, 1993; Lunn et al., 1999; Barro et al., 2020). This includes the grasses which comprise many of the globally most important crops and a wide variety of cultivated forage species (Farrar & Farrar, 1986; Sicher et al., 1986; Schnyder, 1993; Isopp et al., 2000), such as perennial ryegrass (*L. perenne*, C_3),

the model species used in this study. Starch built up in chloroplasts during the day and degraded during the night is also known as an essential diurnal carbohydrate store, sometimes complementary with vacuolar sucrose, in many plants, e.g. *Arabidopsis* (Sulpice et al., 2009; Graf & Smith, 2011; Stitt & Zeeman, 2012), including in grasses (Gordon et al., 1980; Cairns et al., 2002).

Nevertheless, in C_3 grasses, much greater amounts and concentrations of carbohydrates can be stored longer-term (several days to months) as fructans (Kühbauch & Thome, 1989; Pollock & Cairns, 1991). For example, Wagner et al. (1983) observed a fructan concentration of up to 75% of the dry weight of illuminated barley leaves when photosynthate export was slowed down or blocked by cool conditions or detachment of leaves. Fructan molecules are water-soluble oligomers or polymers of fructose, generally containing one glucose residue, and are synthesized from sucrose in vacuoles (Wagner et al., 1983, 1986; Sprenger et al., 1995; Pollock & Cairns, 1991). Fructan synthesis can occur in virtually all immature growing and mature fully-differentiated tissues of C_3 grasses, including leaf blades, leaf sheaths, leaf growth zones, stems, roots, floral and reproductive tissues (Nelson & Spollen, 1987; Pollock & Cairns, 1991; Schnyder et al., 1993; Pavis et al., 2001). Fructan synthesis in vacuoles occurs by different fructosyl transferase enzymes that catalyse the transfer of the fructosyl residue of a donor sucrose molecule onto an acceptor sucrose molecule, thus forming a trisaccharide or onto an (acceptor) fructan molecule, causing fructan chain elongation by one fructosyl residue (Chalmers et al., 2005). These fructosyl transfers cause liberation of the glucosyl residue of sucrose, which is then used for sucrose (re)synthesis in the cytosol (Nguyen-Quoc et al., 2001). Fructan degradation or depolymerization is catalyzed by fructan exohydrolase enzymes releasing fructose, which is subsequently used for sucrose recycling in the cytosol (Lattanzi et al., 2012). Given that fructan synthesis and hydrolysis may coincide in the same compartment (Wagner et al., 1983; Pollock & Cairns, 1991), the fructan pool in a vacuole can be conceived as an extension of the sucrose pool, which permits the maintenance of a very high concentration of stored carbohydrate without the adverse osmotic consequences that would arise from storage of a similar quantity of sucrose (Nelson & Spollen, 1987).

Fructan storage depends on the source-sink relationships in plants, with an overabundance of photo-assimilates relative to growth and maintenance needs stimulating fructan deposition (Kühbauch & Thome, 1989; Pollock & Cairns, 1991). Such relationships are naturally provided by cool conditions (such as are prevailing in the fall; Pollock & Jones, 1979), nutrient limitation (particularly of nitrogen; McGrath et al., 1997; Lattanzi et al., 2012),

mild drought (Chaves et al., 2003; Muller et al., 2011), high irradiance (Savitch et al., 2000) and elevated atmospheric CO_2 concentration ([CO_2]) (Stitt, 1991; Smart et al., 1994; Isopp et al., 2000; Rogers & Ainsworth, 2006). However, whether or not low [CO_2] – such as the ~200 μmol mol^{-1} that existed near the Last Glacial Maximum (LGM), *c.* 20'000 years ago – could have compromised the ability of grasses to store fructan has not been studied to my knowledge.

Generally, it is held that long-term stores of fructan are mobilized during the senescence phase of graminaceous crops that occurs in parallel with grain development and growth (Schnyder, 1993; Smouter & Simpson, 1991; Gebbing et al., 1998) or perennial grasses following the dormant period (Noël et al., 2000), during periods of stress (e.g. drought, Amiard et al., 2003), and after disturbance by fire (de Moraes et al., 2016; Martínez-Vilalta et al., 2016) or defoliation by grazing or mowing (Morvan-Bertrand et al., 2001). Importantly, however, stores also play a constitutive role in supplying substrate for growth and autotrophic respiration of grassland vegetation during undisturbed growth, as indicated by C tracer studies in the field (Gamnitzer et al., 2009; Ostler et al., 2016). Specifically, evidence also supports a constitutive role of fructan in central metabolism, with fructan turnover contributing very significantly to sucrose recycling (regeneration) in leaves even in steady-state conditions when photosynthesis is active and fructan levels remain virtually constant in perennial ryegrass (Lattanzi et al., 2012, see also chapter 1.3, below). Although sucrose is a primary photosynthetic product (Stitt et al., 1987; Goldschmidt & Huber, 1992; Farrar et al., 2000), foliar fructan turnover may participate constitutively in its (re-)cycling, which is vital for understanding the relationship between photosynthetic activity and sucrose availability. The importance is further enhanced by the fact that carbohydrate translocation in grasses (and most other species) occurs in the form of sucrose virtually exclusively (Giaquinta, 1983; Ward et al., 1997). In such a system, sucrose recycled via fructan turnover would become available for growth and respiratory metabolism centers in the heterotrophic plant parts.

Besides carbohydrate stores, soluble proteins have also been discussed as an additional putative source of 'stored' substrate for respiration in connection with protein turnover, particularly under stressful conditions (Araújo et al., 2011; Lehmeier et al., 2012).

As respiration produces 'only' CO_2, there is no metabolic tag in the respired gas that could inform us of its' metabolic origin, that is the specific metabolic pathways visited by the precursors of the respired CO_2 inside intact plants. However, it is known that – in the strict sense – respired CO_2 derives directly from only a few compounds, mainly malate, pyruvate,

isocitrate, α-ketoglutarate, or gluconate-6-P (Heldt, 2005; Tcherkez et al., 2012), which together comprise only a tiny fraction of whole plant biomass (Lehmeier et al., 2008). These compounds must be turned over very rapidly, given the commonly observed respiration rates. However, Lehmeier et al. (2008) demonstrated the presence of a storage pool (with a half-life of ~33 h) that comprised approximately 11.5% of total plant biomass-C feeding whole plant respiration (see chapter 1.3, below). If it is true that stored substrate can be used with a similar CUE as primary photosynthate, then the total size of the store must have been in the order of approximately 35% of shoot biomass-C in the investigations of Lehmeier et al. (2008). That estimate is close to the total metabolic biomass supporting (structural) biomass synthesis of perennial ryegrass in tracer studies in the field (Ostler et al., 2016). At present, a full understanding of the chemical identity of the metabolic pools supporting respiration of perennial ryegrass is still lacking, although it is hypothesized here that fructan plays a central role. In particular, it is presently unknown how the low level of [CO_2] in the LGM and future predicted [CO_2] affect the role of the fructan pool in sucrose recycling and the role of stores in supplying substrate for respiration in grasses.

1.3 Principles and application of carbon isotopes in carbohydrate and respiratory CO_2 measurement

Temporal variation in the transport of C metabolites through metabolic networks and stores of intact plants has been explored by labelling with radioactive (^{11}C- or ^{14}C-CO_2) or stable C isotope ($^{13}C/^{12}C$-CO_2) tracers. Specifically, C tracers have been used to partition CO_2 fluxes, estimate transport velocity, and assess C allocation to different plant parts and partitioning between different biochemical compounds (Schnyder et al., 2012; Kölling et al., 2013). This has included tracing of C through the different metabolites of the reductive pentose phosphate cycle (Bassham et al., 1950), disentangling of photorespiration and gross photosynthesis (Ludwig & Canvin, 1971), distinguishing between dark respiration and net photosynthesis during the light period of the day (Schnyder et al., 2003), and determination of the importance of storage-derived pre-anthesis C to carbohydrate and protein synthesis in wheat grains (Gebbing & Schnyder, 1999). The different isotopes are not equally well suited to studying different physiological questions. For instance, radioactive isotopes (^{11}C, ^{14}C) are a practical tool for studying translocation velocity *in vivo* by using emission/decay detectors/sensors placed along the translocation path (Geiger & Swanson, 1965; Jahnke et al., 1981). Conversely,

the physiology or biochemistry of longer-term storage cannot be studied with ^{11}C due to its short half-life (20 min). Stable isotope mixtures of CO_2 (i.e. $^{13}CO_2/^{12}CO_2$) are preferable, particularly for applications in the field or for large-scale and long-duration (>1 d) experiments in controlled environments, as they avoid health hazards originating from the use of radioactive isotopes and, by using natural or industrial sources of different origin, are relatively inexpensive.

Two different strategies of applying isotopically labelled CO_2 have been employed in the past: pulse- and dynamic (or steady-state) labelling (Schnyder et al., 2012, 2017). Typically, pulse-labelling experiments have employed either the radioactive isotopes (^{11}C or ^{14}C) or ^{13}C at high isotopic enrichment. Pulse-labelling experiments consist of three phases: (1) a pre-labelling period in which the plants are grown in normal, i.e. non-labelled, usually ambient CO_2, (2) a labelling pulse of short duration (normally seconds to hours depending on the research question), followed by (3) a so-called 'chase' period in which the photosynthetically fixed tracer becomes diluted by new, 'non-labelled' C. Commonly, the distribution of the tracer is followed during the chase period. In contrast, dynamic labelling experiments have only two phases: a pre-labelling period and a labelling period in which tracer distribution is monitored. The labelling period may have a variable duration that may extend from seconds to months or longer, depending on the research question (Schnyder et al., 2012, 2017). For the question at hand here, which concerns the role of stores, dynamic labelling experiments are considered more suitable, as long-term stores are labelled only weakly in short-term pulse-labelling experiments and, consequently, the redistribution of the storage derived C compounds during the chase period is associated with a strongly weakened isotopic signal that may easily escape detection against the background noise in the isotopic baseline (Geiger & Swanson, 1965a, b; Schnyder et al., 2012). Here, I present data from 7-day long dynamic labelling experiments with the near-natural abundance $^{13}CO_2/^{12}CO_2$ labelling and gas exchange mesocosm described by Schnyder et al. (2003). This system has been used previously to study the role of stores in central carbohydrate metabolism (Lattanzi et al., 2012) or respiration (Lehmeier et al., 2008; 2010a, b) of *L. perenne*. This technique uses natural and relatively inexpensive sources of CO_2: mineral CO_2 and fossil (or organic) CO_2 derived from industrial processes (Schnyder, 1992). The abundance of ^{13}C ($\delta^{13}C$) is conventionally expressed as the deviation of the isotopic composition of a sample from that of the universal standard, which is carbon in carbon dioxide generated from a fossil belemnite from the Pee Dee Formation, denoted PDB (Farquhar et al., 1989) or nowadays IAEA Vienna-PDB (V-PDB), defined thus: $\delta^{13}C = R_P/R_S - 1$, with R the

molar abundance ratio $^{13}C/^{12}C$ as measured by the mass spectrometer, *P* referring to the sample and *S* to the V-PDB standard. As variations of $\delta^{13}C$ are extremely small in natural systems, the $\delta^{13}C$ values are commonly expressed in permil (‰).

The $\delta^{13}C$ of the CO_2 sources ($\delta^{13}C_{CO2}$) used in experiments have ranged preferably in the region of -3‰ (mineral) or -47‰ (organic) (Schnyder et al., 2003), similar to this thesis. The precision (standard deviation of repeated measurements) of the ^{13}C analysis of plant material or CO_2 in air is typically better than 0.3‰ (e.g. Ostler et al., 2016), providing an isotopic 'signal-to-noise ratio' (SNR) of the labelling system of >100 when SNR is defined as the ratio of the isotopic discrepancy between the contrasting CO_2 sources and the measurement precision for repeated measurements (e.g. SNR is calculated by 44‰ / 0.3‰, for the example cited above).

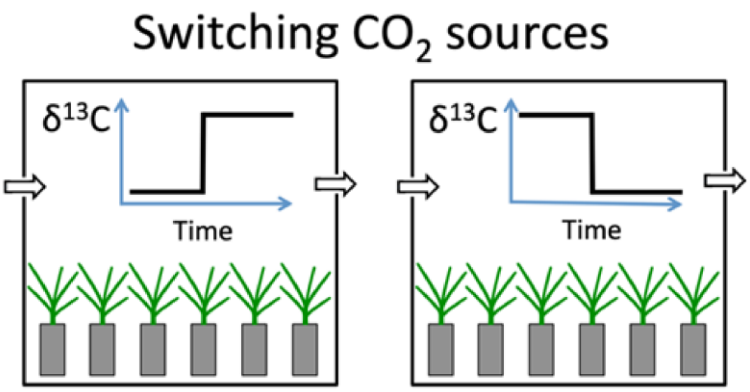

Fig. 1.1 Scheme illustrating the 'switching CO_2 sources' strategy for dynamic $^{13}CO_2/^{12}CO_2$ labelling of plant stands in growth chambers at the laboratory of Grünlandlehre of TUM (from Schnyder et al., 2017). Identical plant stands are established in two growth chambers with the same environmental conditions, but different $\delta^{13}C$ in the CO_2 ($\delta^{13}C_{CO2}$) provided to the chambers during the pre-labelling period (see figure insets). The CO_2 sources are switched at a given time, starting the dynamic labelling in both chambers. Individual plants can be sampled prior to and at intervals during the dynamic labelling period to analyze the tracer kinetics in plant parts or compounds of interest (see text). In parallel, the flux of air through the chambers, the CO_2 concentration and $\delta^{13}C_{CO2}$ entering and leaving the chamber are controlled and monitored, enabling the determination of the $\delta^{13}C$ of CO_2 exchanged in the light or respired in the dark.

For labelling plant stands, the laboratory of Grünlandlehre at TUM has typically applied a CO_2 source-switching strategy (Fig. 1.1), where identical plant stands are grown with the same environmental conditions in two growth chambers supplied with different $\delta^{13}C_{CO2}$ (Schnyder et al., 2003). Labelling is initiated by switching the isotopically contrasting CO_2

sources ($\delta^{13}C_{CO2\ mineral} \Leftrightarrow \delta^{13}C_{CO2\ organic}$) in parallel chambers. Thus, the chamber receiving mineral CO_2 is switched to organic CO_2, and *vice versa*, at the beginning of labelling. Plants are sampled at the time of (or just prior to) the switch and at intervals during the dynamic labelling for subsequent C isotope analysis of plant parts or compounds of interest (e.g. sucrose; Lattanzi et al., 2012). At the same time, the flux of air through the chambers (controlled by mass flow controllers) and the CO_2 concentration (measured by an infrared gas analyzer) and $\delta^{13}C_{CO2}$ (determined by on-line isotope ratio mass spectrometry) entering and leaving the chamber are used to calculate CO_2 exchange rates and the $\delta^{13}C$ of CO_2 exchanged during the light and dark periods (Schnyder et al., 2003).

The fraction of unlabelled C ($f_{unlabelled}$, with $f_{unlabelled} = 1 - f_{labelled}$, the labelled fraction) in a given entity of interest (C pool or CO_2 flux component, e.g. respiration) is obtained by a two-member mixing model as:

$$f_{unlabelled} = (\delta^{13}C_{sample} - \delta^{13}C_{new}) / (\delta^{13}C_{old} - \delta^{13}C_{new}) \qquad \text{Eqn 1.1}$$

where $\delta^{13}C_{sample}$ equals the $\delta^{13}C$ of a specific sample, and $\delta^{13}C_{new}$ and $\delta^{13}C_{old}$ are the end-members of the equation given by the C fixed in the presence of the 'new' (labelling) and 'old' (pre-labelling) CO_2 for the same sample type, respectively (Schnyder et al., 2003). $\delta^{13}C_{new}$ and $\delta^{13}C_{old}$ are typically determined in samples from plants constantly maintained in the presence of the 'new' or 'old' CO_2. However, experimenters often have only one labelling chamber. In that case, the 'new' end-member is estimated from: (1) knowledge of ^{13}C discrimination of a specific sample ($\Delta^{13}C$) as observed in the presence of the 'old' CO_2 (Farquhar et al., 1989):

$$\Delta^{13}C = (\delta^{13}C_{CO2\ old} - \delta^{13}C_{old}) / (1 + \delta^{13}C_{old}) \qquad \text{Eqn 1.2}$$

and (2) knowledge of the $\delta^{13}C_{CO2}$ of the new, i.e. labelling CO_2 ($\delta^{13}C_{CO2\ new}$) as per Schnyder, (1992):

$$\delta^{13}C_{new} = (\delta^{13}C_{CO2\ new} - \Delta^{13}C) / (1 + \Delta^{13}C) \qquad \text{Eqn 1.3}$$

The one-chamber approach uses the fact that $\Delta^{13}C$ is independent of $\delta^{13}C_{CO2}$, as is true based on theory (Farquhar et al., 1989), but also requires that $\delta^{13}C_{CO2\ new}$ and $\delta^{13}C_{CO2\ old}$ (as measured for the tank CO_2 gases) are not negatively affected by experimental artefacts in the labelling compartments (e.g. the plant growth chamber) such as by contamination with extraneous CO_2. A critical condition for a quantitative evaluation of tracer data is the virtual constancy of the isotopic composition of CO_2 in the chamber air in the different phases of the

experiment. For that reason, it is useful to monitor and control these parameters during the experiment (Schnyder et al., 2003). If experimenters have one parallel growth chamber (two-chamber approach), $\delta^{13}C_{new}$ is taken directly from $\delta^{13}C_{old}$, where $\delta^{13}C_{old}$ in one chamber serves as $\delta^{13}C_{new}$ in its counterpart and *vice versa* (Lehmeier et al., 2010a; Lattanzi et al., 2012). The estimate of $f_{unlabelled}$ via the two-chamber approach is independent of experimental artefacts with the assumption that contamination effects on $\delta^{13}C_{sample}$ and $\delta^{13}C_{old}$ are the same in the parallel chambers with the same growth conditions and practical operation.

Notably, there are systematic but often unknown differences between the $\delta^{13}C$ of different C pools or metabolites, even if $\delta^{13}C_{CO2}$ of the CO_2 provided to a chamber is kept constant. This is due to variation of photosynthetic (Farquhar et al., 1989) and post-photosynthetic C isotope discrimination (Cernusak et al., 2009). Generally, however, plant C is variably depleted in ^{13}C due to photosynthetic ^{13}C discrimination, $\Delta^{13}C$, the primary determinant of overall $\Delta^{13}C$, with a variation of $\Delta^{13}C$ as a function of growth conditions and genotype- or functional group-specific biological makeup (Farquhar et al., 1989).

Instantaneous $\Delta^{13}C$ – the $\Delta^{13}C$ of C fixed on a given moment in time – can be determined from on-line $^{13}CO_2/^{12}CO_2$ gas exchange measurements (Evans et al., 1986) as:

$$\Delta^{13}C = [\xi\,(\delta^{13}C_{CO2\ outlet} - \delta^{13}C_{CO2\ inlet})] / [1 + \delta^{13}C_{CO2\ outlet} - \xi\,(\delta^{13}C_{CO2\ outlet} - \delta^{13}C_{CO2\ inlet})] \qquad \text{Eqn 1.4}$$

with $\delta^{13}C_{CO2\ outlet}$ and $\delta^{13}C_{CO2\ inlet}$ the $\delta^{13}C_{CO2}$ at the outlet and inlet of the growth chamber, and

$$\xi = C_{inlet} / (C_{inlet} - C_{outlet}) \qquad \text{Eqn 1.5}$$

with C_{inlet} and C_{outlet} the CO_2 concentration at the inlet and outlet of the chamber, respectively, corrected to standard humidity (i.e. 0). For the plant growth chambers of the Lehrstuhl für Grünlandlehre, C_{outlet} and $\delta^{13}C_{CO2\ outlet}$ are very near to the conditions experienced by plants (Schnyder et al., 2003) due to the strong ventilation of air inside the growth chambers.

Importantly, true $\Delta^{13}C$ is independent of $\delta^{13}C_{CO2}$ (Farquhar et al., 1989; Schnyder, 1992). However, (true) $\Delta^{13}C$ may vary by several thousandths between environments (Cernusak et al., 2013), genotypes (Farquhar & Richards, 1984; Yang et al., 2016), plant parts (Schnyder, 1992) and biochemical compounds (Gleixneret al., 1993; Tcherkez et al., 2011). Environmental and genotypic variation of $\Delta^{13}C$ is valuable physiological information for C_3 plants, as it correlates closely with intrinsic water-use efficiency (iWUE), the ratio of

photosynthesis (A) to stomatal conductance (g_s): iWUE = A / g_s (Farquhar et al., 1989; Yang et al., 2016). However, differences in $\Delta^{13}C$ between plant parts or biochemical compounds are still not fully understood (Cernusak et al., 2009). Whatever the cause, variation of $\Delta^{13}C$, including via experimental artefacts, must be considered in labelling data evaluation, as it directly affects the isotopic end-members ($\delta^{13}C_{new}$ and $\delta^{13}C_{old}$), as seen above. Therefore, organ- and compound-specific $\Delta^{13}C$ values (Schnyder, 1992) should be used to calculate $f_{unlabelled}$ (Eqn 1.1).

Contamination by extraneous $^{13}CO_2/^{12}CO_2$ (Gong et al., 2015) is a paramount concern, as it may affect all members of the equation, i.e. $\delta^{13}C_{sample}$, $\delta^{13}C_{new}$, and $\delta^{13}C_{old}$. Contamination by extraneous $^{13}CO_2/^{12}CO_2$ may occur through gas leaks (Gong et al., 2015) in the growth chamber or during the opening of the chambers for plant sampling or other works requiring access to the growth compartment. Such an effect can be explained by the incursion of a mixture of CO_2 from the free atmosphere ($\delta^{13}C$ ~ -10‰) and CO_2 exhaled ($\delta^{13}C$ ~ -23‰; Epstein & Zeiri, 1988) by people (e.g. experimenters) in the room housing the plant growth chambers. Contamination with extraneous $^{13}CO_2/^{12}CO_2$ can be minimized by maintaining a slightly positive atmospheric pressure inside relative to outside of the chambers (Schnyder et al., 2003) and by placing air-locks in chamber doors (Lehmeier et al., 2008). Eventual contamination with extraneous (organic) C sources during the handling and processing of samples is another factor that should be considered in labelling experiments. Given that all plant samples are handled and processed in identical ways, any contamination would reduce the isotopic spread between $\delta^{13}C_{new}$ and $\delta^{13}C_{old}$. In a theoretical, although extreme scenario, where the contaminated samples are composed entirely of the contaminant, the (artefactual) estimate of $\delta^{13}C_{new}$ would equal that of $\delta^{13}C_{old}$. Such extreme cases are most likely for tiny samples, where contamination would cause an extreme 'dilution' of the true (original) C isotope signal in the sample. Again, such artefacts would cause an (erroneous) effect on $\delta^{13}C_{CO2}$ on $\Delta^{13}C$, generating errors in tracer data evaluation. In principle, one should expect that tracer experiments at different [CO_2] would be particularly susceptible to such artefacts. Except for the investigation of leak problems with clamp-on leaf chamber $^{13}CO_2/^{12}CO_2$ exchange measurements by Gong et al. (2015), however, this problem (termed 'isotopic end-member problem' in the following) has not been examined systematically, to the best of my knowledge.

1.4 Compartmental modelling of the respiratory substrate supply system and central carbohydrate metabolism

Compartmental modelling is a mathematical tool for interpreting the tracer time course in a particular entity, e.g. sucrose or respired CO_2, in terms of the metabolic system that generates it (Atkins, 1969; Farrar & Farrar, 1986; Jacquez, 1996; Lattanzi et al., 2012; Schnyder et al., 2012, 2017). Basically, the compartmental model characterises the system, for instance, the respiratory substrate supply system, by the number of kinetically distinct pools, the connections between the pools, the residence time of the tracer in each pool, the size of each pool, the fluxes of material (tracer) through each pool and the environment (including any parts exterior to the system under investigation). Commonly, it is assumed that pools are well-mixed, thus obeying first-order kinetics, with practical support from many systems (e.g. Lattanzi et al. 2005). This means that the time course of the tracer in the parts (pools) of the system can be described by a set of differential equations. Another assumption is that the system is in a steady state, namely that pool sizes and fluxes are constant. In the strict sense, that condition is rarely met, even if plants are grown in controlled conditions. However, the condition may be approximate sufficiently closely, even with plants grown in day-night cycles, when analysing data on a day-by-day timescale over limited periods of time, as shown by Lattanzi et al. (2005, 2012), Lehmeier et al. (2010a), and Gong et al. (2017).

Compartmental models should provide a biologically meaningful description of the system under investigation (Schnyder et al., 2012). At the same time, a compartmental model should be parsimonious, that is, it should not be more complex than is necessary for an unbiased representation of the tracer data. Lehmeier et al. (2008) analysed the tracer time courses in respired CO_2 (i.e. the temporal changes of $f_{\text{unlabelled}}$ over time) of shoots of perennial ryegrass grown in continuous light and labelled for periods of 1 h to 25 d and detected three kinetically distinct phases that indicated the existence of a respiratory substrate supply system composed of three pools, with different half-lives (<0.2 h, ~3 h, and 33 h) and sizes (equivalent to 0.2, 10 and 70 mg g^{-1} biomass-C). Interestingly, the tracer kinetics of the roots were (1) very similar to that for the shoots, but (2) exhibited a temporal delay in tracer appearance that was consistent with assumptions for the time needed for transport of the substrate of respiration from the shoot to the root (~0.8 h), and (3) indicated a total size of the respiratory substrate supply system supporting root respiration that was several times larger than the total quantity of non-structural, i.e. metabolizable C present in the roots. Together, these features (1-3) indicated that at least

the largest and most slowly turning over pool supporting root respiration must have been located outside the root system, i.e. in the shoot. These results revealed new biological insight into the biological system supporting respiration obtained by combining quantitative tracer application and compartmental modelling. A simplified version of that model, that is, a two-pool model (inset in Fig. 1.2a) that ignored the presence of the most rapidly turned-over and smallest pool in the system, was subsequently used to study the role of long-term stores in the respiratory substrate supply system of perennial ryegrass grown in continuous light or regular day-night cycles (Lehmeier et al., 2010a; Fig. 1.2) and of [CO_2] in sunflower (Gong et al., 2017).

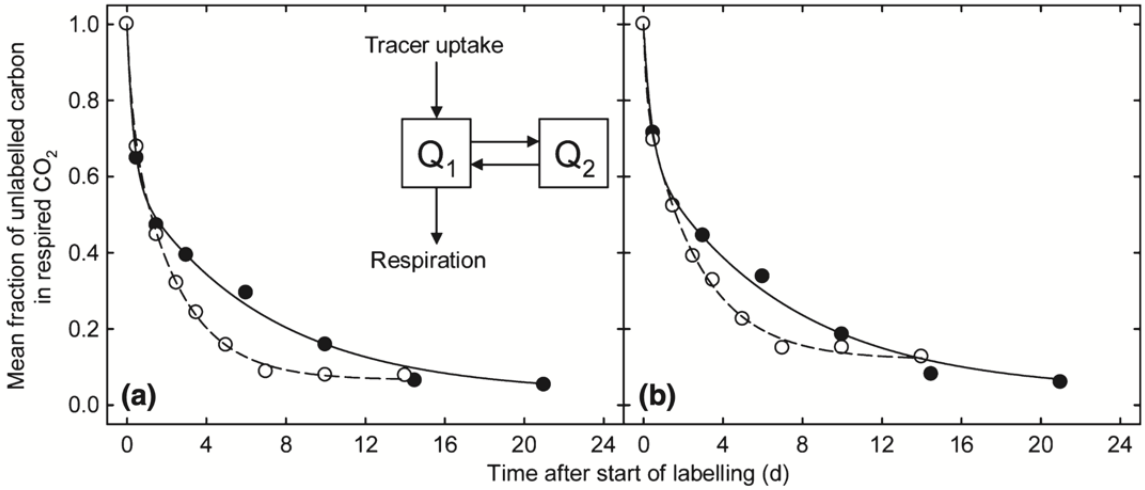

Fig. 1.2 Time course of the fraction of unlabelled C ($f_{unlabelled}$) in dark-respired CO_2 of shoots (a) and roots (b) during dynamic $^{13}CO_2/^{12}CO_2$ labelling of *L. perenne* grown in continuous light (closed symbols) or a 16:8 h day:night regime (open symbols) (from Lehmeier et al., 2010a). Lines denote the predictions of the two-pool model shown as an inset in (a) for plants grown in continuous light (solid lines) or in the 16:8 h day:night cycle (dashed lines). For details, see Lehmeier et al. (2010a).

Lattanzi et al. (2012) devised a four-pool compartmental model of central carbohydrate metabolism for a photosynthetically active leaf of a C_3 grass (Fig. 1.3). Among other things, that model was used to study the effect of nitrogen nutrition on the role of fructan metabolism in the recycling (re-synthesis) of sucrose. In that model, (1) current photosynthesis supplied central carbohydrate metabolism *via* the sucrose pool, (2) sucrose was consumed in three types of processes: export, fructan synthesis (with the fructosyl moiety of a donor sucrose molecule transferred to an acceptor sucrose or fructan molecule, and simultaneous release of one glucose

molecule), and sucrose hydrolysis by invertase-like processes (generating equimolar amounts of fructose and glucose), (3) fructan hydrolysis produced fructose, (4) fructan turnover in a steady-state yielded equimolar amounts of fructose (released during fructan hydrolysis) and glucose (released during the synthesis step, see above), and (5) all fructose and glucose was (re)utilized in sucrose (re)synthesis. This model provided a virtually perfect fit (R^2=0.97) to the combined tracer kinetics in sucrose, fructan, glucose, and fructose (Fig. 1.4), supporting the basic assumptions of compartmental analysis, as outlined above. In particular, the model fit to the data also supported stoichiometric constraints, i.e. that equimolar amounts of glucose were produced per fructosyl unit transferred to the fructan pool, and equimolar use of fructose and glucose in sucrose re-synthesis related to invertase activity and fructan metabolism. In other words, in a statistical sense, the stoichiometrically-constrained four-pool model (Fig. 1.3) performed equally well or better than more complex models (Lattanzi et al., 2012). To the best of my knowledge, the approach of Lattanzi et al. (2012) (or equivalent) has not been applied to other research questions, such as scaling up to the whole plant level or investigations of the effect of [CO_2] on the role of fructan metabolism in sucrose recycling.

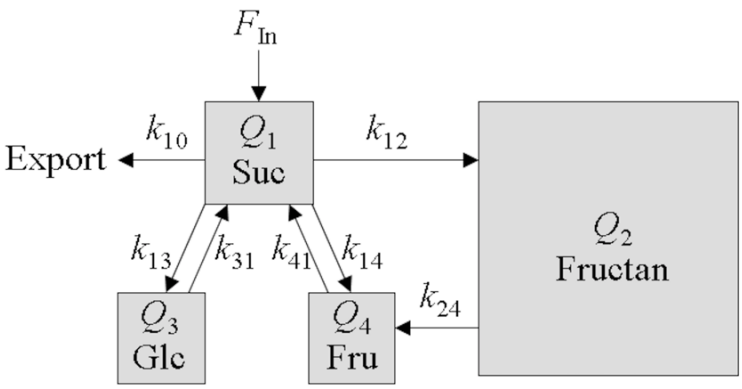

Fig. 1.3 Four-pool compartmental model of central carbohydrate metabolism in source leaves of *L. perenne* (from Lattanzi et al., 2012). Suc, sucrose; Glc, glucose; Fru, fructose; F_{in}, tracer flux into the system. Q_i represents the size of the carbohydrate pool *i* ($Q_{1\text{-}4}$ mean sucrose, fructan, glucose, and fructose pools, respectively), and k_{ij} is the rate constant for the flux from pool *i* to pool $_j$. Thus, k_{10} denotes the export of sucrose from the system, k_{12} the fructosyl transferase-catalysed transfer of the fructosyl residue of donor sucrose to a fructan (or sucrose) acceptor molecule, k_{13} glucose production by fructosyl transferase *plus* invertase(-like) activities, k_{14} fructose production by invertase(-like) activity, k_{24} cleavage of fructose from fructan by fructan exohydrolase, k_{31} glucose use in sucrose resynthesis, and k_{41} fructose use in sucrose resynthesis. For mathematical details of the model, including the differential equations describing the fluxes, see Lattanzi et al. (2012).

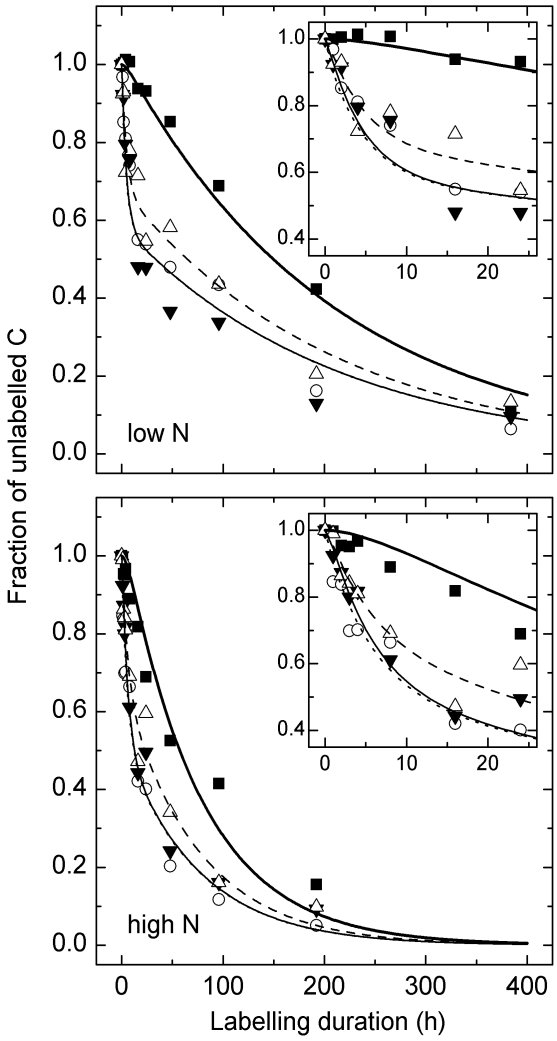

Fig. 1.4 The fraction of unlabelled C ($f_{unlabelled}$) in fructan (filled squares), sucrose (open circles), glucose (filled triangles), and fructose (open triangles) with labelling duration in the youngest fully expanded leaf blade of *L. perenne* grown at low N (upper panel) and high N supply (lower panel) (from Lattanzi et al., 2012). The insets expand the first 24 h of the dynamic labelling. The curves represent the fits of the four-pool model shown in Fig. 1.3. Carbohydrates were extracted from the blade of the youngest fully expanded leaf of perennial ryegrass grown with either 1 mM nitrate (low N) or 7.5 mM nitrate (high N) in the nutrient solution. Plants were labelled during normal growth in swards kept in $^{13}CO_2/^{12}CO_2$ mesocosms. In both treatments, swards grew in continuous light with a photosynthetic photon flux density of 275 μmol mol^{-1}at 20 °C air temperature and 85% relative humidity. For details on carbohydrate extraction, separation and isotope analysis, see Lattanzi et al. (2012).

1.5 Aim and outline of the thesis

This thesis aims to explore the effects of [CO_2] on the role of stores for recycling sucrose in whole shoots and supplying substrate to respiration of intact plants or stands of perennial ryegrass (*L. perenne*, cv Acento) by use of a modernized version of the mesocosm-scale near-natural abundance $^{13}CO_2/^{12}CO_2$ dynamic labelling technique developed at the former TUM Lehrstuhl für Grünlandlehre and described by Schnyder et al. (2003). Perennial ryegrass was chosen as a model perennial C_3 grass of high economic value (Chapman et al., 2017), whose biology, breeding, and agronomy have been studied comparatively intensively in the past. The cultivar Acento was selected, as it had already been the subject of previous physiological studies at the TUM Lehrstuhl für Grünlandlehre (e.g. Lehmeier et al., 2008). My work was based on mesocosm-scale tracer experiments that were performed subsequent to extensive experimental works with the same plant stands during the (pre-labelling) establishment phase (see chapter 3.2 and Baca et al., 2020). As these works might have caused inadvertent

$^{13}CO_2/^{12}CO_2$ contamination issues, my work also included investigations on basic methodical assumptions of tracer data evaluation.

Thus, my work addressed the following specific questions and objectives (addressed in chapter 3):

(1) Do $^{13}CO_2/^{12}CO_2$ artefacts (e.g. through gas leaks or contamination during carbohydrate extraction and separation by HPLC) affect the isotopic end-member of the two-member mixing model used to analyze the labelling kinetics of gas exchange-, biomass- and carbohydrate-components? If so, were such artefacts sensitive to [CO_2] treatments? (chapter 3.1)

(2) Does the four-pool compartmental model of leaf-level central carbohydrate metabolism of a C_3 grass proposed by Lattanzi et al. (2012) also apply to the whole shoot level? Moreover, if so, does [CO_2] affect the role of the fructan store in sucrose recycling? (chapter 3.2)

(3) Does [CO_2] affect the importance of the store in supplying substrate for whole plant respiration? (chapter 3.3)

(4) Does a comparative analysis of the tracer kinetics of carbohydrate components (at shoot level) and whole plant respiration provide clues to the identity of substrates fueling dark respiration? (chapter 3.4).

Perennial ryegrass plants (*L. perenne*) were grown in dense swards in growth chambers at three different [CO_2] levels (treatments): 'half ambient' (approximately equivalent to the [CO_2] at the Last Glacial Maximum), current 'ambient', and 'double ambient' (as projected for the end of this century, IPCC, 2007). Stands in parallel (paired) plant growth chambers were grown in the presence of fossil-organic (industrial) CO_2 ($\delta^{13}C$ -43.5‰ as determined for the CO_2 at chamber inlet) and CO_2 from a mineral source ($\delta^{13}C$ -5.6‰). The swards were grown using a hydroponic culture system with optimal water supply but reduced nitrogen concentration in the standard nutrient solution (Kavanová et al., 2008; Lehmeier et al., 2008; 2013; Baca et al., 2020; see chapter 2).

In addition, in this thesis, I have included as Appendices two publications in which I am a coauthor. These formed part of the publication-based thesis of Juan C Baca Cabrera ("The key role of stomatal conductance in controlling the grassland vegetation response to a changing environment" passed with distinction in 2022) and were performed in the same experiments as

my studies. I contributed experimentally to these works by performing leaf-level gas exchange measurements (photosynthesis, stomatal conductance, and transpiration), assisting in the sampling of plant material, and carbohydrate analysis, and maintaining the experimental facility. Also, I contributed to the discussion of these works, as acknowledged in the author's contributions of these papers. These include one paper published in *New Phytologist* (Baca et al., 2020) and a preprint published in *ResearchSquare* (Baca et al., 2021). However, the specific topics of these papers are outside the scope of my thesis. Therefore, I did not include these papers in my thesis, although I cite them for some methodical details, which were common also to my work, and findings of interest to the interpretation of my results.

2. Materials and Methods

2.1 Experiment design

The treatments presented in this thesis formed part of a 3 × 2 factorial experiment with three atmospheric CO_2 concentrations ([CO_2]: 200, 400, and 800 µmol mol^{-1}) corresponding to the Last Glacial Maximum (LGM; sub-ambient), current ambient, and end of the century projections (double-ambient), and two air relative humidity (RH) levels of 50% and 75% during day-time. Night-time RH was 75% in all treatments. A total of five sequential experimental runs were performed using four growth chambers (Table 2.1). My thesis research was limited to the (day-time) 50% RH treatment in the first two runs. A day-time RH of 50% is a typical scenario for local temperate grassland (Hirl et al., 2019). Treatment replicates (*n*=3-5) were allocated to different chambers between sequential runs to minimize chamber effects. Plant management details were the same in all experimental runs. However, I observed no chamber effect on the parameters reported in this study (see also Baca et al., 2020).

Table 2.1 Experiment with a 3 x 2 experimental design: three [CO_2]: 200, 400 or 800 µmol mol^{-1} (C1, C2 or C3) and two RH levels: 50% or 75% during daytime. Nighttime RH was 75%, the same in all treatments. The treatment replicates were distributed between four growth chambers (no. 1-4). The corresponding treatments in this thesis are given in bold.

	Treatment					
Run	C1 (50%)	C2 (50%)	C3 (50%)	C1 (75%)	C2 (75%)	C3 (75%)
	Chamber no.					
1st	**1 / 2**	**3 / 4**	**-**	**-**	**-**	**-**
2nd	**-**	**1 / 2**	**3 / 4**	**-**	**-**	**-**
3rd	-	-	-	3 / 4	1 / 2	-
4th	-	3	-	-	4	1 / 2
5th	3	-	1	2	-	4

Plants of *L. perenne* were established and grown singly in individual plastic pot (350 mm height, 50 mm diameter) filled with 800 g of washed quartz sand (0.3-0.8 mm grain size). Pots were arranged at a density of 383 plants m^{-2} in plastic containers (770 × 560 × 300 mm), and two of such containers were placed in each growth chamber (PGR15, Conviron, Winnipeg,

Canada). Plants were supplied with a modified 5 mM nitrate-N Hoagland nutrient solution with a hydroponic culture system (Fig. 2.1). This nitrate-nitrogen (N) concentration corresponded to a nutrient solution with a 33% reduced nitrate-N concentration relative to normal and nominal concentrations of the other nutrients (compared to Kavanová et al., 2008). Thus, the nutrient solution contained 1.7 mM $Ca(NO_3)_2$, 1.7 mM KNO_3, 1.0 mM $MgSO_4$, 0.5 mM KH_2PO_4, 0.5 mM NaCl, 0.125 mM iron as EDTA, 46.1 µM H_3BO_3, 9.1 µM $MnSO_4$, 0.8 µM $ZnSO_4$, 0.3 µM $CuSO_4$, and 0.15 µM Na_2MoO_4. A nutrient solution with reduced nitrate-N concentration was chosen as most terrestrial ecosystems, including temperate grassland, are typically N-limited (LeBauer & Treseder, 2008; Terrer et al., 2019; Baca et al., 2020).

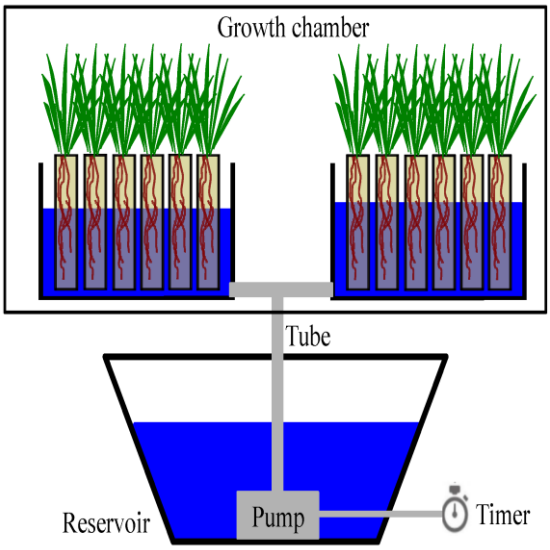

Fig. 2.1 Schematic representation of a flood-tide hydroponic culture system used in the present study. Nutrient solution (for composition, see text) was contained in a reservoir (size: 1770 × 690 × 520 mm; CEMO, Rems-Murr, Germany) close to the growth chamber (PGR15, Conviron, Winnipeg, Canada), a water pump (JP5BBCVBP, Grundfos, Bjerringbro, Denmark), and a timer (AX-801A, Duwi, Hagen, Germany) which activated the irrigation cycle every six hours. After the pot/container was irrigated for nine minutes, gravity drained the solution back down into the reservoir for *c.* 45 minutes.

Growth chambers were operated with day/night cycles, with a 16 h-long photoperiod and an 8 h-long dark period. The light was supplied by cool-white fluorescent tubes and warm-white LED bulbs. Irradiance was measured at regular intervals with a quantum sensor (Li-190R, LI-COR Inc., Lincoln, NE, USA), and the distance between the light source and the canopy was adjusted so that a photosynthetic photon flux density of 800 µmol m^{-2} s^{-1} was maintained at canopy height. The temperature of chamber air was held at 20 °C during the photoperiod and at 16 °C during darkness. RH of the chamber air was kept near the nominal level (SD ± 0.9%) by using a high-pressure water vapour generator (FINESTFOG, Ottobrunn, Germany) that added a known amount of water vapour to the chamber air whenever the nominal RH dropped below a specified threshold (1-2% RH lower than the chamber setpoint). The chamber-based humidification system was inactivated during that period. Air temperature and RH in the chamber were measured continuously with the chamber control system (CMP6050, Conviron, Winnipeg, Canada).

The target [CO_2] inside the chamber was obtained by mixing dry CO_2-free air and tank CO_2 of known carbon isotope composition ($\delta^{13}C$, with $\delta^{13}C = [(^{13}C/^{12}C)_{sample} / (^{13}C/^{12}C)_{VPDB\ standard}] - 1$) (Linde AG, Unterschleißheim, Germany or CARBO Kohlensäurewerke, Bad Hönningen, Germany) using mass flow controllers. Each [CO_2] treatment had two growth chamber replicates, one replicate chamber was supplied with ^{13}C-organic CO_2 ($\delta^{13}C$, -43.5‰) while the other replicate chamber received ^{13}C-mineral CO_2 ($\delta^{13}C$, -5.6‰). The $\delta^{13}C$ of supplied CO_2 was determined at the chamber inlet with a precision (SD) of <0.17‰ for repeated measurements. The airflow and CO_2 concentration of the chamber inlet air were periodically adjusted. The rate of CO_2 supply to the chamber exceeded the CO_2 exchange rate of the stands in light by a factor of 10. This minimised the effects of photosynthesis, respiration, and recycling of respiratory CO_2 on the $\delta^{13}C$ of chamber CO_2, so that the growing stands always experienced closely similar $\delta^{13}C$ and target [CO_2] in the growth chamber air during the photoperiod. One tank typically contained *c.* 30 kg of CO_2, so one experiment employed two ^{13}C-organic CO_2 tanks and two ^{13}C-mineral CO_2 tanks. The $\delta^{13}C$ of tank CO_2 was tested before each experimental run and was typically very similar (<0.27‰ SD) between tanks of the same type of CO_2 source (mineral or fossil-organic). The CO_2 concentrations and $\delta^{13}C_{CO2}$ measured in the chamber outlet air represented the growth chamber atmosphere (Schnyder et al., 2003).

Disturbance of air conditions in the chambers during handling of plants was minimized by maintaining *c.* 200 Pa positive atmospheric pressure inside relative to the outside of the chambers (Schnyder et al., 2003) and installing air-locks in chamber doors (Lehmeier et al., 2008) as shown in Fig. 2.2. Experimental operations, which included chamber maintenance activities and plant sampling, carried out with opening growth chamber doors, may have nevertheless resulted in some disturbance of growth chamber air CO_2 and $\delta^{13}C_{CO2}$. The total time that the chamber was open for one entire experiment during daylight was approximately 110 minutes. This time included a total of 20 minutes spent changing the broken light and 90 minutes spent sampling and handling the plants approximately 20 times (see next paragraph).

Fig. 2.2 Picture of air-lock. One air-lock consists of two PVC plates (770 × 460 mm) and two plastic sheets (570 × 400 mm). Two PVC plates were installed above and below the door. The middle area was left for the operation window, covered with two plastic sheets. The air-lock covered the growth chamber door completely.

2.2 Experiment timeline

The experiment was set up based on the plant growth stage, as shown in Table 2.2. The first irrigation of the sown seeds, which signifies the initiation of seed imbibition, was considered the start of the experiment (Day 0). The seedling development (Day 0 - 12), plant canopy expansion (Day 13 - 48), and full canopy (Day 49 - 72) are designated the three phases of a complete experiment (10 weeks).

Growth chambers were supplied with ambient air during the seedling development phase (until day 12). RH was maintained at 80% in both the light and dark periods. The air temperature was kept at target levels. Plants were irrigated with nutrient solution for the whole day. [CO_2] and RH treatments were implemented on day 13, in the canopy expansion phase. Plants were irrigated with the nutrient solution every six hours. In that: nutrient solution entered the plastic containers holding the plants for nine minutes and then drained back down into the reservoir over *c.* 45 minutes by gravity. The nutrient solution was renewed every three weeks throughout the duration of each experiment, in all experimental runs. For gas measurements in the chamber inlet or outlet, the concentration of CO_2 was measured from day 13 and $\delta^{13}C$ from day 20. All experiment operations were conducted in the full canopy phase. This experimental phase included two 2-d long intensive plant sampling periods, starting on day 49 and day 63, leaf-scale gas exchange measurements from day 49 to day 60, plant leaf temperature measurements from day 49 to day 63, leaf-elongation measurements from day 49 to day 62, and sampling of leaf morphometry measurements on day 64. The labelling experiments (and associated sampling activities) reported in this thesis were started between day 65 and day 72.

Table. 2.2 Timeline of one experiment. Day *X*, designates time during an experimental run, with time 0 defined as when the sown seed was first imbibed. The experiment was started on day 0 (refers to seed imbibition) and ended on day 72. The period consisted of the seedling development phrase, canopy expansion phase, and full canopy phase. The labelling experiment was conducted during the full canopy phase.

Experiment timeline		
Time	Stage description	Details
Day 0-12	Seedling development	Three seeds were sown per plastic tube; One week after seed imbibition, plants were reduced to one per tube (Fig. 2.3 A).
Day 13-48	Plant canopy expansion	On day 13, canopy-scale gas exchange measurement was started; On day 20, carbon isotopes measurements on chamber gas exchange were started.
Day 49-72	Full plant canopy	A series of measurements were performed during this period, including two plant sampling phases starting on day 49 and day 63, leaf-scale gas exchange, leaf temperature, leaf-elongation (Baca et al., 2020) and leaf morphometry measurements (see also Fig. 2.3 B).
Day 65-72	**Labelling experiment**	Dynamic $^{13}CO_2/^{12}CO_2$ labelling of stand-scale dark respired CO_2 and whole-shoot water-soluble carbohydrate fractions (fructan, sucrose, glucose and fructose).

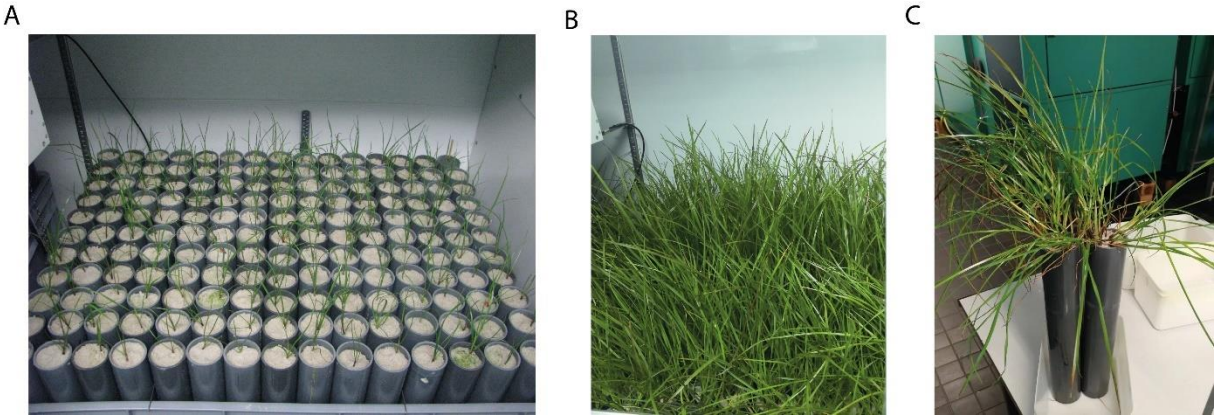

Fig. 2.3 Typical stages of plant and stand development during the experiment. A: Arrangement of plants in the growth chamber on day 18. B: Dense canopies had developed by day 49. C: Individual plants removed from the stands on day 65. Treatments did not exhibit differences in development rate or leaf dimensions (Baca et al., 2020). Also, all canopies were closed with a leaf area index >5.5 at the time of harvests (Baca et al., 2020).

2.3 Gas exchange measurement and isotope analysis

The experiment used a new version of the experimental infrastructure described by Schnyder et al. (2003; see also Baca et al., 2020) shown in Fig. 2.3, which consisted of four plant growth chambers. Sample air was collected at the inlet and outlet of each growth chamber and passed on to an infrared gas analyser (Li-840, LI-COR Inc., Lincoln, NE, USA) for measuring CO_2 and H_2O concentrations and to an isotope ratio mass spectrometer (IRMS, Delta plus, Advantage equipped with GasBench II, ThermoFinnigan, Bremen, Germany) for measuring "on-line" $\delta^{13}C$ of the sample air. Air for mass spectrometric analysis was pumped continuously via a steel capillary from the gas sampling system to a 0.25 mL sample loop which was attached to an eight-port Valco valve of the GasBench II. Sample air in the loop was introduced into the IRMS via an open split after the passage of a dryer (Nafion) and a GC column (25 m × 0.32 mm Poraplot Q; Chrompack, Middleburg, the Netherlands). After every second sample, a VPDB-gauged CO_2 reference gas was injected into the IRMS via the open split. The precision (SD) of repeated measurements was <0.2‰. The entire measurement cycle of four growth chambers was completed within 30 minutes, including measurement of CO_2 and H_2O concentration and $\delta^{13}C$ of the sample air on the inlet and outlet of each growth chamber.

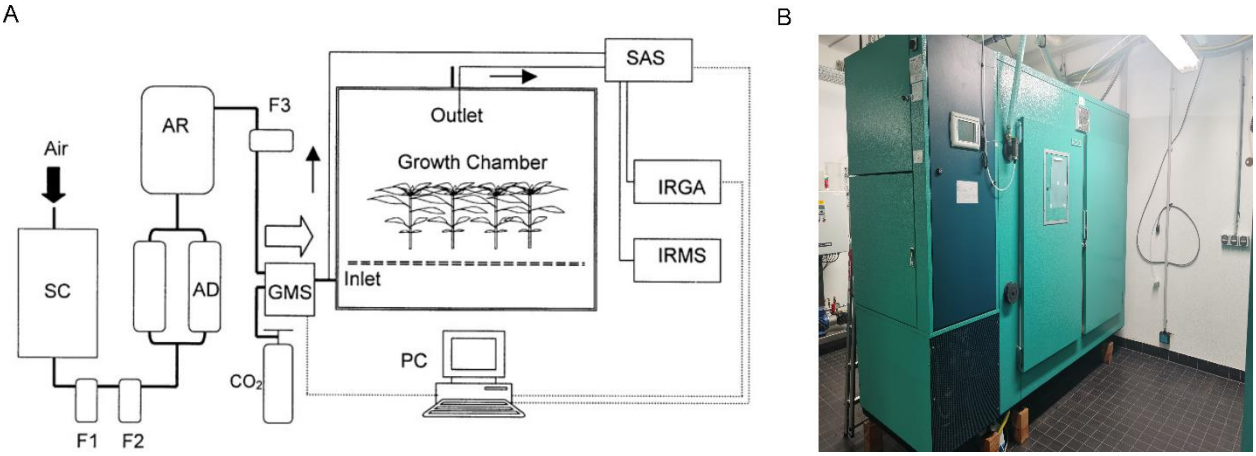

Fig. 2.4 Schematic representation of $^{13}CO_2/^{12}CO_2$ gas exchange and labelling system (A; from Schnyder et al., 2003) and growth chamber picture (B). SC, screw compressor (S40; Boge, Bielefeld, Germany); AD, adsorption dryer (KEN 3100; Zander, Essen, Germany; and molecular sieve: activated aluminium oxide F200; Alcoa, Houston, TX, USA); AR, air receiver (1 m^3) (Magnet Kft, Magocs, Hungary); F1, oil and water condensate drain (CSP005; Hiross, Mönchengladbach, Germany), F2 oil, water and particle filter (≥0.01 µm; G12XD and filter element: 2030X, Zander), F3, universal filter (≥1 µm; G12ZHD and filter element: 2030Z, Zander); GMS, gas mixing system consisting of CO_2 flow controller (Red-y, Vögtlin, Muttenz, Switzerland) and air flow controller (EL-FLOW, Bronkhorst, Veenendaal, Netherlands); CO_2, tank containing CO_2 of mineral or fossil–organic origin (Linde AG, Unterschleißheim, Germany or CARBO Kohlensäurewerke, Bad Hönningen, Germany); Growth chamber (PGR15, Conviron, Winnipeg, Canada); SAS, sample air selector (Type 6012, Bürkert, Ingelfingen, Germany); IRGA, CO_2 and H_2O infrared gas analyser (Li-840, LI-COR Inc., Lincoln, NE, USA); IRMS, $^{13}CO_2/^{12}CO_2$ isotope ratio mass spectrometer (IRMS, Delta plus, Advantage equipped with GasBench II, ThermoFinnigan, Bremen, Germany); PC, central control and data acquisition systems (DMP). For more details on the design and its operation, see Schnyder et al. (2003).

2.4 ^{13}C-labelling and sampling

On day 66, in each experiment, ^{13}C-labelling of the total photosynthetic carbon flux of all canopies was initiated by switching the CO_2 sources: a growth chamber that had received the ^{13}C-rich CO_2 henceforth received ^{13}C-depleted CO_2 and *vice versa* (see Fig. 1.1, chapter 1). The switch occurred during the night of day 65, at approximately three hours before the onset of the light period of the next day. This procedure ensured that virtually all of the isotopically "old" (i.e. "pre-switch") CO_2 had been entirely replaced by the "new" CO_2 at the beginning of the 1st labelling light period. The labelling period lasted for a total duration of 8 days.

Plants were collected at the beginning of the dark period (Fig. 2.3 C), just before the switch of the CO_2 source that initiated the $^{13}CO_2/^{12}CO_2$ labelling, and then at the beginning of the dark periods following the 1st, 2nd, 3rd, 4th and 7th photoperiod after the CO_2 switch. Two replicate samples from each growth chamber were collected at each harvest, with one replicate consisting of three randomly selected plants. Plants were removed from the pots, their roots washed to free them of sand, and dissected into their shoot and root parts. The plant parts were weighed to determine their fresh weight, then frozen in liquid nitrogen and stored at -18 °C before freeze-drying for 72 h. Dry weights were subsequently determined. After that, plant material was ground to a fine powder in a ball mill and stored again at -18 °C until further use.

2.5 Elemental and carbon isotopes analysis

The carbon (C) and nitrogen (N) contents and $\delta^{13}C$ of biomass samples were determined for all shoot and root replicates as in Lattanzi et al. (2005). The stored samples were thawed, re-dried at 40 °C for 24 h and stored in desiccator vessels. Aliquots of 0.70 ± 0.05 mg of the shoot and root materials were weighed and packed into tin cups (3.3 x 5 mm, IVA Analysentechnik, Meerbusch, Germany). They were then combusted in an elemental analyzer (NA 1110, Carlo Erba Instruments, Milan, Italy) and interfaced (Conflo III, Finnigan MAT, Bremen, Germany) to a continuous-flow isotope-ratio mass spectrometer (CF-IRMS, Delta Plus, Finnigan MAT, Bremen, Germany), which measured concentrations of carbon and nitrogen, and $\delta^{13}C$ of the sample. A solid internal laboratory standard (SILS, fine ground wheat flour) was measured as a reference after every tenth sample to correct for possible instrument drift. All samples and SILS were measured against a laboratory working standard CO_2 gas, which was previously calibrated against a secondary isotope standard (IAEA-CH6; calibration accuracy ± 0.06‰ SD). The precision given as the SD of repeated measurements of the SILS was better than 0.2‰.

The C and N masses of plants and plant parts were obtained as the product of elemental contents (g per g dry mass) of plants and plant parts times their corresponding dry mass. C content of shoot tissue was closely similar for all tissues (44.7% ± 0.54% SD), meaning that sample dry mass was virtually proportional to C mass. For that reason and to avoid redundancy I do not present dry mass data in this work. Fresh and dry masses of root samples were somewhat contaminated by sand, as reflected in low (but variable) root C contents (average: 40.8%; range 30.1% to 45.5%). This artefact was eliminated by calculating root C mass which corrected the error of the erroneously high dry mass by the correspondingly lower C content, as determined by elemental analysis.

2.6 Water-soluble carbohydrate extraction, separation, quantification, and ^{13}C analysis

Water-soluble carbohydrate (WSC) fractions (fructan, sucrose, glucose, and fructose) were extracted from shoot and root samples and separated using the procedures described by Gebbing & Schnyder (2001). Briefly, aliquots of 200 mg of milled sample material were weighed into 2-mL capped Eppendorf tubes and topped off with 1.8 mL of deionized water. Samples were briefly vortexed (Vortex-Genie 2, Scientific Industries, New York, USA), held in a water bath at 93 °C for 10 min, shaken for 45 min (Shaker, Heidolph Instruments, Schwabach, Germany) at room temperature, and centrifuged at 9500 *g* for 15 min (Universal 320, Merck, Tuttlingen, Germany). The supernatant, which contained the dissolved WSC, was passed through nylon-membrane filters with a pore size of 0.45 µm and then stored in clean 2-mL capped Eppendorf tubes at -18 °C.

WSC fractions (fructan, sucrose, glucose and fructose) were separated, quantified and collected using a high-performance liquid chromatography (HPLC) system similar to Gebbing & Schnyder (2001). Briefly, 0.2 mL aliquots of the filtered supernatant were passed through a guard column (Shodex KS-LG, Showa Denko, Tokyo, Japan) and a preparative column (Shodex KS, Showa Denko, Tokyo, Japan) held at 50 °C, with HPLC-grade water (Carl Roth, Karlsruhe, Germany) as the eluent, at a flow rate of 0.75 mL min^{-1} and a system pressure of approximately 21 bar. The WSC was detected by refractive index measurement (Shodex RI-101, Showa Denko, Tokyo, Japan) and concentrations quantified by comparing sample peak area against reference calibration curves of pure and mixed standards of analytical grade inulin, sucrose, glucose and fructose (all from Merck, Darmstadt, Germany). Knowing when the individual carbohydrates eluted from the preparative column (Fig. 2.4), I collected fractions of fructan, sucrose, glucose, and fructose individually in test tubes. Aliquots of approximately 0.7 mg of the different carbohydrates were then transferred to tin cups (Capsules, Lüdi Swiss AG, Flawil, Switzerland), dried at 60 °C for 24 h, and then analysed for their $\delta^{13}C$ using a continuous-flow isotope ratio mass spectrometer (CF-IRMS) as described above.

The accuracy of HPLC system separation for specific water-soluble carbohydrate was tested as by González et al. (1999): individual stand materials of fructan, sucrose, glucose, and fructose (inulin from chicory, sucrose, D-glucose and D-fructose) were prepared and measured for their $\delta^{13}C$ (Pure group). I prepared a 10 ml mixed standard solution containing inulin (413.96 mg), sucrose (25.02 mg), glucose (20.41 mg) and fructose (20.71 mg), which were similar to the concentration of WSCs in the plant, and injected 0.2 mL aliquots of mixed solution into the

HPLC system, recollected the individual carbohydrates after separation, and measured their $\delta^{13}C$ as described above (Mixture group).

I used the iodine-potassium iodide solution test to detect starch in plants. Shoot and root powders were taken from plant material of the 800 µmol mol^{-1} [CO_2] treatment. I placed a 0.70 mg sample on a glass slide, added two drops of iodine-potassium iodide solution, and watched the colour change with a microscope (475110, Carl Zeiss, Wetzlar, Germany) after 1 minute.

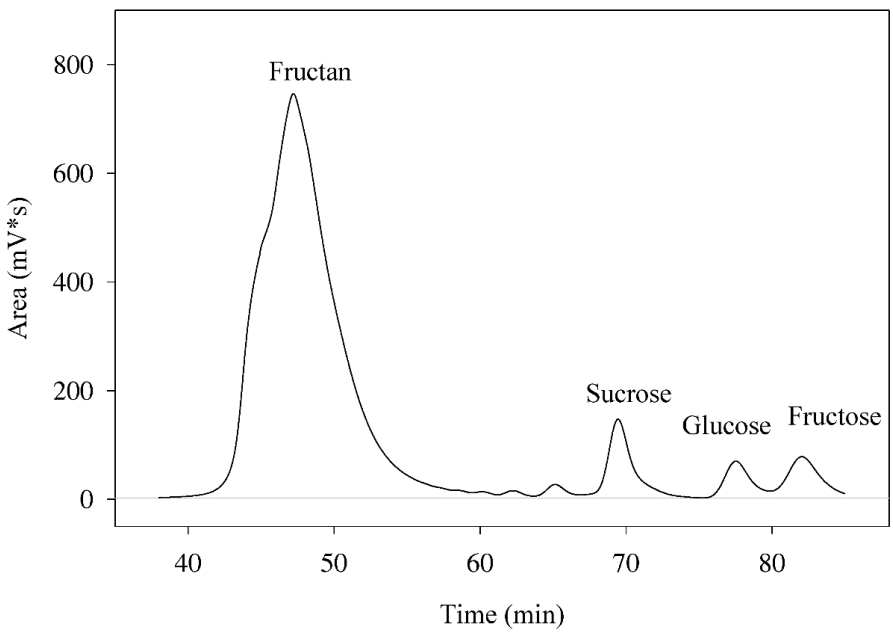

Fig. 2.5 Typical HLPC chromatogram of carbohydrates in the shoot of *L. perenne.* The fractions corresponding to the fructan, sucrose, glucose and fructose peak were separated and detected separately. The thin grey line represents the baseline. The total elution time was about 90 minutes following sample injection. The sample was taken from a plant grown in 800 µmol mol^{-1} [CO_2].

2.7 Compartmental modelling

Four-pool model for carbohydrates (see chapter 3.2)

I used the same four-pool compartmental model (Fig. 1.2) as Lattanzi et al. (2012) based on the same set of differential equations and implemented this in ModelMaker to analyse the time course of $f_{\text{unlabelled}}$ in the different carbohydrate pools at the whole-shoot scale. Accordingly, for any carbohydrate pool Q_i (with Q_1, Q_2, Q_3 and Q_4 representing the size of the sucrose, fructan, glucose and fructose pools, individually), it is assumed that $dQ_i/dt = 0$. This implies

that the sum of all fluxes of substrate carbon into and out of Q_i have the same magnitude, i.e. the system was in steady-state with respect to pool sizes and fluxes at the day-by-day time-scale. The assumptions also imply that a given flux out of a donor pool *i* to a receiving pool *j* (F_{ij}) is the product of a rate constant (k_{ij}) and the size of the donor pool (Q_i) ($F_{ij} = k_{ij}\ Q_i$). *j*=0 denotes a flux leaving the four-pool system and reflects sucrose consumption in all growth and maintenance processes in the entire shoot. The half-life of a pool ($T_{1/2\ Qi}$) is $T_{1/2\ Qi} = \ln(2) / k_{In}$, with k_{In} the sum of the rate constants for all fluxes leaving pool Q_i.

The change in the amount of unlabelled carbon in pool *i* with time *t* was given by the sum of all fluxes of unlabelled carbon into that pool minus the sum of all fluxes of unlabelled carbon leaving the pool. Accordingly, for the four pools in the system (Lattanzi et al., 2012):

$$df_{\text{unlabelled Q1}}(\text{t}) / dt\ (t) \cdot Q_1 = f_{\text{unlabelled In}}\ (t) \cdot F_{\text{In}} + f_{\text{unlabelled Q3}}\ (t) \cdot k_{31} \cdot Q_3 + f_{\text{unlabelled Q4}}\ (t) \cdot k_{41} \cdot Q_4 - f_{\text{unlabelled Q1}}\ (t) \cdot (k_{10} + k_{12} + k_{13} + k_{14}) \cdot Q_1$$

Eqn 2.1

$$df_{\text{unlabelled Q2}}(\text{t}) / dt\ (t) \cdot Q_2 = f_{\text{unlabelled Q1}}\ (t) \cdot k_{12} \cdot Q_1 - f_{\text{unlabelled Q2}}\ (t) \cdot k_{24} \cdot Q_2$$

Eqn 2.2

$$df_{\text{unlabelled Q3}}(\text{t}) / dt\ (t) \cdot Q_3 = f_{\text{unlabelled Q1}}\ (t) \cdot k_{13} \cdot Q_1 - f_{\text{unlabelled Q3}}\ (t) \cdot k_{31} \cdot Q_3$$

Eqn 2.3

$$df_{\text{unlabelled Q4}}(\text{t}) / dt\ (t) \cdot Q_4 = f_{\text{unlabelled Q1}}\ (t) \cdot k_{14} \cdot Q_1 + f_{\text{unlabelled Q2}}\ (t) \cdot k_{24} \cdot Q_2 - f_{\text{unlabelled Q4}}\ (t) \cdot k_{41} \cdot Q_4$$

Eqn 2.4

where $f_{\text{unlabelled } Qi}\ (t)$ denotes the fraction of unlabelled C in pool *i* at time *t*, F_{In} the flux into the system (which is equal to the rate of photosynthetic sucrose synthesis in the plant), and $f_{\text{unlabelled In}}\ (t)$ the fraction of unlabelled C in F_{In} with $f_{\text{unlabelled In}}\ (t) = 1$ before the switch of $\delta^{13}C_{CO2}$ (i.e. at $t < 0$) and $f_{\text{unlabelled In}}\ (t) = 0$ after the switch ($t \geq 0$).

Based on Eqns 2.1 - 2.4, the rate constants were optimized in such a way that $f_{\text{unlabelled } Qi}\ (t)$ fitted best the observed $f_{\text{unlabelled } Qi}\ (t)$ for the tracer kinetics of sucrose (Q_1), fructan (Q_2), glucose (Q_3), and fructose (Q_4) pools. In this, I constrained the model with the pool size ratios Q_i / Q_j as observed in the experiments. The mean residence time (τ) of carbon in the system was calculated as $\tau = (Q_1 + Q_2 + Q_3 + Q_4) / F_{01}$, with F_{01} the influx of carbon into the sucrose pool, the entry point of the system.

Two-pool model of the respiratory substrate supply system (see chapter 3.3)

The rate of respiration in darkness (R_n, µmol m^{-2} s^{-1}) was obtained as per (Schnyder et al., 2003):

$$R_n = (F_{inlet} - F_{outlet}) / A \qquad \text{Eqn 2.5}$$

F_{inlet} and F_{outlet} are the fluxes of CO_2 (µmol s^{-1}) entering and leaving the chamber, and A is the chamber ground area (m^2).

The $\delta^{13}C$ of the sample air in the light and dark period were obtained as:

$$\delta^{13}C_{sample} = (\delta^{13}C_{inlet} \cdot F_{inlet} - \delta^{13}C_{outlet} \cdot F_{outlet}) / (F_{inlet} - F_{outlet}) \qquad \text{Eqn 2.6}$$

with $\delta^{13}C_{inlet}$ and $\delta^{13}C_{outlet}$ denoting the $\delta^{13}C$ of CO_2 entering and leaving the growth chamber, respectively.

I used the same two-pool compartmental model (Fig. 1.4) as Lehmeier et al. (2010a) based on the set of differential equations and implemented this in ModelMaker to analyse the time course of $f_{unlabelled}$ in the respiratory CO_2 of plant stands. $f_{unlabelled}$ of the respiratory CO_2 was calculated using Eqn 1.1 (chapter 1).

For the two pools in the system:

$$df_{unlabelled\ Q1}(t) / dt\ (t) \cdot Q_1 = f_{unlabelled\ In}\ (t) \cdot F_{01} + f_{unlabelled\ Q2}\ (t) \cdot k_{21} \cdot Q_2 - f_{unlabelled\ Q1}\ (t) \cdot (k_{10} + k_{12}) \cdot Q_1 \qquad \text{Eqn 2.7}$$

$$df_{unlabelled\ Q2}(t) / dt\ (t) \cdot Q_2 = f_{unlabelled\ Q1}\ (t) \cdot k_{12} \cdot Q_1 - f_{unlabelled\ Q2}\ (t) \cdot k_{21} \cdot Q_2 \qquad \text{Eqn 2.8}$$

where $f_{unlabelled\ Qi}(t)$ denotes the fraction of unlabelled C in pool i at time t, F_{01} the flux into the system (which is equal to export flux; the respiratory rate) and $f_{unlablled\ In}(t)$ the fraction of unlabelled C in F_{01} with $f_{unlabelled\ In}(t) = 1$ before the switch of $\delta^{13}C_{CO2}$ (i.e. at $t < 0$), and $f_{unlabelled\ In}(t) = 0$ after the switch ($t \geq 0$).

The pool sizes were given as by Lehmeier et al. (2010a):

$$Q_1 = F_{01} / k_{10} \qquad \text{Eqn 2.9}$$

$$Q_2 = F_{01} / k_{10} \cdot k_{12} / k_{21} \qquad \text{Eqn 2.10}$$

Based on optimized fluxes and pool sizes, the half-life $t_{1/2}$ (Q_i) was obtained by

$t_{1/2}$ (Q_i) = ln(2)/k_i Eqn 2.11

where k_i is the sum of all rate constants leaving the pool Q_i.

The contribution of pool Q_i to respiratory carbon released is defined as the probability that tracer leaves the system without cycling through Q_2 (i.e. current assimilate that was not stored), while the fractional contribution of stores to respiration is the probability that the tracer cycles through Q_2 at least once before it is respired (i.e. that the tracer underwent storage). These fractional contributions are given by:

Contribution of current assimilates = $k_{10}/(k_{10}+k_{12})$ Eqn 2.12

Contribution of temporary stores = $k_{12}/(k_{10}+k_{12})$ Eqn 2.13

The mean residence time of carbon in the respiratory supply system (τ) was calculated as:

τ (h) = Q_{total}/r_{plant} Eqn 2.14

where Q_{total} is the total size of all respiratory substrate pools and r_{plant} is the respiration rate of the whole plant.

2.8 Statistical analysis

For the dataset from gas exchange measurements, the measurements in the first 45 minutes of one light and dark period and following the opening of the chamber were removed. In addition, measurements more than 1.5 × IQR (Interquartile Range) away from the mean were removed as outliers. All statistical analyses were conducted in R version 3.6.1 (R Core Team, 2019) and Rstudio version 1.1.383 (Rstudio Team, 2016). The R-packages ggplot2 (Wickhan, 2016) and Agricolae (Mendiburu, 2017) were used for data plotting and ANOVA analysis, respectively. Type III Wald test was used to determine the significance of the CO_2 effects, and the post hoc Tukey's HSD test was performed for pairwise comparison among treatments. T-tests were used to test the $\delta^{13}C$ differences of reference carbohydrates between pure and mixture samples The number of replicates varied between measured parameters and treatments and is indicated in the Figure legends and Table captions.

3. Results and Discussion

3.1 Accuracy and precision of the near-natural abundance $^{13}CO_2/^{12}CO_2$ labelling system

Constancy and consistency of the concentration and isotopic composition of CO_2 inside the plant growth chambers

One key methodical criterion of quantitative labelling experiments at different [CO_2] is the accuracy and precision of maintaining [CO_2] near target levels and the constancy of the $\delta^{13}C_{CO2}$ inside the growth chambers during the different phases of the labelling experiment. This includes the pre-labelling phase studied here that determines the so-called end-members of the isotopic mixing model (objective 1, chapter 1). The [CO_2] and $\delta^{13}C_{CO2}$ inside the growth chamber are closely reflected by [CO_2] and $\delta^{13}C_{CO2}$ at the chamber outlet ($[CO_2]_{outlet}$; $\delta^{13}C_{CO2\ outlet}$) in these highly ventilated chambers (Schnyder et al., 2003). Besides the technical capabilities and limitations (for specifications, see chapter 2), there are two biological (and hence inescapable) drivers that oppose the constancy of $[CO_2]_{outlet}$ and $\delta^{13}C_{CO2\ outlet}$ in plant growth chambers: the photosynthetic drawdown of [CO_2] which intensifies over time due to the expansion of the plant canopy and resulting canopy photosynthetic activity, and photosynthetic ^{13}C discrimination ($\Delta^{13}C$) which causes a ^{13}C-enrichment of the chamber CO_2 that is mainly proportional to the photosynthetic CO_2 flux. In principle, the effect of these drivers on the constancy of [CO_2] close to the target value and maintenance of a stable $\delta^{13}C_{CO2}$ in the chambers can be counterbalanced by adjustments of [CO_2] at the chamber inlet ($[CO_2]_{inlet}$) and/or increases in the rates of air injection into the chambers. Here, I balanced these variables in such a way that the [CO_2] and $\delta^{13}C_{CO2}$ differences between the chamber inlet and outlet also permitted quasi-continuous measurements of the CO_2 exchange rate (net photosynthesis in the light period and respiration in the dark) and photosynthetic ^{13}C discrimination ($\Delta^{13}C$). Accordingly, as soon as the drawdown of [CO_2] between the chamber inlet and outlet started to exceed 10% of the inlet value, decreasing the ξ-value in Eqn 1.3 to <10 (Evans et al., 1986), I adjusted airflow rates in such a way that the drawdown of CO_2 would be kept near-constant while [CO_2] at the chamber outlet remained close to the target value, so that the resulting ξ-values were 5.12 (±0.09 SD), 5.87 (±0.24 SD) and 7.66 (±0.22 SD) for 200, 400 and 800 $\mu mol\ mol^{-1}$ [CO_2] respectively, after approximately Day 30. The result of these adjustments is shown in Fig. 3.1.1, which presents the deviation of the daytime mean $[CO_2]_{outlet}$ from the target

values (200, 400 or 800 μmol mol^{-1} depending on treatment) during the pre-labelling period between day 20 and day 65 of the different experimental runs. These data revealed that $[CO_2]_{outlet}$ actually averaged somewhat higher than the target value in all $[CO_2]$ treatments: +4.0 (±4.3 SD), +7.2 (±6.2 SD) and +13.9 (±8.3 SD) μmol mol^{-1} for target $[CO_2]$ of 200, 400 and 800 μmol mol^{-1}, respectively. These deviations of $[CO_2]_{outlet}$ from target values were virtually identical (P<0.05) in the presence of the ^{13}C-organic and -mineral CO_2 sources, and corresponded to mean %-deviations from target $[CO_2]$ of <2% in all treatments. Meanwhile, the enhancement of $\delta^{13}C_{CO2\ outlet}$ relative to the inlet increased by several ‰ during the first 30 to 35 days of an experimental run, when ξ first attained a value of ≤10, and thereafter was kept relatively stable (<0.31‰ SD) until day 65, the end of the pre-labelling period (Fig. 3.1.2). That temporal pattern was very similar in the chambers receiving ^{13}C-organic and -mineral CO_2.

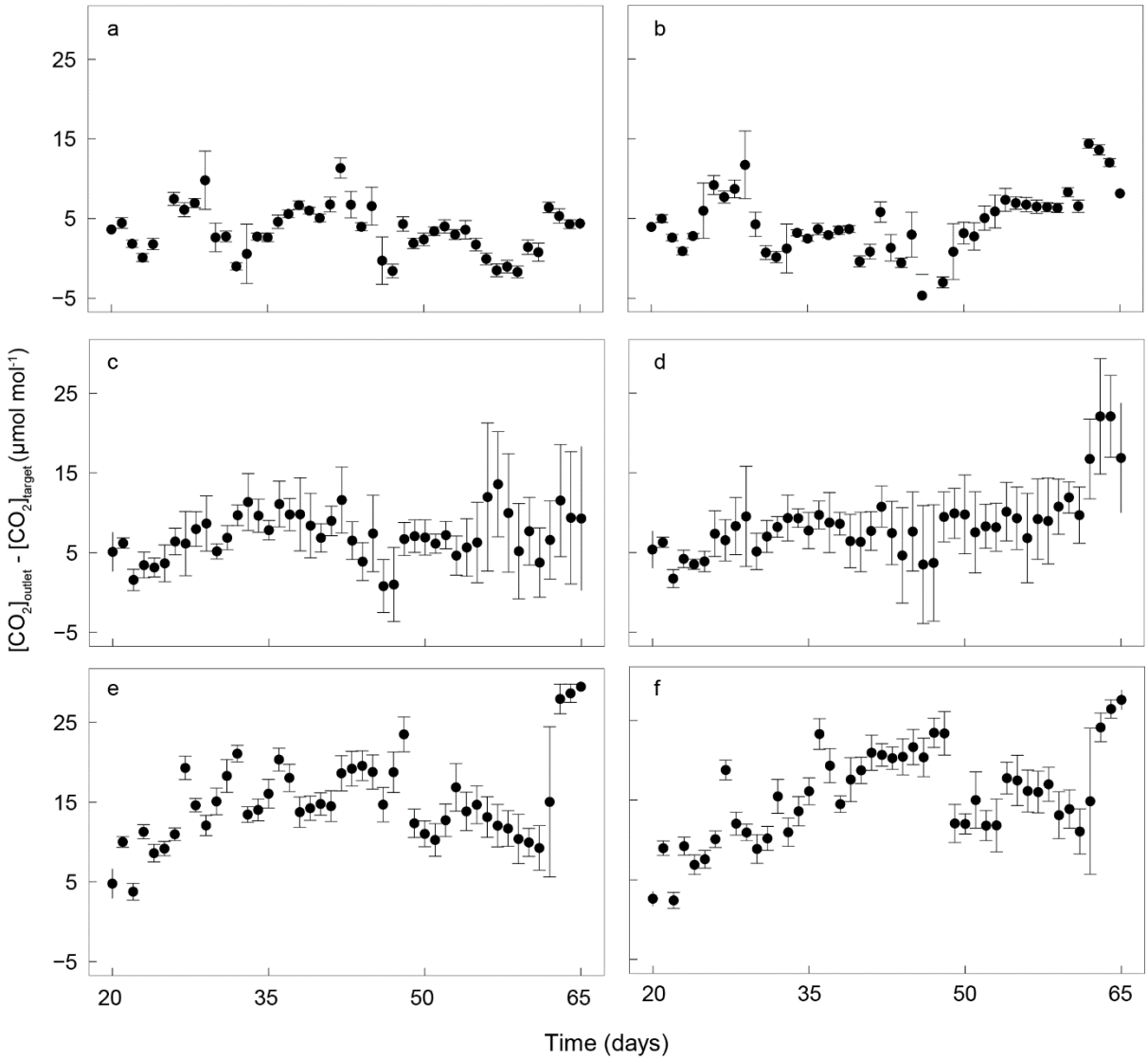

Fig. 3.1.1 CO_2 concentration difference between chamber outlet ($[CO_2]_{outlet}$) and target $[CO_2]$ ($[CO_2]_{target}$) with time ($[CO_2]_{outlet}$ - $[CO_2]_{target}$). Target $[CO_2]$: (a, b) 200, (c, d) 400 and (e, f) 800 µmol mol^{-1}. Growth chambers were supplied with either ^{13}C-organic ($\delta^{13}C_{CO2}$ -43.5‰; left) or ^{13}C-mineral CO_2 ($\delta^{13}C_{CO2}$ -5.6‰; right). The criterion of data evaluation was that measurements in the first 45 min of a light period or following the opening of the chamber were removed, and values over 1.5 × IQR (Interquartile Range) away from the mean were removed as outliers. Data points and error bars represent daily means ± SD (*n* = 9-23). Note that the dataset included the 14-d long period (day 49 to day 63) in which intensive sampling and leaf elongation measurements were performed.

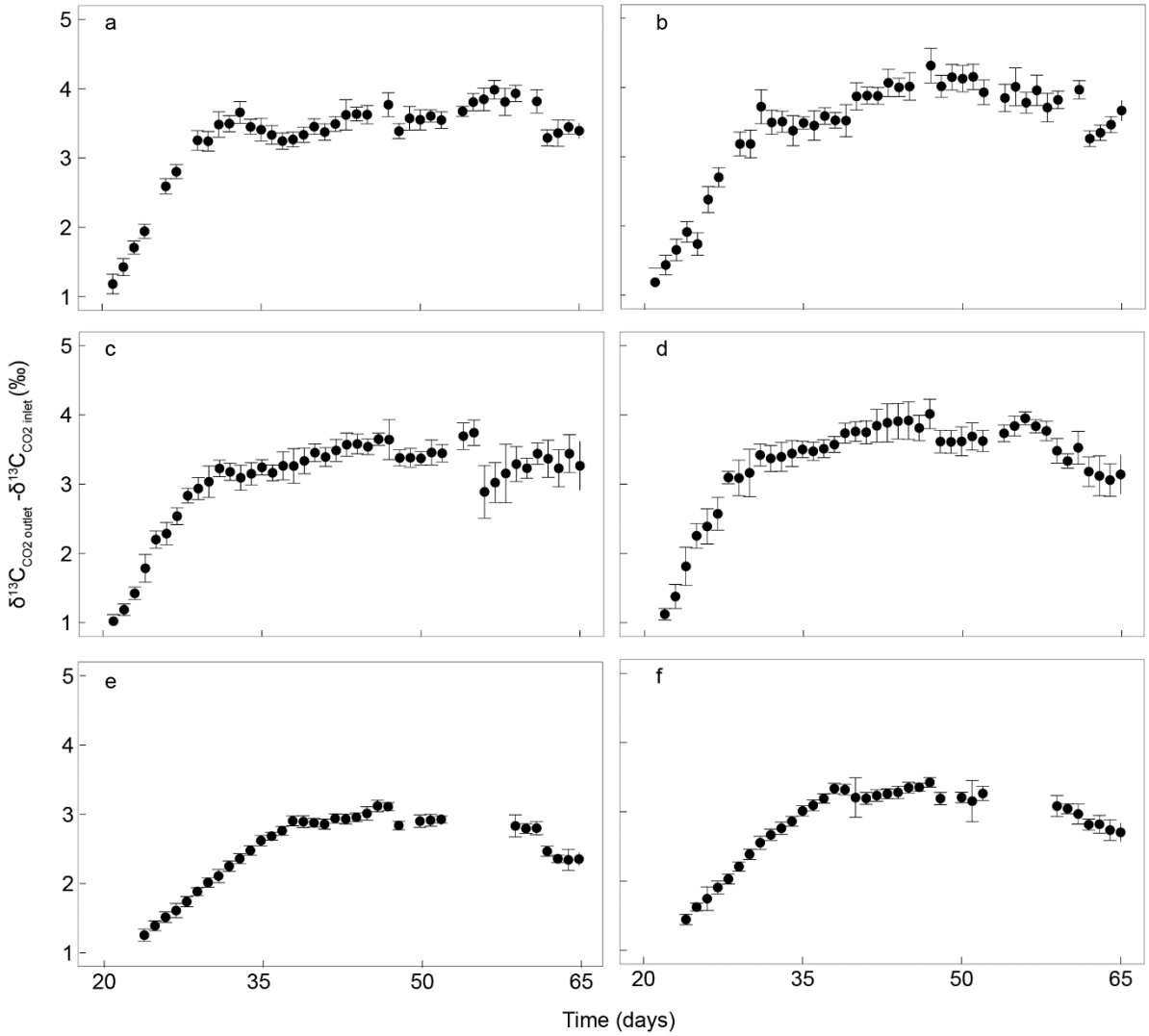

Fig. 3.1.2 The $\delta^{13}C$-difference between $\delta^{13}C_{CO2\ outlet}$ and $\delta^{13}C_{CO2\ inlet}$ with time ($\delta^{13}C_{CO2\ outlet}$ - $\delta^{13}C_{CO2\ inlet}$). CO_2 concentration at chamber outlet ($[CO_2]_{outlet}$) was maintained near target $[CO_2]$: 200 (a, b), 400 (c, d) and 800 (e, f) μmol mol^{-1}. Growth chambers were supplied with either ^{13}C-organic ($\delta^{13}C_{CO2}$ -43.5‰; left) or ^{13}C-mineral CO_2 ($\delta^{13}C_{CO2}$ -5.6‰; right). The criterion of data evaluation was that measurements in the first 45 min of a light period or following the opening of the chamber were removed, and values over 1.5 × IQR (Interquartile Range) away from the mean were removed as outliers. Data points and error bars represent daily means ± SD (*n* = 9-23). Note that the dataset included the 14-d long periods (day 49 to day 63) in which intensive sampling and leaf elongation measurements were performed.

Isotopic distance (spread) between chambers receiving ^{13}C-depleted and -enriched CO_2 as observed for components of CO_2 exchange, biomass and water-soluble carbohydrates

The isotopic distance ($d\delta^{13}C$, termed 'spread') between two parallel chambers run with the same target $[CO_2]$ but receiving CO_2 with a different $\delta^{13}C_{CO2}$ (i.e. either ^{13}C-organic or -mineral CO_2)

was highly similar for measurements at the inlet ($d\delta^{13}C_{CO2\ inlet}$, Table 3.1.1). The same was true for measurements at the outlet ($d\delta^{13}C_{CO2\ outlet}$, Table 3.1.1). Meanwhile, the spread for the $\delta^{13}C$ of net CO_2 exchange rates in daylight (net photosynthesis, $d\delta^{13}C_{Nd}$) and at night (dark respiration, $d\delta^{13}C_{Rn}$) appeared to be slightly smaller than that of CO_2 at the chamber inlet ($d\delta^{13}C_{inlet}$). Thus, $d\delta^{13}C_{Nd}$ was 97 - 99% and $d\delta^{13}C_{Rn}$ 93 - 97% of $d\delta^{13}C_{inlet}$, pointing to a small, and not always significant, contamination (e.g. leak) effect on the $\delta^{13}C$ of gas exchange components, particularly of dark respiration.

Minor CO_2 contamination effects on the $\delta^{13}C$ were also evident for the shoot and root biomass based on their $d\delta^{13}C_{shoot}$ and $d\delta^{13}C_{root}$, although the effects were not always significant. $d\delta^{13}C_{shoot}$ and $d\delta^{13}C_{root}$ averaged 96% of $d\delta^{13}C_{inlet}$, with no apparent significant difference between [CO_2] levels or plant parts. The $d\delta^{13}C$ for water-soluble carbohydrate components ($d\delta^{13}C_{fructan}$, $d\delta^{13}C_{sucrose}$, $d\delta^{13}C_{glucose}$, and $d\delta^{13}C_{fructose}$) was virtually the same as that of $d\delta^{13}C_{shoot}$, indicating that protocols for extraction and separation of the carbohydrates did not introduce any additional contamination that would have further adulterated the original ^{13}C signal of the carbohydrates.

The consistently slightly smaller $d\delta^{13}C$ of biomass and water-soluble carbohydrate components relative to $d\delta^{13}C_{Nd}$ must be related to the fact that determination of $d\delta^{13}C_{Nd}$ only considered periods of near isotopic steady-state, that eliminated measurements made during the first 45 min after 'lights-on' during daytime and periods during which chambers had to be opened for operations within the chamber (such as for sampling or making leaf elongation rate measurements). The fact that $d\delta^{13}C$ of biomass and water-soluble carbohydrate components averaged ~96% of $d\delta^{13}C_{inlet}$, means that the integrated effect of all artefacts, including disturbances of the chamber atmosphere during daylight opening times of chambers, accounted for an average error (bias) of ~4% in all [CO_2] treatments. In other words, on average, 4% of the total C in plant biomass was not derived from the ^{13}C-organic or -mineral CO_2 sources supplied to the chambers.

Cross-contamination of different carbohydrates due to imperfect separation on the preparative HPLC column (see chapter 2, Fig. 2.2) appeared to be a minor factor in determinations of the $\delta^{13}C$ of sugars. This assessment was supported by comparing $\delta^{13}C_{glucose}$ with $\delta^{13}C_{sucrose}$ or $\delta^{13}C_{fructose}$ in pure reference material and after HPLC passage of a reference mixture of fructan, sucrose, glucose and fructose (Table 3.1.3). This is illustrated by the deviation between pure and mixture-derived $\delta^{13}C_{glucose}$ (0.39‰), which was 2.6% of the $\delta^{13}C$-distance between glucose and sucrose or fructose. Given the comparatively short separation

(elution) times differences between glucose and sucrose or fructose compared to fructan, and the low concentration of glucose in the reference mixture, the observed 2.6% cross-contamination likely represents near-maximum contamination.

Table 3.1.1 Isotopic difference (termed 'spread') between paired plant growth chambers receiving ^{13}C-organic and -mineral CO_2 for different gas exchange, biomass and water-soluble carbohydrate components. Spread ($d\delta^{13}C_X$) was calculated as $d\delta^{13}C_X = \delta^{13}C_{X\ 13C\text{-mineral}} - \delta^{13}C_{X\ 13C\text{-organic}}$), with *X* designating the parameter of interest, e.g. bulk biomass or sucrose. Spread was calculated for $\delta^{13}C_{CO2}$ at the inlet ($d\delta^{13}C_{CO2\ inlet}$) and outlet ($d\delta^{13}C_{CO2\ outlet}$) of paired growth chambers in the light and dark period of days 61 to 64, daytime canopy CO_2 exchange ($d\delta^{13}C_{Nd}$) and respiration in the dark ($d\delta^{13}C_{Rn}$) for days 61 to 64, bulk shoot ($d\delta^{13}C_{shoot}$) and root C ($d\delta^{13}C_{root}$), and fructan ($d\delta^{13}C_{fructan}$), sucrose ($d\delta^{13}C_{sucrose}$), glucose ($d\delta^{13}C_{glucose}$) and fructose ($d\delta^{13}C_{fructose}$) extracted and purified from shoot biomass sampled at the beginning of the light period on day 65. Growth chambers were maintained at near target [CO_2] of 200, 400 or 800 μmol mol^{-1} using one of two CO_2 sources, a ^{13}C-organic ($\delta^{13}C$ -43.5‰) or a ^{13}C-mineral source ($\delta^{13}C$ -5.6‰). $\delta^{13}C_{Nd}$ and $\delta^{13}C_{Rn}$ were determined during periods of steady-state gas exchange of chambers, measurements in the first 45 min of a light period or following the opening of the chamber were removed, and values over 1.5 × IQR (Interquartile Range) away from the mean were removed as outliers. Except for [CO_2] and $\delta^{13}C_{CO2}$, all conditions were kept the same in all chambers (see Materials and Methods). Daily means (± SD) for *n* = 2 to 10.

Spread	CO_2 concentration (μmol mol^{-1})		
	200	400	800
	---------- (‰) ----------		
$d\delta^{13}C_{inlet}$	37.7 (0.1)	37.6 (0.1)	37.4 (0.0)
$d\delta^{13}C_{outlet\ day}$	37.7 (0.2)	37.5 (0.2)	37.8 (0.1)
$d\delta^{13}C_{outlet\ night}$	37.3 (0.1)	37.0 (0.2)	36.9 (0.1)
$d\delta^{13}C_{Nd}$	37.2 (0.1)	36.9 (0.3)	36.2 (0.4)
$d\delta^{13}C_{Rn}$	35.0 (1.2)	35.5 (1.0)	36.4 (0.3)
$d\delta^{13}C_{shoot}$	35.9 (0.1)	35.7 (0.8)	36.2 (1.0)
$d\delta^{13}C_{root}$	35.8 (0.2)	35.5 (0.5)	36.5 (0.5)
$d\delta^{13}C_{fructan}$	35.9 (0.3)	36.4 (0.6)	35.4 (1.1)
$d\delta^{13}C_{sucrose}$	36.1 (1.6)	36.2 (1.0)	36.0 (1.9)
$d\delta^{13}C_{glucose}$	36.2 (1.6)	35.4 (0.9)	36.0 (1.9)
$d\delta^{13}C_{fructose}$	36.0 (1.2)	35.5 (0.5)	36.5 (2.8)

Table 3.1.2 $\delta^{13}C$ of reference carbohydrates measured pure or after HPLC separation of an 80:5:5:4 (wt:wt:wt:wt) mixture of analytical grade inulin-fructan, sucrose, glucose and fructose (all from Merck, Darmstadt, Germany). The concentration of the individual carbohydrates in the mixture corresponded to typical concentrations in shoot extracts of plants grown at [CO_2] of 400 μmol mol^{-1}. Data shown are means ± SD (*n* = 2-3). "Pure" represents the pure individual component before being mixed. The $\delta^{13}C$ of individual carbohydrates was not significantly different between pure and mixture groups (*P* > 0.05).

	$\delta^{13}C_{fructan}$ (‰)	$\delta^{13}C_{sucrose}$ (‰)	$\delta^{13}C_{glucose}$ (‰)	$\delta^{13}C_{fructose}$ (‰)
Pure	-25.14 ± 0.03	-25.32 ± 0.04	-10.61± 0.14	-25.25 ± 0.09
Mixture	-25.20 ± 0.20	-24.94± 0.37	-11.00± 0.87	-25.02 ± 0.4

Post-photosynthetic C isotope discrimination

Although the (isotopic) spread was very similar for dark respired CO_2, shoot biomass-C, and water-soluble carbohydrate-C extracted and isolated from shoot biomass, I did detect some systematic differences between their $\delta^{13}C$ values. These differences are shown as deviations from the $\delta^{13}C$ of shoot bulk biomass ($\delta^{13}C_X - \delta^{13}C_{shoot}$) in Fig. 3.1.3 and were independent of the isotopic composition of the $\delta^{13}C$ of source CO_2 supplied to the plant growth chambers. Of these differences, the deviation between $\delta^{13}C_{sucrose}$ and $\delta^{13}C_{shoot}$ was the most consistent, as it was significant and manifest in all [CO_2] treatments. Overall, sucrose was ^{13}C-enriched by ~1‰ relative to shoot biomass and by ~1.5‰ relative to dark respired CO_2, glucose, fructose and structural biomass. Conversely, the relative ^{13}C-enrichment of fructan (i.e. $\delta^{13}C_{fructan} - \delta^{13}C_{shoot}$) was only about half that for sucrose. In part, this must have been due to the very high fructan concentration in biomass: fructan accounted for >80% of all water-soluble carbohydrates and up to 60% of total shoot biomass in all [CO_2] treatments (see chapter 3.2). Therefore, its $\delta^{13}C_{fructan}$ must have had a strong effect on $\delta^{13}C_{shoot}$, of which it formed the main component. This also largely explains why the $\delta^{13}C$ of water-soluble carbohydrate-free shoot biomass, a proxy of shoot structural biomass ($\delta^{13}C_{structure}$), was ^{13}C-depleted relative to $\delta^{13}C_{shoot}$.

$\delta^{13}C$-differences among biochemical or flux components have been previously discussed in terms of developmental (temporal), compartmental and true biochemical ^{13}C fractionation effects (Bowling et al., 2008; Cernusak et al., 2009; Ghashghaie & Badeck, 2014), but are still not fully understood. However, the relatively close match of the $\delta^{13}C$ of whole-plant respiration ($\delta^{13}C_{Rn}$) with $\delta^{13}C_{shoot}$ does agree with observations of Klumpp et al. (2005) and Schnyder & Lattanzi (2005), who found only a tiny ^{13}C discrimination in whole plant dark

respiration, although shoot respired CO_2 was systematically ^{13}C-enriched and root respiration ^{13}C-depleted in two herbaceous dicot species and in *L. perenne*. Also, the ^{13}C-enrichment of sucrose and fructan relative to shoot structural biomass agrees with observations of relative ^{13}C-enrichment of leaf non-structural carbohydrates (sugars and starch) in comparison with whole-leaf biomass (Bowling et al., 2008), although comparisons of the leaf- and whole shoot- ^{13}C may not be entirely straightforward, due to the presence of both ^{13}C-enriched autotrophic (leaf) and ^{13}C-depleted heterotrophic (i.e. non-photosynthetic) tissues (Cernusak et al., 2009) in whole shoot biomass samples. The stronger relative ^{13}C-enrichment of sucrose compared to all other biomass components would also agree with the observed ^{13}C-enrichment of leaf sugars, as sucrose concentration in leaf blades was much higher than in any other plant part in the present investigations (Dorn, 2019). In the same work, Dorn (2019) observed the highest fructose and glucose concentrations in the immature growing, fully-heterotrophic shoot tissues, a factor that could be related to their relative ^{13}C-depletion.

Finally, differences in residence time of C within a pool (e.g. of sucrose relative to shoot structural biomass) could also affect the relationship between their $\delta^{13}C$. Sucrose is turned over rapidly (in a few hours; chapter 3.2), while C in structural shoot biomass resides in that pool throughout the life span of the plant part (several months). If it is true that ^{13}C discrimination and post-photosynthetic fractionation remained unchanged throughout the experiment, some relatively ^{13}C-depleted C must have been incorporated into the structural pool during the early phase (e.g. prior to 30 d) of an experimental run when the $\delta^{13}C$ of photosynthate was more depleted in ^{13}C than in later phases (e.g. past 40 d) due to the increase of $\delta^{13}C_{CO2}$ in the chamber atmosphere (Fig. 3.1.2). By contrast, the $\delta^{13}C$ of sucrose obtained from samples collected on day 65 would be determined only by the more ^{13}C-enriched CO_2 in the chamber near that sampling time.

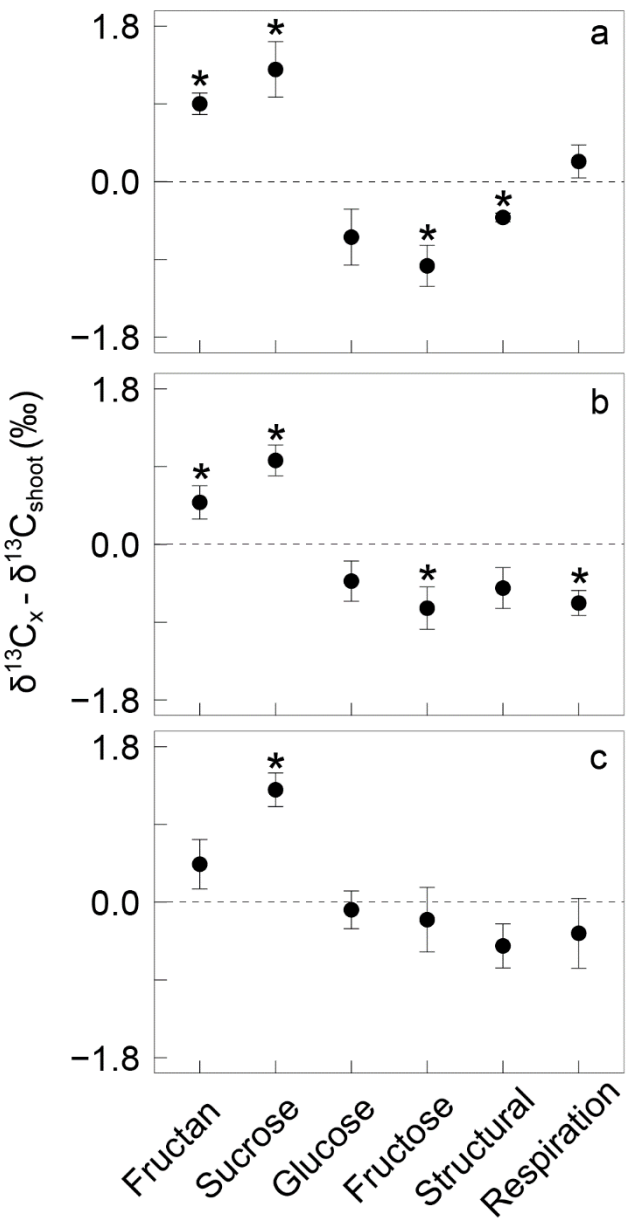

Fig. 3.1.3 The $\delta^{13}C$-difference between parameters *X* and shoot bulk biomass ($\delta^{13}C_X$ – $\delta^{13}C_{shoot}$), with *X* referring to the $\delta^{13}C$ of fructan, sucrose, glucose, fructose, structural biomass or dark respiratory CO_2. The $\delta^{13}C$ of shoot bulk biomass ($\delta^{13}C_{shoot}$), structural biomass, and the different carbohydrate fractions refer to samples collected on day 65 of the different experimental runs, i.e. before labelling. The $\delta^{13}C$ of structural biomass was determined as the difference between $\delta^{13}C_{shoot}$ and $\delta^{13}C$ of water-soluble carbohydrates and determined by isotopic mass balance. The $\delta^{13}C$ of dark respired CO_2 ($\delta^{13}C_{Rn}$) was determined during dark periods between days 61 to 65. Data (means ± SE, *n* = 4-8) represent the average of equinumerous samples derived from chambers supplied with ^{13}C-mineral and -organic CO_2 and maintained near target [CO_2] of 200 (a), 400 (b), or 800 (c) μmol mol^{-1}. Stars mark a significant difference ($P < 0.05$) between a parameter *X* and shoot bulk biomass ($\delta^{13}C_X$ – $\delta^{13}C_{shoot}$).

The estimation of end-members for isotopic mixing models in labelling experiments

The fraction of unlabelled C ($f_{unlabelled}$) in C pools and CO_2 flux components (e.g. respiration) was quantified by the use of a two-member isotopic mixing model (Eqn 1.1, chapter 1). Estimates of the isotopic composition of the two end-members, i.e. of $\delta^{13}C_{new}$ and $\delta^{13}C_{old}$, can be obtained in two different ways: a one-chamber approach, which is employed when only one growth and labelling facility is available, or a two-chamber approach, which can be used in facilities with more than one labelling unit, as in this study. In both approaches, $\delta^{13}C_{old}$ is determined by measuring the $\delta^{13}C$ of the parameter of interest immediately before the switch of the CO_2 source. This $\delta^{13}C_{old}$ should be flux-, component- or compound specific to account for possible post-photosynthetic fractionation (Fig. 3.1.3). In the one-chamber approach,

s$\delta^{13}C_{new}$ is calculated using the parameter-specific $\Delta^{13}C$ (calculated with $\delta^{13}C_{CO2\ old}$) and the $\delta^{13}C$ of the labelling CO_2, i.e. $\delta^{13}C_{CO2\ new}$ (Eqn 1.2 and 1.3, chapter 1). However, data in Table 3.1.1 show that approximately 4% of the C fixed was not derived from tank CO_2 but from contaminating CO_2. Hence, the "true" source CO_2 must have been slightly different from $\delta^{13}C_{outlet\ day}$, which was calculated after eliminating data when chambers were not in isotopic equilibrium. This applies to both the pre-labelling and the labelling phases. Consequently, $\Delta^{13}C$ is associated with some errors (although that error was comparatively small here). Also, the estimation of $\delta^{13}C_{new}$ is subject to a further error, as $\delta^{13}C_{CO2\ new}$ for the labelling phase is not precisely reflected by $\delta^{13}C_{outlet\ day}$.

In the two-chamber approach, $\delta^{13}C_{old}$ in one chamber can be taken as $\delta^{13}C_{new}$ of the parallel chamber (following the change of the CO_2 source) and *vice versa*. Hence, any uncertainties concerning the pre-labelling and labelling of CO_2 sources are avoided. A prerequisite for this approach is that the extent of contamination is identical before and after the switch of the source CO_2. This assumption seems warranted because (1) experimental operations were virtually the same during the pre-labelling and labelling phases, and (2) there was no difference in the isotopic spread in parameters in temporal integration (Table 3.1.1).

In conclusion, the present work offered the unique opportunity to compare the analyses of tracer kinetics using a one-chamber and a two-chamber approach. It should be noted that possible artefacts associated with the one-chamber approach, namely the uncertainties in determining the exact value of the $\delta^{13}C$ of the source CO_2, became noticeable and quantifiable only by the two-chamber approach. Still, the analysis revealed a maximum 4% error due to contamination of the source CO_2 in the labelling experiments. Moreover, this work indicated that in investigations of photosynthetic and post-photosynthetic $\Delta^{13}C$, contamination with extraneous CO_2 must be avoided by additional tests (Lehmeier et al., 2008), as those studies must be capable of capturing minute differences in $\Delta^{13}C$. The present study also demonstrated that water-soluble carbohydrates in plant material can be extracted and separated via the HPLC system without cross contamination and adulteration of their $\delta^{13}C$. This is very important for studying the turnover of carbohydrate pools (subsequent chapter) and for studying post-photosynthetic fractionation. As it allowed the quantification of (although minor) artefacts, I used the two-chamber approach to evaluate tracer data in the following chapters (3.2, 3.3, and 3.4).

3.2 The role of stores in recycling sucrose

Plant biomass, leaf area, canopy nitrogen status and water-soluble carbohydrates

Elevating atmospheric CO_2 concentration from 200 to 400 and 800 μmol mol^{-1} CO_2 increased the C mass of whole plants by 34% and 59%, and decreased the N mass of whole plants by 12% and 23%, respectively (both P<0.001; Table 3.2.1). These effects of rising [CO_2] were very similar for shoots and roots, as the shoot : root C mass ratio was not affected significantly by [CO_2] (P>0.05). Meanwhile, leaf area per plant was reduced by 6% and 14%, respectively, a statistically significant reduction (P<0.05) for the high [CO_2] level (Table 3.2.1). The nitrogen nutrition index (NNI) of the plant canopies averaged 0.79 at 200 μmol mol^{-1} CO_2 and decreased by 38% and 52% (both P<0.001) by elevating CO_2 concentration to 400 and 800 μmol mol^{-1} respectively (Table 3.2.1).

Elevating [CO_2] from 200 to 400 and 800 μmol mol^{-1} increased the total mass of water-soluble carbohydrates-C (WSCs-C) per shoot by 65% and 116%, respectively (both at P<0.001), in association with increases in the concentration of WSCs-C (mg g^{-1} biomass-C) in shoot biomass of 23% and 37%, respectively (P<0.001; Table 3.2.2). Since leaf area per plant decreased with increasing [CO_2], these relationships corresponded to 66% and 147% enhancements of whole-shoot WSCs-C per unit leaf area resulting from the elevation of [CO_2] from 200 to 400 and 800 μmol mol^{-1}, respectively.

Of all WSC-fractions (Table 3.2.3), fructan contents showed the strongest response to the [CO_2] treatments. They accounted for 83-87% of total WSCs in the different treatments and increased by 74% and 161% on a leaf area basis when [CO_2] was increased from 200 to 400 and 800 μmol mol^{-1}, respectively. This CO_2 response of fructan was almost paralleled by that of fructose which increased by 37% and 121% from 200 to 400 and 800 μmol mol^{-1} CO_2 in the air, respectively. Sucrose and glucose contents also increased with increasing [CO_2], but those increases were distinctly smaller. These relationships were stable during the 7 d-long labelling period. No starch was detected in the samples.

Table 3.2.1 Growth parameters of *L. perenne* grown in the presence of [CO_2] of 200, 400 or 800 μmol mol^{-1} in the growth chamber atmosphere. Means (±SE) are of biomass parameters and leaf area measurements based on a total of 24 (200 and 800 μmol mol^{-1} CO_2) or 48 (400 μmol mol^{-1} CO_2) replicates sampled at the beginning of the dark period on the first day after the switch of $\delta^{13}C_{CO2}$ (day 66) and on the following 2nd, 3rd, 4th and 7th days. Determinations of canopy nitrogen nutrition index (NNI, according to Lemaire et al., 2008) are based on 16 (200 and 800 μmol mol^{-1} CO_2) or 32 (400 μmol mol^{-1} CO_2) replicates sampled on day 63. Shoot and root growth rates were calculated based on biomass change over three weeks (day 49 to day 72). Different superscript letters indicate statistically significant differences among CO_2 treatments, see Table 3.2.5.

	Atmospheric CO_2 concentration (μmol mol^{-1})		
	200	400	800
Dry plant biomass (g plant^{-1})	11.53^{c} (0.48)	14.75^{b} (0.42)	17.33^{a} (0.41)
Dry shoot biomass t (g plant^{-1})	9.21^{c} (0.34)	12.35^{b} (0.40)	14.45^{a} (0.38)
Dry root biomass (g plant^{-1})	2.33^{b} (0.19)	2.40^{b} (0.11)	2.88^{a} (0.13)
Whole plant C (g plant^{-1})	1.61^{a} (0.06)	2.15^{b} (0.06)	2.57^{c} (0.06)
Shoot C (g plant^{-1})	1.37^{a} (0.05)	1.84^{b} (0.06)	2.17^{c} (0.06)
Root C (g plant^{-1})	0.24^{a} (0.02)	0.31^{b} (0.01)	0.40^{c} (0.01)
Shoot C : root C ratio	6.17^{a} (0.44)	5.94^{a} (0.33)	5.44^{a} (0.17)
Whole plant N (mg plant^{-1})	74^{a} (7)	65^{ab} (3)	58^{b} (2)
NNI	0.79^{a} (0.02)	0.49^{b} (0.03)	0.38^{c} (0.01)
Leaf area (dm^{2} plant^{-1})	10.2^{a} (0.4)	9.6^{a} (0.2)	8.8^{b} (0.2)
Growth rate			
shoot (mg C plant^{-1} d^{-1})	39^{a} (5)	51^{b} (4)	59^{b} (4)
root (mg C plant^{-1} d^{-1})	2^{a} (2)	2^{a} (2)	3^{a} (3)

Table 3.2.2 Total water-soluble carbohydrates (WSCs) in shoot of *L. perenne*. Means (±SE) of WSC are based on a total of 24 (200 and 800 μmol mol^{-1} CO_2) or 48 (400 μmol mol^{-1} CO_2) replicates sampled at the beginning of the dark period on the first day after the switch of $\delta^{13}C_{CO2}$ (day 66) and on the following 2nd, 3rd, 4th and 7th days. Different superscript letters indicate statistically significant differences among CO_2 treatments at *P* <0.001, see Table 3.2.5.

	Atmospheric CO_2 concentration (μmol mol^{-1})		
	200	400	800
WSCs-C			
per shoot (mg plant^{-1})	573^{a} (36)	947^{b} (43)	1240^{c} (65)
per shoot biomass-C (mg g^{-1} biomass-C)	418^{a} (20)	515^{b} (11)	571^{c} (27)
per leaf area (g m^{-2})	39.0^{a} (1.9)	64.8^{b} (1.4)	96.5^{c} (4.6)

Table 3.2.3 Content of individual water-soluble carbohydrates (sucrose, fructan, glucose and fructose) in the shoot of *L. perenne*. Means (±SE) of individual WSC are based on a total of 24 (200 and 800 μmol mol^{-1} CO_2) or 48 (400 μmol mol^{-1} CO_2) replicates sampled at beginning of the dark period on the first day after the switch of $\delta^{13}C_{CO2}$ (day 66) and on the following 2nd, 3rd, 4th and 7th days. Different superscript letters within a row indicate statistically significant differences among CO_2 treatments at *P* <0.001, see Table 3.2.5.

	Atmospheric CO_2 concentration (μmol mol^{-1})		
	200	400	800
Sucrose (g m^{-2})	3.0^{a} (0.3)	3.9^{b} (0.2)	5.2^{c} (0.2)
Fructan (g m^{-2})	32.3^{a} (1.5)	56.3^{b} (1.3)	84.4^{c} (4.4)
Glucose (g m^{-2})	1.8^{a} (0.2)	2.0^{a} (0.1)	2.7^{b} (0.1)
Fructose (g m^{-2})	1.9^{a} (0.1)	2.6^{b} (0.1)	4.2^{c} (0.2)

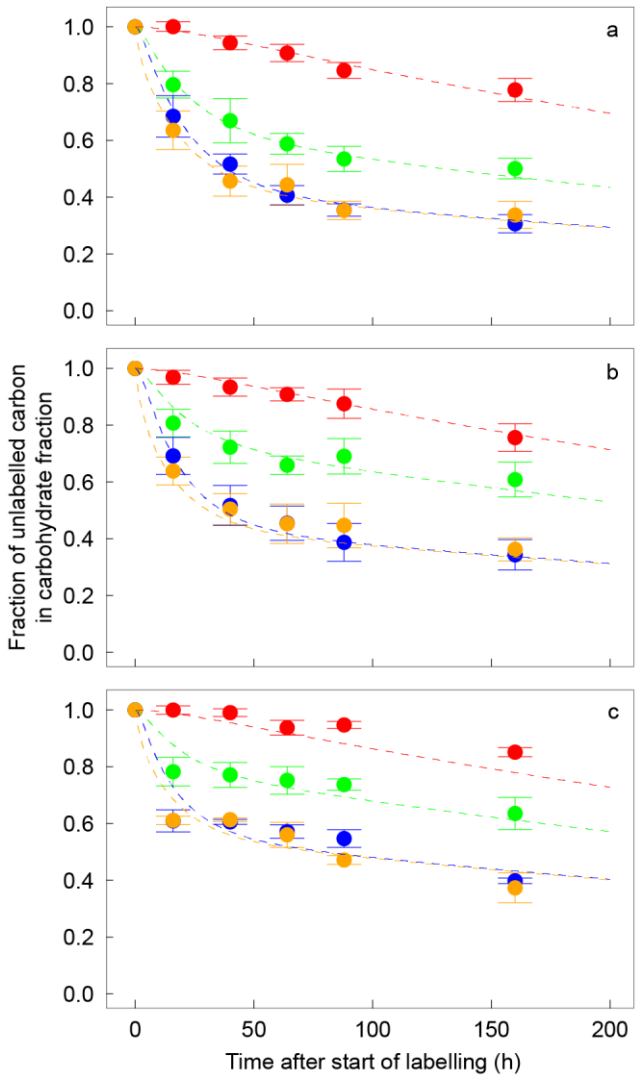

Fig. 3.2.1 Time course of the fraction of unlabelled C ($f_{unlabelled}$) in fructan (red), fructose (green), glucose (blue) and sucrose (orange) with labelling duration. Carbohydrates were extracted from the whole shoot of *L. perenne* grown at [CO_2] of 200 (a), 400 (b) or 800 (c) μmol mol^{-1}. The curves represent the fits of the 4-pool compartmental model shown in Fig. 1.2 (chapter 1). Each value is the mean (± SE) of four (200 and 800 μmol mol^{-1} CO_2) or eight (400 μmol mol^{-1} CO_2) replicates.

Fructan concentration in whole-shoot biomass was very high (≥35% of biomass) even at sub-ambient [CO_2] (Table. 3.2.1 and 3.2.2). That result was likely connected with an overabundance of assimilate availability (Wagner et al., 1983; Pollock & Cairns, 1991) determined by the high photosynthetically active radiation received by the canopies over the 16 h-long photoperiod and a simultaneously limited sink activity of the plants at reduced nitrogen fertilizer supply (Baca et al., 2020). Indeed, the nitrogen nutrition index of the canopies (defined as in Lemaire et al., 2008) was suboptimal even at sub-ambient [CO_2] (Table 3.2.1). In the same experiment, Baca et al. (2020) also observed that leaf elongation rates and epidermal cell lengths in all CO_2 treatments were typical of the effects of nitrogen limitation as observed in the same cultivar of *L. perenne* by Kavanova et al. (2008). Remarkably, the present data do not support a fundamental penalty to fructan storage in this C_3 grass under sub-ambient [CO_2], at least under the conditions of this experiment. Although I do not know of any other study of fructan levels under glacial maximum [CO_2], I assume that nitrogen limitation and cool climate

conditions, both conducive to fructan storage, may have prevailed together under glacial maximum [CO_2].

Still, increasing [CO_2] generated an additional increase in fructan accumulation, while the nitrogen nutrition index of the canopies continued to decline even further (compare Table 3.2.1 and 3.2.2), in line with observations in free-air CO_2 enrichment (FACE) studies (Isopp et al., 2000; Kimball et al., 2002; Högy et al., 2013). However, the whole-shoot fructan concentration at double ambient [CO_2] observed here (57%) was much higher than any reported FACE effect on fructan concentration (Högy et al., 2009, 2013). In fact, the whole-shoot fructan concentration observed here is the highest that I am aware of in an entire system of a C_3 grass, and again, likely resulted from several factors combining to enhance fructan accumulation (see above), including the [CO_2] fertilizer effect and the decrease in the nitrogen nutrition status. This [CO_2] effect on fructan storage occurred while non-WSC biomass of shoots increased very little with [CO_2]. Thus, non-WSC biomass at 800 μmol mol^{-1} CO_2 was only 11% higher than at 400 and 28% higher than at 200 μmol mol^{-1} CO_2. In comparison, fructan mass in the shoot increased by 74% and 129%, respectively.

Compartmental modelling of central carbohydrate metabolism

Estimates of the half-life of individual carbohydrate pools, the substrate fluxes among pools and the environment, and the partitioning of sucrose between fructan synthesis, hydrolysis or utilization in growth and maintenance activities (including sucrose export to the root system) were obtained based on optimization of the rate constants when fitting the four-pool model to the time courses of $f_{\text{unlabelled}}$. The four-pool model of carbohydrate metabolism of a fructan storing grass species (Fig.1.2, chapter 1) provided a virtually perfect fit to the dynamic labelling data of the whole-shoot carbohydrate system at sub-ambient and ambient [CO_2]. The goodness of fit was near-perfect for the sub-ambient (R^2=0.99) and ambient (R^2=0.98) [CO_2], and somewhat less so for the double-ambient [CO_2] (R^2=0.89). Fits with the 'free' (that is stoichiometrically unconstrained) four-pool model, or free models, without consideration of fructose-glucose interconversions (Lattanzi et al., 2012) did not improve the quality of the fit in any [CO_2] treatment. Such a good fit of a compartmental model may not be intuitive given the assumptions of compartmental modelling: that the system is in a steady state at the day-by-day timescale, i.e. that fluxes into and out of pools are the same and constant, and that all pools are well-mixed, given the compartmental and developmental heterogeneity of the plant parts that are combined in the system. This includes leaves of different developmental stages and a variety of functionally distinct tissues in both the lamina and sheath parts of each leaf. However,

all plants remained vegetative during the experiment, meaning that the shoot was composed virtually entirely of leaves. In support of modelling assumptions, I found no significant day-by-day variation of carbohydrate concentrations during the 7-d long dynamic labelling experiment, as I only sampled near the end of light periods. Also, the shoot growth rate was <3% d^{-1} (Table 3.2.1) in these well-developed closed stands. This slight deviation from the constancy-of-shoot-size assumption was deemed acceptable, as it implied, for instance, that the actual rate of fructan synthesis on a given day underestimated the rate of hydrolysis by less than 3% d^{-1}, as whole shoot fructan concentration did not vary significantly with labelling time. An analogous evaluation and qualification of the steady-state assumption was also performed by Lattanzi et al. (2008 and 2012) in their compartmental modeling of C and N substrate fluxes into leaf growth zones and of central carbohydrate analysis in mature leaves of perennial ryegrass. In comparison, errors in model estimates for the other pools (sucrose, glucose, fructose) must have been minor, as they were turned over much faster. Also, the effects of potential physical compartmentation did not affect model features in Lattanzi et al. (2012). Overall, the present observations may be taken to indicate that biochemical (functional) features of central carbohydrate metabolism were much more critical than potential compartmentation (structural) effects, as the four-pool model described only the broad features of the biochemistry of water-soluble carbohydrate metabolism and yielded excellent fits to tracer data at least under half-ambient and ambient [CO_2].

Interestingly, the stoichiometrically-constrained model provided the most parsimonious, best fit to the labelling kinetics of the whole shoot carbohydrate system. That is, more complex models that permitted glucose-fructose interconversion activities or non-stoichiometrically-constrained sucrose re-synthesis from free glucose and fructose, did not demonstrate a statistically superior fit (data not shown). This result is also consistent with the idea that sucrose cycling *via* hydrolysis/re-synthesis and passage *via* the fructan pool may principally occur independently of each other. Whether or not the relative activities of the two cycling mechanisms occurred at the same relative rates in leaves of different ages or leaf blades and sheaths, however, cannot be deduced from this analysis, as all shoot tissues were combined in one sample. However, if the relative magnitude of the two activities did change between developmental stages or tissue types, the fact that the activities occurred independently would explain why the model nevertheless provided an excellent fit to the carbohydrate systems' labelling kinetics.

Tracer kinetics and compartmental analysis

The labelling time courses of the different carbohydrates (i.e. the changes of $f_{unlabelled}$ with time) were qualitatively similar in the different treatments (Fig. 3.2.1): initial label incorporation was fastest and similar in sucrose and glucose, and slowest in fructan. In comparison, fructose demonstrated a labelling time course that was intermediate between that of fructan and sucrose. These time courses of $f_{unlabelled}$ in the carbohydrate system (Fig. 3.2.1) of the whole shoot were well fitted with the so-called 'stoichiometrically constrained' four-pool compartmental model presented by Lattanzi et al. (2012).

The results indicated that [CO_2] had no significant effect on the half-life of any carbohydrate (sucrose, fructan, glucose or fructose) (Table 3.2.4). Also, at all [CO_2], the predicted half-lives were relatively short and similar for the sucrose (~2.4 h), glucose (~3 h) and fructose (~4 h) pools, while that of the fructan pool (~180-190 h) was almost two orders of magnitude higher than that of the sucrose pool. The residence time of carbohydrate-C in the system increased from about 8.9 d to 13.6 d between 200 and 800 μmol mol^{-1} [CO_2], essentially due to greater sucrose partitioning to fructan synthesis. The half-life ($T_{1/2}$) of fructan observed here (~7.7 d) was much longer than that in mature photosynthesising leaf blades of the same cultivar of *L. perenne* grown in continuous light with high ($T_{1/2}$ = 1.1 d) or low nitrogen fertilizer supply ($T_{1/2}$ = 2.6 d). As the studies addressed different scales and were performed in different environments, it is unclear which factor explained the difference in half-lives. It is possible, however, that fructan contents in the sheath part of leaves were more prominent and possibly turned over more slowly than in leaf blades (Thomas & James, 1999). The fructan half-life observed here was equivalent to a mean residence time of about 11 d, close to the leaf appearance interval observed by Baca et al. (2020) in the same study. Also, the half-life of fructan corresponded to about one-quarter to one-fifth of the average leaf life span of *L. perenne* observed elsewhere (Schleip et al., 2013, and compilation therein). Although these relationships do not prove that fructan storage was constrained by leaf life span directly, I cannot rule out that perhaps developmental cues associated with leaf senescence were involved in the control of fructan storage and mobilisation.

Although, I know of no other studies of the half-lives of sucrose, glucose or fructose at the whole shoot level, the half-life estimates here appear to be realistic when compared with studies on the scale of mature leaves (Farrar & Farrar 1985, 1986; Borland & Farrar, 1988; Lattanzi et al., 2012) or leaf growth zones (Schnyder et al., 1987), and the short delays in the system that may be connected with sucrose transport times (Windt et al., 2006) between leaves

and sheaths. Clearly, the idea that the sucrose pool is homogeneous is a significant simplification, given the fact that sucrose may be found in several cellular compartments (cytoplasm, vacuole, apoplast) and in various functionally distinct tissue types, including sieve tubes and companion cells (Ruan 2012, 2014; Du et al., 2019). Indeed, the half-life estimate of sucrose must have been dominated by those tissues that contained the bulk of the sucrose, particularly the cytoplasm of lamina and sheath parenchyma cells. Also, I sampled only near the end of the light period, meaning that a certain fraction of the sucrose in the leaf blades may have been vacuolar (Farrar et al., 1989) if plants used a diurnal sucrose storage mechanism. This factor would tend to increase the half-life of the 'average' sucrose molecule. However, the half-life of sucrose as obtained here was close to (or not much longer) than that of the "transport" sucrose pool (Farrar & Farrar, 1985), which was assumed to include all sucrose not stored in the vacuole of barley leaf blades. Additionally, I would not expect a strong effect of carbohydrate metabolism within sink tissue (that is the leaf growth-and-differentiation zones of the vegetative tillers that composed the shoot, Baca et al., 2020) on the tracer dynamics in the shoot as described by the model, since carbohydrate contents of that tissue accounted for only a tiny fraction (i.e. <10%) of the total quantity of water-soluble carbohydrates in the shoot in the different treatments. For that reason, any eventual discrepancy between labelling patterns of carbohydrates in sinks compared with the vastly greater mass of fully-developed remaining plant parts (source and storage tissue) would have a minimal effect at the scale of the whole shoot tracer kinetics. Together, the predominance of sucrose in the cytoplasm of parenchyma in leaf blades and sheaths, and the short transit times in the transport system linking the plant parts, may have combined to yield a half-life of whole-shoot sucrose that was close to that of the "transport" pool of individual leaves as found in several studies (Geiger et al., 1983; Farrar & Farrar, 1986; Rocher & Prioul, 1987; Borland & Farrar, 1988).

For the different treatments, the model results indicated that about equal fractions of sucrose were partitioned between the three alternative functions: (1) supply of growth and maintenance of the shoot and export to roots, or use in (2) fructan synthesis or (3) hydrolysis (Table 3.2.4). The approximately equal partitioning was true, except for the low [CO_2] treatment, where sucrose partitioning to fructan synthesis (0.22) was significantly lower than its use in the other processes, also by comparison with the treatments with higher [CO_2]. In particular, at low [CO_2], sucrose use in hydrolysis was almost double that for fructan synthesis. For a system in steady-state, that [CO_2] effect implied that sucrose recycling from the products of hydrolysis was almost twice as important as that from fructose released during fructan breakdown at 200 μmol mol^{-1} CO_2, while at 400 and 800 μmol mol^{-1} CO_2, fructan metabolism

and sucrose hydrolysis contributed approximately equally to sucrose recycling. The summed proportion of the gross flux of sucrose cycling through fructan and hydrolysis was insensitive to [CO_2], and, accordingly, the proportion of sucrose used in growth and maintenance (including export to roots) was also practically constant (Table 3.2.4). At the same time, partitioning of the gross flux of sucrose use between hydrolysis and fructan synthesis did change considerably. The rate of sucrose consumption in hydrolysis was about two times that in fructan synthesis at low [CO_2] while partitioning between hydrolysis and fructan synthesis was approximately equal at ambient and high [CO_2]. Although effects of low [CO_2] on sucrose cycling via hydrolysis/resynthesis have not been studied so far, to my best knowledge, it is well known that sucrose cycling via hydrolysis/resynthesis is common and active in photosynthesizing leaves of dicots and grasses (Wagner et al., 1986; Lemoine, 2000; Du et al., 2020), including in *L. perenne* (Lattanzi et al., 2012) as well as in sink tissue, such as tap roots of sugar beet (Giaquinta, 1979) or tomato fruits (Nguyen-Quoc & Foyer, 2001) or other heterotrophic systems (Kruger et al., 2007). The estimates for the rates of cycling via hydrolysis in the present study were comparable in magnitude to estimates for leaves of *Arabidopsis* by Nägele et al. (2010), soybean and tobacco by Huber (1989) and cotyledons of germinating *Ricinus communis* by Geigenberger & Stitt (1991). It has been proposed that leaf sucrose cycling through hydrolysis should increase as photosynthesis acclimates to elevated [CO_2] (Moore et al., 1999). However, my results do not support that hypothesis in terms of sucrose partitioning, although I cannot rule out that a possible enhancement of sucrose cycling *via* hydrolysis in leaf blades was compensated by decreased cycling elsewhere in the shoot (i.e. in sheaths). Indeed, Lattanzi et al. (2012) observed much greater cycling via hydrolysis in leaf blades. Also, my modelling indicated that the gross flux through hydrolysis at the whole shoot level may have increased with [CO_2], although that result was not statistically significant.

In addition, differences in [CO_2] during growth caused significant differences in the scale of fluxes within and out of the system (Table 3.2.4). For instance, the total flux of sucrose out of the system (F_{10}), supplying growth, maintenance and sucrose export to roots, increased 1.7-fold between 200 and 800 μmol mol^{-1} [CO_2]. The strongest [CO_2] effect on fluxes was connected with fructan synthesis (F_{12}) and associated fructan hydrolysis (F_{24}). Thus, increasing [CO_2] from 200 to 800 μmol mol^{-1} caused a 2.8-fold increase in the flux of C through the fructan pool. On the other hand, I found no significant effect of [CO_2] on the sucrose flux through hydrolysis.

In conclusion, increasing [CO_2] from 200 to 800 μmol mol^{-1} increased total shoot biomass 1.6-fold, fructan mass 2.3-fold and its concentration in shoot biomass from 35% to 51%. Compartmental modelling indicated that the biggest impact of increasing [CO_2] on central carbohydrate metabolism was to increase carbon cycling through the fructan pool. By contrast, the half-life of the fructan pool (~7.7 d) was insensitive to [CO_2] change, as were the half-lives of sucrose, glucose and fructose (2.3-4.5 h). Sucrose re-synthesis from breakdown products of fructan (fructose) accounted for an increasing proportion of total sucrose synthesis and was similar in magnitude to sucrose neo-synthesis at double-ambient [CO_2]. The data indicate fructan as the main factor explaining the turnover time of the metabolic pool serving growth and respiration of a temperate perennial grassland species during undisturbed growth.

Table 3.2.4 Parameters of the four-pool compartmental model of central carbohydrate metabolism in the shoot of *L. perenne*. Parameters were numerically optimized as described in chapter 2, based on the tracer kinetics data shown in Fig. 3.2.1. Fluxes are expressed as g C m^{-2} leaf area h^{-1} and calculated by the differential equations given in chapter 2, using the carbohydrate contents per leaf area as shown in Table 3.2.3. The results of the fluxes predicted by the optimized rate constants are given in bold. Numbers in a row or column with different superscript letters indicate a statistically significant difference at 95% confidence intervals.

	Atmospheric CO_2 concentration (μmol mol^{-1})		
	200	400	800
Pool half-life			
Sucrose ($T_{1/2\ Q1}$, h)	2.4^a (0.2)	2.5^a (0.2)	2.3^a (0.4)
Fructan ($T_{1/2\ Q2}$, h)	190.5^a (14.5)	181.6^a (16.4)	178.7^a (39.1)
Glucose ($T_{1/2\ Q3}$, h)	3.7^a (0.3)	3.3^a (0.3)	2.9^a (0.5)
Fructose ($T_{1/2\ Q4}$, h)	3.8^a (0.3)	4.3^a (0.3)	4.5^a (0.8)
C flux			
F_{10} (g m^{-2} h^{-1})	**0.18^a (0.02)**	**0.25^b (0.02)**	**0.30^b (0.04)**
F_{12} (g m^{-2} h^{-1})	**0.12^a (0.01)**	**0.21^b (0.02)**	**0.33^b (0.07)**
F_{13} (g m^{-2} h^{-1})	0.34^a (0.04)	0.42^{ab} (0.04)	0.65^b (0.12)
F_{14} (g m^{-2} h^{-1})	**0.23^a (0.03)**	**0.21^a (0.03)**	**0.33^a (0.10)**
F_{24} (g m^{-2} h^{-1})	0.12^a (0.01)	0.21^b (0.02)	0.33^b (0.07)
F_{31} (g m^{-2} h^{-1})	0.34^a (0.05)	0.42^{ab} (0.04)	0.65^b (0.12)
F_{41} (g m^{-2} h^{-1})	0.34^a (0.04)	0.42^{ab} (0.04)	0.65^b (0.13)
Sucrose partitioning			

To growth, maintenance, and export	0.34^{Aa} (0.04)	0.38^{Aa} (0.03)	0.31^{Aa} (0.06)
To fructan synthesis	0.22^{Ba} (0.03)	0.32^{Ab} (0.04)	0.35^{Ab} (0.09)
To hydrolysis	0.43^{Aa} (0.07)	0.31^{Aa} (0.04)	0.34^{Aa} (0.11)
Residence time in the system (h)	213^{a} (23)	255^{ab} (17)	327^{b} (45)
Goodness of model fit (R^2)	0.99	0.98	0.89

Table 3.2.5 Results of one-way ANOVA, testing the effect of [CO_2].

Parameter	*F*-value	*P*-value
Dry plant biomass (g plant^{-1})	30.39	<0.001
Dry shoot biomass (g plant^{-1})	30.59	<0.001
Dry root biomass (g plant^{-1})	3.93	0.23
Plant C (g plant^{-1})	39.88	<0.001
Plant N (mg plant^{-1})	4.31	0.08
Shoot C (g plant^{-1})	32.67	<0.001
Root C (g plant^{-1})	33.24	<0.001
Shoot C : root C ratio	1.99	0.14
NNI	109.7	<0.001
Leaf area (dm^2 plant^{-1})	4.67	0.01
WSC mass (g plant^{-1})	34.47	<0.001
WSC concentration (mg g^{-1})	15.34	<0.001
WSC content (g m^{-2})	104.3	<0.001
Fructan (g m^{-2})	96.53	<0.001
Sucrose (g m^{-2})	24.91	<0.001
Glucose (g m^{-2})	12.14	<0.001
Fructose (g m^{-2})	55.3	<0.001

3.3 The role of stores in supplying respiratory substrate

Respiration rate

In this section, I report the analysis of the response of plant respiration rate to a change of [CO_2] during growth (object 3, chapter 1). Canopy dark respiration (R_n), that is dark respiration rate per unit chamber ground area, was calculated as specified in Eqn 2.5 (chapter 2). Relative to [CO_2] of 400 μmol mol^{-1}, R_n was 19% lower (P<0.05) at [CO_2] of 200 μmol mol^{-1}. However, increasing [CO_2] from 400 to 800 μmol mol^{-1} had no significant effect (Table 3.3.1 and 3.3.2). The latter result aligns with the study of Ryle et al. (1992), that found no significant response of R_n on a ground area basis when *L. perenne* was grown at [CO_2] of 680 μmol mol^{-1} relative to 340 μmol mol^{-1}. Also, the fact that area-based R_n was reduced under low [CO_2] is consistent with the study of Ayub et al. (2011), who reported that area-based *R*n of *Eucalyptus saligna* decreased under [CO_2] of 280 μmol mol^{-1} relative to 400 μmol mol^{-1}.

Meanwhile, R_n per unit plant-C (which is also termed specific respiration rate, e.g. Lötscher et al., 2004) did not differ significantly between the [CO_2] treatments (Table 3.3.1 and 3.3.2). This indicated that the significant [CO_2] effect on canopy respiration rate (i.e. R_n per unit ground area) observed when increasing [CO_2] above 200 μmol mol^{-1} was primarily a function of [CO_2] effects on canopy biomass.

In the following compartmental modelling, I used R_n per unit of chamber ground area, as this is also the normal basis for respiration measurements at the plant community level (Amthor, 1991).

Table 3.3.1 Canopy dark respiration rate of *L. perenne*. Respiration was expressed per unit chamber area or per unit plant-C. Plants were grown in the growth chamber with [CO_2] of 200, 400, or 800 μmol mol^{-1} CO_2, 20/16 °C air temperature and 50%/75% relative humidity during the 16/8 h light/dark period. Photosynthetic photon flux density (PPFD) was 800 μmol m^{-2} s^{-1}.at canopy height. Measurements were conducted from day 66 to day 72. Shown are means ± SE of 2 - 4 replicates. Different superscript letters within a row indicate statistically significant differences between CO_2 treatments.

	Atmospheric CO_2 concentration (μmol mol^{-1})		
	200	400	800
Dark respiration rate			
per unit **ground area** (μmol C m^{-2} s^{-1})	-4.26^a (0.18)	-5.23^b (0.08)	-4.99^b (0.21)
per unit **plant-C** (μmol C mol^{-1} plant C s^{-1})	-0.19^a (0.03)	-0.18^a (0.02)	-0.14^a (0.005)

Table 3.3.2 Results of one-way ANOVA testing effect of CO_2 on plant dark respiration rate.

Parameter	*F*-value	*P*-value
Dark respiration rate		
per unit **ground area** (μmol C m^{-2} s^{-1})	154.8	<0.05
per unit **plant-C** (μmol C mol^{-1} plant C s^{-1})	2.4	0.19

Tracer kinetics and compartmental analysis

The tracer kinetics in respired CO_2 were very similar between all [CO_2] treatments, each consisting of two major phases (Fig. 3.3.1): first, the fraction of unlabeled C ($f_{unlabelled}$) decreased rapidly by ~0.25 during the first day of labelling, and then it continued to decrease at a distinctly slower rate during the following phase of continuous labelling. After 7 days of continuous labelling, the value of $f_{unlabelled}$ had decreased to ~0.42. The change of $f_{unlabelled}$ over time appeared to occur only during the 16 h-long photoperiods, as hourly $f_{unlabelled}$ in respired CO_2 did not change significantly during the night, as indicated by the data for the 1st and 2nd night following the start of labelling (Fig. 3.3.2).

In each [CO_2] treatment, fitting two-exponential functions to the tracer kinetics of respired CO_2 gave the best fit, indicating that the respiratory substrate supply system could be

separated into two pools. This compared well with the single-shoot, two-pool compartmental model used by Lehmeier et al. (2010a; see Fig. 1.4, chapter 1) in investigations of day-length effects on the compartmental structure of the system supplying substrate for respiration. In my work, the goodness-of-fit of the two-pool model, given by the R^2, was >0.99 in all [CO_2] treatments. A one-pool model exhibited a significant lack of fit to the data, while a three-pool model did not improve fit quality compared to the two-pool model, as in Lehmeier et al. (2010a) (data not shown).

In the two-pool compartmental model, the R_n on a ground area basis represents the efflux of the model, which equals the respiratory substrate influx into the system in the steady state. The half-life ($T_{1/2}$) and size (Q) of each pool did not differ significantly between [CO_2] treatments (Table 3.3.3). The $T_{1/2}$ of Q_1, the fast pool, was in the order of ~11 - 15 h, and that of Q_2, the slow pool, ranged between 3 - 5 d. Relative to the pool size of Q_2 in ambient [CO_2], Q_2 was 34% smaller at low [CO_2] and 32% larger at high [CO_2]. The proportional contribution of Q_2 to total respiratory substrate supply was very large and highly similar between all [CO_2] levels (58-60%). The carbon residence time in the entire respiratory supply system ranged between 194 h (200 μmol mol^{-1} CO_2) and 291 h (800 μmol mol^{-1} CO_2).

The fact that $f_{unlabelled}$ did not change significantly during the course of dark periods (Fig. 3.3.2) is consistent with results by Schnyder et al. (2003), who also reported a constant hourly $f_{unlabelled}$ during the dark period. This finding supports the idea that the respiratory substrate pool is well mixed with “labelled” and “unlabelled” carbon at the whole plant (and community) level.

Within a continuous labelling experiment (as practiced here), unlabelled carbon in the respiratory substrate is gradually replaced by labelled carbon until $f_{unlabelled} = 0$. In a study by Lehmeier et al. (2010a), they found that $f_{unlabelled}$ of shoot or root respired CO_2 decreased to < 0.2 on the 7th day of continuous labelling when *L. perenne* was grown at [CO_2] of 360 μmol mol^{-1}. This progression of labelling was faster than that I observed at all [CO_2] levels. This difference between Lehmeier et al. (2010a) and my investigations may be related to plant growth conditions. Compared with the study of Lehmeier et al. (2010a), in my study, plants were grown at a much higher light intensity (PPFD: 800 compared to 425 μmol m^{-2}s^{-1}) and with a lower N supply (N concentration: 5.1 compared to 7.5 mM). The higher photosynthetically active radiation may have led to a higher assimilate availability (Wagner et al., 1983; Pollock & Cairns, 1991), while, simultaneously, the lower nitrogen supply could

have caused sink limitation (Baca et al., 2020). Both factors would lead to a greater accumulation of respiratory substrate in the form of water-soluble carbohydrates (mainly fructan, see chapter 3.2). The slower rate of change of $f_{unlabelled}$ in my work may be because the turnover of a much larger respiratory substrate store would take much longer, even if the absolute rate of tracer addition to that pool were the same.

In all [CO_2] treatments, the tracer kinetics in respired CO_2 could be fitted with a two-exponential curve. This finding is consistent with the study by Lehmeier et al. (2010a), who reported a tracer time course with two distinct phases in respired CO_2 of shoot and root in *L. perenne* when plants grown in [CO_2] of 360 μmol mol^{-1} were labelled continuously over 14 days. Gong et al. (2017) observed a similar tracer kinetic pattern in respired CO_2 of sunflower stands grown in [CO_2] of 200 or 1000 μmol mol^{-1} over a 5-d labelling period. Conversely, Lehmeier et al. (2018, 2010b) also found a third, very fast phase immediately at the beginning of labelling. I could not observe this first initial labelling phase, as my first determination of $f_{unlabelled}$ only occurred at 16 h after the start of labelling.

The $T_{1/2}$ of Q_1 (12.7 h), the fastest labelled pool detected here, agreed reasonably well with that of the transport and metabolic pool (2 to 8 h), discussed by Lehmeier et al. (2010a). However, I cannot discount the possibility that Q_1 included some contribution from a short-term or diurnal store (Lehmeier et al., 2010b), which may have included vacuolar sucrose (Farrar & Farrar, 1986; Borland & Farrar; 1988).

In contrast, Q_2 is a long-term storage pool, forming the primary carbon source to feed plant respiration (Table 3.3.3). This finding was in agreement with observations by Lehmeier et al. (2010a, b), who reported that the respiratory storage pool (Q_2) contributed *c.* 60% to total respired C of *L. perenne* when grown in continuous light, regular day-night cycles, or under nitrogen-limited conditions. Nogués et al. (2004) found that the products of current photosynthesis supplied less than 50% of the substrate feeding leaf respiration of French beans. Together, these results highlight that the long-term storage pool formed a central part of the integral C supply system to feed plant respiration. I also found that the carbon stored in Q_2 exceeded the total demand for respiration during a dark period by comparing the size of Q_2 to the rate of F_{10} (Table 3.3.3), indicating this pool may act as a buffer accommodating fluctuating respiratory substrate supply in day-night cycles. This result differs from a study with a starch-storing plant by Gong et al. (2017). Who reported that the long-term storage pool contributed

<36% of carbon respired by sunflowers, an amount that was insufficient to meet the demand of dark respiration in one night.

The residence time of respiratory substrate in the plant (τ) is determined by respiratory substrate pool size and efflux rate (F_{10}) (Table 3.3.3). I observed no difference in τ between [CO_2] treatments, despite F_{10} being significantly smaller at [CO_2] of 200 μmol mol^{-1}. τ was more than two times longer than the $T_{1/2}$ of C in the storage pool (Q_2) (234 h vs 93 h) (Table 3.3.3). This result also agreed with the observation that the tracer entered the long-term storage compartment more than once before being respired (Lehmeier et al., 2010b).

In conclusion, R_n was enhanced with increasing [CO_2] from 200 to 400 μmol mol^{-1} and was insensitive to increasing [CO_2] from 400 to 800 μmol mol^{-1}. Compartmental modelling indicated that an increase of [CO_2] from 200 μmol mol^{-1} to 800 μmol mol^{-1} increased the size of the long-term storage pool by 197% and its $T_{1/2}$ by 148%. This highlights the great importance of Q_2 in supplying respired substrate.

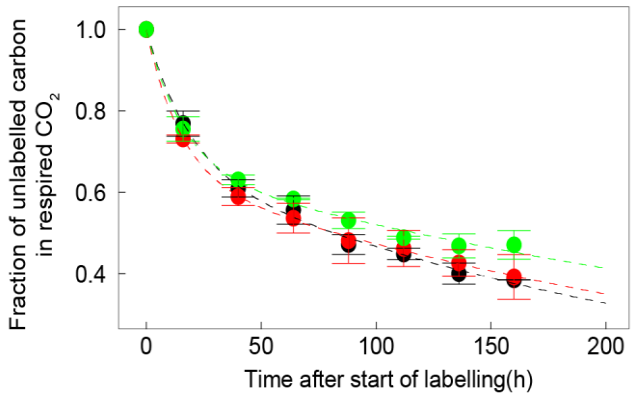

Fig. 3.3.1 Time course of the fraction of unlabelled carbon ($f_{unlabelled}$) in respired CO_2 of stands of *L. perenne*. Plants were grown at [CO_2] of 200 (black), 400 (red) or 800 (green) μmol mol^{-1}. The labelling experiment started at day 65. Each value is the mean (± SE) of two (200 and 800 μmol mol^{-1} CO_2) or four (400 μmol mol^{-1} CO_2) chamber-scale replicates. The dashed line represents the two-pool model prediction.

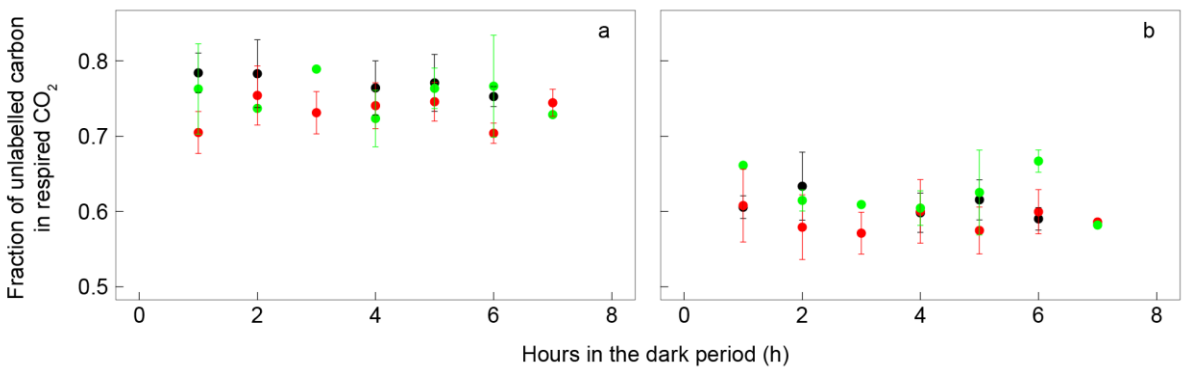

Fig. 3.3.2 Time course of the fraction of unlabelled carbon ($f_{unlabelled}$) in respired CO_2 by stands of *L. perenne* during the 1st (a) and 2nd night (b) after the beginning of labelling. Plants were grown at [CO_2] of 200 (black), 400 (red) or 800 (green) µmol mol^{-1}. The labelling experiment started on day 65. Shown are means (± SE) of hourly values of stands during the dark period on the first and second labelling day. *n* = 2-4.

Table 3.3.3 Effect of atmospheric CO_2 concentration during growth on the parameters of the two-pool compartmental model of respiratory substrates in stand *L. perenne*. Parameters were optimized as described in chapter 2, based on the tracer kinetics data shown in Fig. 3.3.1. Fluxes are expressed as g C m^{-2} h^{-1}, which is dark respiration rate expressed on a chamber ground area basis. The results of the fluxes predicted by the optimized rate constants are given in bold. Different superscript letters indicate a statistically significant difference at 95% confidence intervals.

	Atmospheric CO_2 concentration (μmol mol^{-1})		
	200	400	800
C flux			
F_{10} (g C m^{-2} h^{-1})	**0.183^a**	**0.223^b**	**0.214^b**
F_{12} (g C m^{-2} h^{-1})	**0.242^a (0.059)**	**0.309^a (0.029)**	**0.326^a (0.078)**
F_{21} (g C m^{-2} h^{-1})	**0.242^a (0.059)**	**0.309^a (0.029)**	**0.326^a (0.078)**
Pool half-life			
$T_{1/2}$ (Q_1) (h)	15^a (2)	11^a (1)	12^a (2)
$T_{1/2}$ (Q_2) (h)	76^a (17)	90^a (7)	112^a (28)
Pool sizes			
Q_1 (g C m^{-2})	9.1^a (0.9)	8.6^a (0.4)	9.5^a (1.0)
Q_2 (g C m^{-2})	26.5^a (8.7)	40.0^a (4.9)	52.7^a (18.2)
Residence time in the system (h)	194^a (48)	218^a (22)	291^a (85)
Fractional contribution			
Current assimilation	0.43^a (0.07)	0.42^a (0.03)	0.40^a (0.07)
Store	0.57^a (0.15)	0.58^a (0.06)	0.60^a (0.15)
Goodness of model fit (r^2)	0.998	0.999	0.996

3.4 A connection between carbohydrate and respiratory substrate supply systems

Comparison of tracer kinetics in non-structural carbohydrates and dark respired CO_2

In this section, I explore the relationships between the tracer kinetics in the dark respired CO_2 at the whole plant level and in the water-soluble carbohydrates (WSCs) of the shoot to seek further clues as to the likely chemical identity of the main mediator carbohydrate substrate feeding respiration (object 4, chapter 1). I first assessed $\Delta f_{\text{unlabelled } X}$, the deviation between the fraction of unlabelled C in a given carbohydrate species *X* and that in respired CO_2 ($\Delta f_{\text{unlabelled } X} = f_{\text{unlabelled } Rn} - f_{\text{unlabelled } X}$) and its temporal pattern during the labelling period (Fig. 3.4.1). This analysis demonstrated that for any given carbohydrate, the magnitude of $\Delta f_{\text{unlabelled } X}$ and its temporal pattern was highly similar for all [CO_2] treatments. $\Delta f_{\text{unlabelled}}$ of sucrose ($\Delta f_{\text{unlabelled suc}}$) was generally positive throughout labelling. In addition, for glucose, the magnitude and temporal pattern of $\Delta f_{\text{unlabelled}}$ ($\Delta f_{\text{unlabelled glc}}$) closely resembled that of sucrose. Similar relationships did not exist for fructan ($\Delta f_{\text{unlabelled fructan}}$) and fructose ($\Delta f_{\text{unlabelled fru}}$), which exhibited consistently negative values. Moreover, $\Delta f_{\text{unlabelled fructan}}$ and $\Delta f_{\text{unlabelled fru}}$, tended to increase with labelling time, a pattern that was most evident for fructan (Fig. 3.4.1). On average across the three [CO_2] treatments, $\Delta f_{\text{unlabelled suc}}$ decreased with the duration of labelling from approximately 0.13 after the first labelling photoperiod to approximately 0.06 on day 7 (Fig. 3.4.1a, b and c). The time lag for dark respired CO_2 to reach the same degree of labelling as whole-shoot sucrose was around 6 h throughout labelling, an estimate associated with an uncertainty (SE) of around 2 h. This pattern was not evident for the other sugars for which $\Delta f_{\text{unlabelled } X}$ stayed constant (glucose) or even increased with the labelling duration (fructan and fructose).

The positive $\Delta f_{\text{unlabelled suc}}$ observed throughout the labelling period means sucrose was labelled faster than whole plant (or stand-scale) respiration. This observation supported Schnyder et al. (2012) that sucrose in a leaf blade was labelled faster than the whole shoot respired CO_2 in *L. perenne*. Assuming all substrates feeding respiration are derived from sucrose, the 6 h delay represents the time span between exiting the shoot sucrose pool and passage through the different metabolic events associated with, or preceding, the release of respired CO_2. These results may support the idea that sucrose is indeed the main mediator carbohydrate substrate supplying the respiratory machinery (see below). The fact that $\Delta f_{\text{unlabelled glc}}$ was similar to $\Delta f_{\text{unlabelled suc}}$ may be unsurprising as both sugars followed similar labelling kinetics, and glucose was turned over rapidly, most likely in connection with sucrose recycling

(see chapter 3.2). Conversely, the results of $\Delta f_{\text{unlabelled fructan}}$ and $\Delta f_{\text{unlabelled fru}}$ demonstrate that fructan and fructose were labelled much more slowly than the whole plant respired CO_2, a disparity that even increased with labelling duration. This result is consistent with the idea that fructan and fructose did not serve as *immediate* precursors of respiratory substrates at the whole-plant level, although they had a critical mediator role via their involvement in the recycling of sucrose, as discussed in chapter 3.2.

Table 3.4.1 Results of a one-way ANOVA, testing the differences of $\Delta f_{\text{unlabelled X}}$ among different labelling days.

Parameter	*F*-value	*P*-value
[CO_2] 200 μmol mol^{-1}		
$\Delta f_{\text{unlabelled fructan}}$	12.36	0.008
$\Delta f_{\text{unlabelled suc}}$	2.14	0.21
$\Delta f_{\text{unlabelled glu}}$	2.78	0.15
$\Delta f_{\text{unlabelled fru}}$	1.49	0.33
[CO_2] 400 μmol mol^{-1}		
$\Delta f_{\text{unlabelled fructan}}$	5.07	0.009
$\Delta f_{\text{unlabelled suc}}$	0.53	0.71
$\Delta f_{\text{unlabelled glu}}$	4.13	0.02
$\Delta f_{\text{unlabelled fru}}$	4.27	0.02
[CO_2] 800 μmol mol^{-1}		
$\Delta f_{\text{unlabelled fructan}}$	11.7	0.009
$\Delta f_{\text{unlabelled suc}}$	8.82	0.02
$\Delta f_{\text{unlabelled glu}}$	97.06	<0.001
$\Delta f_{\text{unlabelled fru}}$	30.38	0.001

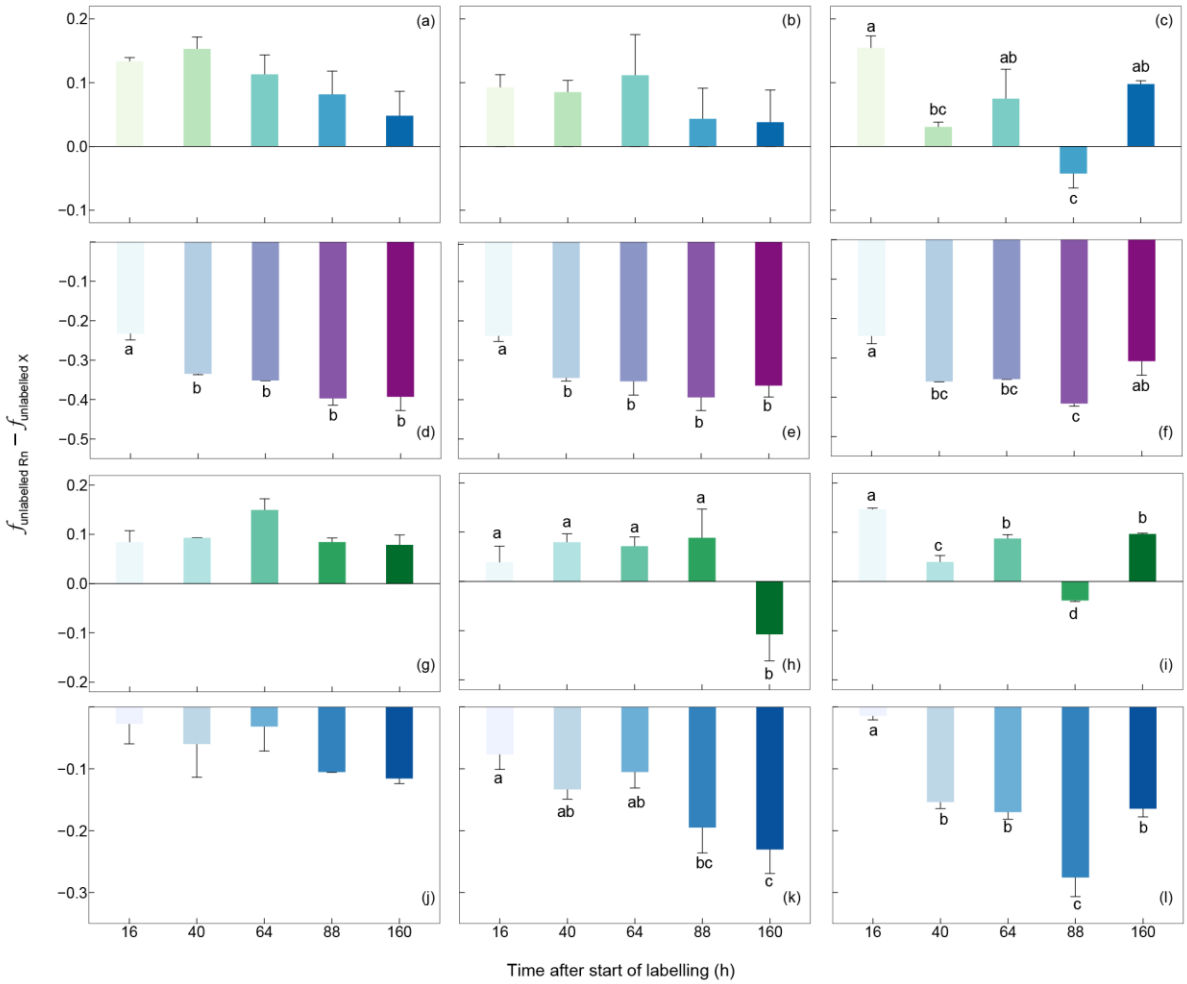

Fig. 3.4.1 Deviation between fractions of unlabelled C between respired CO_2 and individual WSC of *L. perenne*. The deviation ($\Delta f_{unlabelledl\ X}$) between the fractions of unlabelled C in a given carbohydrate *X* and that in respired CO_2 was expressed by $\Delta f_{unlabelled\ X} = f_{unlabelled\ Rn} - f_{unlabelled\ X}$. Individual carbohydrates include sucrose (a, b, and c), fructan (d, e, and f), glucose (g, h, and i), and fructose (j, k, and l). Plants grown at [CO_2] of 200 (left), 400 (middle) and 800 (right) μmol mol^{-1}. Shown are means ± SE of chamber replicates during the whole labelling period from day 65 and the following 7 days, (*n*= 2-4). Different letters indicate significant differences at *P* <0.05.

Further comparative features of the respiratory substrate system and carbohydrate pools

Respiratory substrate-C accounted for *c.* 14% of total plant C across all [CO_2] treatments. By comparison, the average percentage of C in total WSCs in the shoot was 50% across all [CO_2] treatments (Table 3.4.2). The size of the fructan pool (in units of C) was more than two times bigger than the total size of the respiratory substrate pools (Q_1 + Q_2). On average, the size of the sucrose pool was close to that of Q_1, the fast pool, and the size of sum of sucrose, glucose and fructose pools was more than two times greater than that of Q_1, but two times smaller than

Q_2. Again, in comparison, the $T_{1/2}$ of Q_1 was around 5 times longer than that of the sucrose pool (12.7 h vs 2.4 h), but Q_2 had a shorter $T_{1/2}$ than the fructan pool (92.6 h vs 183.6 h).

Table 3.4.2 Plant respiratory substrate pool size and water-soluble carbohydrate (WSC) concentration in the shoot of *L. perenne*. The respiratory substrate system included a fast pool (Q_1) and a slow pool (Q_2), with their sizes predicted from the two-pool compartmental model. Contents of sucrose, fructan, glucose, and fructose were based on a total of 24 (200 and 800 μmol mol^{-1} CO_2) or 48 (400 μmol mol^{-1} CO_2) replicates sampled on days 66 to 69 and 72 after seed imbibition during the 7-dlong labelling experiments. Shown are means with SEs indicated in brackets. Different superscript letters within a row indicate statistically significant differences among CO_2 treatments at P <0.001.

Size	Atmospheric CO_2 concentration (μmol mol^{-1})		
(mg C g^{-1} biomass-C)	200	400	800
Respiratory substrate			
Q_1	34^a (4)	25^b (4)	22^b (3)
Q_2	100^a (43)	116^a (48)	121^a (45)
WSC			
Sucrose	31^a (3)	30^a (1)	30^a (1)
Fructan	351^a (17)	451^b (10)	504^c (26)
Glucose	18^a (2)	15^b (1)	15^b (1)
Fructose	19^a (1)	19.0^a (1)	23^b (1)
Total WSC	418^a (20)	515^b (11)	571^c (27)

Thus, no simple match between carbohydrate fractions and respiratory pool sizes or half-lives were clearly apparent. However, carbohydrates serve not only as a substrate for respiration but also contribute to C skeletons for structural biomass synthesis (i.e. biomass growth). Therefore, the proportion of carbohydrates in biomass should be much greater than that of the respiratory substrate estimated from the tracer kinetics. Thus, assuming that water-soluble carbohydrates (WSCs) were the sole substrate for respiration, only approximately 28% of the WSCs-C was allocated to respiration. Accordingly, the remainder (72%) would be allocated to new (structural) biomass, indicating a carbon use efficiency (CUE) of 72% for the WSCs. This estimate of the CUE of WSCs was greater than that (53%) in the study of Lehmeier et al. (2008). Nevertheless, the CUE reported here was close to the estimate of CUE (~0.6-0.7) calculated by comparing the current photosynthesis and respiration of herbaceous plants in diverse environmental contexts (Thornley, 2011; Gong et al., 2017). In addition, a very high

CUE was estimated for stored carbohydrates in the vegetative plant tissues of wheat during grain filling (Gebbing et al., 1999).

The $T_{1/2}$ of Q_1 (12.7 h) was in a range that corresponds closely to that of the vacuole sucrose pool of C_3 grasses (12 to 24 h; Farrar & Farrar, 1985), indicating that perhaps vacuolar sucrose could have served an essential function in supplying substrate to respiration. In most C_3 and C_4 plant families, vacuolar sucrose in leaf blades and other photosynthetically active tissues is the primary source of assimilation exported to other plant parts during the dark period (Jenner & Rathjen, 1972; Schnyder, 1993; Lunn et al., 1999; Barro et al., 2020). Also, in parallel studies in the same experiment, Dorn (2019) found the highest sucrose concentration in leaf blades at the end of the light period and substantial decreases in that concentration until the end of the dark period. This pattern was not observed in other tissue types, highlighting some carbohydrate-related structural-functional heterogeneity within the whole shoot. At the whole shoot scale, I found no evidence for a vacuole sucrose pool based on the estimate of the $T_{1/2}$ of sucrose (~2.4 h) which was close to that of the cytoplasmic and transport pool of sucrose (see chapter 3.2). Therefore, I can only speculate that perhaps functional-structural heterogeneity within plants may have obscured a better agreement between carbohydrate and respiratory substrate pool features.

Nevertheless, the $T_{1/2}$ and size of Q_2 suggested a long-term organic carbon storage pool. Considering the size of Q_2, fructan was probably the main source of carbon for Q_2, as only its size was larger than Q_2 (Table 3.4.1). This interpretation aligns with that of Lehmeier et al. (2010a), although they only analyzed the pool size of fructan but did not study its labelling kinetics. As already discussed, fructan may supply carbon for the respiratory substrate system via its involvement in the recycling of sucrose (chapter 3.2.). The fact that the half-life of the fructan pool was longer than that of Q_2 (183.6 h compared to 92.6 h), could also be associated with functional structural heterogeneity within plants, or the inclusion and participation of other substrates (non-WSC) to Q_2. It also needs to be acknowledged that tracer kinetics are often unable to resolve pools with half-lives that differ by less than 3-fold, or sometimes even within one order of magnitude (Cheesman, 1986; Lehmeier et al., 2008). For instance, proteins could form a part of Q_2, as their half-lives in the range of 84 to 192 h (Simpson et al., 1981; Dungey & Davies, 1982) are close to that of Q_2. Protein metabolism is intimately connected with respiratory activity (Lea & Ireland, 1999) and products of protein degradation could perhaps serve as an alternative respiratory substrate (Araújo et al., 2011).

Chapter 4 Conclusion and Outlook

This work assessed the performance of the isotope technique in dynamic $^{13}CO_2/^{12}CO_2$ labelling of plant respired CO_2 and carbohydrate fractions under sub-, current-, or double-ambient [CO_2] conditions. The data show that the continuous $^{13}CO_2/^{12}CO_2$ labelling system works well with high accuracy and precision in terms of gas exchange rate and isotope measurements over long experimental periods (up to more than 10 weeks). I demonstrated that contamination of the growth chamber atmosphere, the labelling vessel, was not greater than 4% at all [CO_2] levels analysed, despite intensive sampling and maintenance operations requiring regular access to the chamber interior. In part that precision must have been related to the maintenance of a slight atmospheric overpressure inside the chambers relative to the outside conditions, and the instalment of air-locks that reduced air exchange with the chamber interior when chambers had to be opened. Also, I observed a minimal (max. 2.6%) contamination of carbohydrates during separation with a preparative HPLC system. These minor errors were corrected by using a so-called two-chamber approach to determine the isotopic end-members for the mixing model used to quantify the proportion of labelled and unlabeled C in a sample (gas exchange component, biomass or carbohydrate). Growth conditions inside the growth chambers led to very high fructan concentrations in shoot biomass even at sub-ambient [CO_2], likely due to high photosynthetic activity at high irradiance over long days, and restricted assimilate use in growth processes due to reduced nitrogen availability in the nutrient solution of the hydroponic system used here. A stoichiometrically constrained four-pool compartmental model provided an accurate fit to the whole-shoot carbohydrate (sucrose, fructan, glucose, and fructose) tracer data and yielded an accurate quantitative description of the fundamental features of central carbohydrate metabolism at the shoot scale. This demonstrated that [CO_2] had no significant effect on the half-lives of the different carbohydrate pools. Sucrose re-synthesis from breakdown products of fructan (fructose) was similar in magnitude to sucrose neo-synthesis, but accounted for an increasing proportion of total sucrose synthesis at double-ambient [CO_2]. This result revealed an important constitutive role of fructan in central carbohydrate metabolism, a role that is likely to become even more important at future elevated [CO_2]. It is likely that fructan serves a central and constitutive role in supplying substrate for growth and respiration of C_3 grasses even during undisturbed growth. Dark respiration rate on a ground area basis (canopy respiration) was reduced at sub-ambient [CO_2], but insensitive to ambient or double-ambient [CO_2], broadly aligning with [CO_2] effects on plant biomass production. The interpretation was tentatively supported by the observation that [CO_2] had no significant

effect on the specific respiration rate, i.e. respiration per unit biomass. The tracer kinetics of stand-scale dark respiration were well fitted by a compartmental model that indicated the existence of two pools (Q_1 and Q_2) that orchestrate the respiratory substrate supply system. The sizes and half-lives of both pools were independent of [CO_2]. Pool Q_1 was small in size (equivalent to ~3% of total shoot-C) and had a half-life of approximately half a day. Pool Q_2, termed the respiratory substrate storage pool, had a (specific) size that was equivalent to ~10-12% of total shoot-C, and featured a half-life of approximately four days. Compartmental modelling indicated that ~60% of all respiratory substrate-C cycled through Q_2 at least once independently of [CO_2], meaning that Q_2 was the main source of substrate for whole plant respiration at all [CO_2] levels. A comparative analysis of the tracer kinetics of carbohydrate fractions (at the shoot level) with canopy-scale respiration suggested that sucrose was the mediator substrate that fed metabolic activity connected with respiration, while the role of the fructan pool was indirect, connected through recycling of sucrose. The analysis additionally indicated that the CUE of stored carbohydrates was comparatively high, meaning that <30% of the total water-soluble carbohydrates were lost in respiration.

Based on the methodical and physiological findings of this work, I conclude that the following research topics should be addressed in greater detail in future research. First, my methodological analyses highlight the usefulness of the continuous $^{13}CO_2/^{12}CO_2$ labelling strategy in conjunction with compartmental modelling to quantify the importance of carbon stores in whole plant metabolism in response to environmental drivers, such as CO_2 as studied here. This approach could be expanded in the future to address the physiological role and importance of stores in response to interactive environmental drivers, such as the interaction of nutrient availability and/or temperature with [CO_2]. Second, although a biochemically-based four-pool compartmental model of central carbohydrate metabolism provided a near-perfect fit to the whole-shoot carbohydrate data, the comparison with a compartmental model of the tracer kinetics in whole plant respired CO_2 was not entirely conclusive. This may have been a consequence of not accounting for alternative mediator substrates for respiration (such as protein) or functional-structural heterogeneity (e.g. differences between the locations of greatest carbohydrate storage and metabolic activity). The latter could likely be addressed by tracer kinetic studies at the organ level, with making distinctions between different developmental stages of different plant organs. Thirdly, it could be interesting to combine such studies with investigations of phloem loading and unloading in the source and sink tissues of plants.

Reference

Ainsworth EA, Davey PA, Hymus GJ, Osborne CP, Rogers A, Blum H, Nösberger J, Long SP. 2003. Is stimulation of leaf photosynthesis by elevated carbon dioxide concentration maintained in the long term? A test with Lolium perenne grown for 10 years at two nitrogen fertilization levels under free air CO_2 enrichment (FACE): photosynthetic acclimation of L. perenne to elevated [CO_2]. *Plant, Cell & Environment* **26**: 705–714.

Ainsworth EA, Long SP. 2005. What have we learned from 15 years of free-air CO_2 enrichment (FACE)? A meta-analytic review of the responses of photosynthesis, canopy. *New Phytologist* **165**: 351–371.

Amiard V, Morvan-Bertrand A, Billard J-P, Huault C, Keller F, Prud'homme M-P. 2003. Fructans, but not the sucrosyl-galactosides, raffinose and loliose, are affected by drought stress in perennial ryegrass. *Plant Physiology* **132**: 2218-2229.

Amthor JS. 1991. Respiration in a future, higher-CO_2 world. *Plant, Cell & Environment* **14**: 13-20.

Amthor JS. 1997. Plant respiratory responses to elevated carbon dioxide partial pressure. *Advances in Carbon Dioxide Effects Research* **61**: 35-77.

Araújo WL, Tohge T, Ishizaki K, Leaver CJ, Fernie AR. 2011. Protein degradation–an alternative respiratory substrate for stressed plants. *Trends in Plant Science* **16**: 489-498.

Atkins GL. 1969. Multicompartment models for biological systems. London, UK: Methuen &Co. Ltd.

Ayub G, Smith RA, Tissue DT, Atkin OK. 2011. Impacts of drought on leaf respiration in darkness and light in Eucalyptus saligna exposed to industrial-age atmospheric CO_2 and growth temperature. *New Phytologist* **190**: 1003-1018.

Ayub G, Zaragoza-Castells J, Griffin KL, Atkin OK. 2014. Leaf respiration in darkness and in the light under pre-industrial, current and elevated atmospheric CO_2 concentrations. *Plant Science* **226**: 120-130.

Baca Cabrera JC, Hirl RT, Zhu JJ, Schäufele R, Schnyder H. 2020. Atmospheric CO_2 and VPD alter the diel oscillation of leaf elongation in perennial ryegrass: compensation of hydraulic limitation by stored-growth. *New Phytologist* **227**: 1776-1789.

Baca Cabrera, J.C., Hirl, R.T., Schäufele, R., Zhu, J., Liu, H., Ogée, J. et al. 2021. ^{18}O enrichment of leaf cellulose correlated with ^{18}O enrichment of leaf sucrose but not bulk leaf water in a C_3 grass across contrasts of atmospheric CO_2 concentration and air humidity. https://doi.org/10.21203/rs.3.rs-596094/v1.

Barros KA, Esteves-Ferreira AA, Inaba M, Meally H, Finnan J, Barth S, Davis SJ, Sulpice R. 2020. Diurnal patterns of growth and transient reserves of sink and source tissues are affected by cold nights in barley. *Plant, Cell & Environment*.

Bassham JA, Benson AA, Calvin M. 1950. The path of carbon in photosynthesis VIII. The role of malic acid. *Journal of Biological Chemistry* **185**: 781-787.

Borland AM, Farrar JF. 1988. Compartmentation and fluxes of carbon in leaf blades and leaf sheaths of *Poa annua L.* and *Poa x jemtlandica* (Almq.) Richt. *Plant, Cell & Environment* **11**: 535-543.

Bowling DR, Pataki DE, Randerson JT. 2008. Carbon isotopes in terrestrial ecosystem pools and CO_2 fluxes. *New Phytologist* **178**: 24-40.

Cairns AJ, Begley P, Sims IM. 2002. The structure of starch from seeds and leaves of the fructan- accumulating ryegrass, *Lolium temulentum*. *Journal of Plant Physiology* **159**: 221-230.

Casella E, Soussana JF. 1997. Long-term effects of CO_2 enrichment and temperature increase on the carbon balance of a temperate grass sward. *Journal of Experimental Botany* **48**: 1309– 1321.

Cernusak LA, Tcherkez G, Keitel C, Cornwell WK, Santiago LS, Knohl A, Barbour MM, Williams DG, Reich PB, Ellsworth DS, *et al.* 2009. Why are non-photosynthetic tissues generally ^{13}C enriched compared with leaves in C_3 plants? Review and synthesis of current hypotheses. *Functional Plant Biology* **36**: 199-213.

Cernusak LA, Ubierna N, Winter K, Holtum JA, Marshall JD, Farquhar GD. 2013. Environmental and physiological determinants of carbon isotope discrimination in terrestrial plants. *New Phytologist* **200**: 950-965.

Chalmers J, Lidgett A, Cummings N, Cao Y, Forster J, Spangenberg G. 2005. Molecular genetics of fructan metabolism in perennial ryegrass. *Plant Biotechnol Journal* **3**: 459-474.

Chapin III FS, Schulze ED, Mooney HA. 1990. The ecology and economics of storage in plants. *Annual Review of Ecology and Systematics* **21**: 423-447.

Chapman DF, Bryant JR, Olayemi ME, Edwards GR, Thorrold BS, McMillan WH, Kerr GA, Judson G, Cookson T, Moorhead A, *et al*. 2017. An economically based evaluation index for perennial and short-term ryegrasses in New Zealand dairy farm systems. *Grass and Forage Science* **72**: 1-21.

Chaves MM, Maroco JP, Pereira JS. 2003. Understanding plant responses to drought—from genes to the whole plant. *Functional Plant Biology* **30**: 239-264.

Dippery JK, Tissue DT, Thomas RB, Strain BR. 1995. Effects of low and elevated CO_2 on C_3 and C_4 annuals. I. Growth and biomass allocation. *Oecologia* **101**: 13– 20.

Dorn L. 2019. Die Wirkung der atmosphärischen CO_2-Konzentration auf die tageszeitliche Dynamik derwasserlöslichen Kohlenhydrate in Source-, Sink und Reserveorganen von Deutschem Weidelgras (*Lolium perenne* L.). Master thesis, Technical University of Munich, Munich, Germany.

Drake BG, Gonzàlez-Meler MA, Long SP. 1997. More efficient plants: a consequence of rising atmospheric CO_2? *Annual Review of Plant Physiology and Plant Molecular Biology* **48**: 609– 639.

Du YL, Zhao Q, Chen LR, Yao XD, Zhang W, Zhang B, Xie FT. 2020. Effect of drought stress on sugar metabolism in leaves and roots of soybean seedlings. *Plant Physiology and Biochemistry* **146**: 1-12.

Dungey NO, Davies DD 1982. Protein turnover in isolated barley leaf segments and the effects of stress. *Journal of Experimental Botany* **33**: 12-20.

Epstein S, Zeiri L. 1988. Oxygen and carbon isotopic compositions of gases respired by humans. *Proceedings of the National Academy of Sciences* **85**: 1727-1731.

Evans JR, Sharkey TD, Berry JA, Farquhar GD. 1986. Carbon isotope discrimination measured concurrently with gas exchange to investigate CO_2 diffusion in leaves of higher plants. *Functional Plant Biology* **13**: 281-292.

Farquhar GD, Richards RA. 1984. Isotopic composition of plant carbon correlates with water-use efficiency of wheat genotypes. *Functional Plant Biology* **11**: 539-552.

Farquhar GD, Ehleringer JR, Hubick KT. 1989. Carbon isotope discrimination and photosynthesis. *Annual Review of Plant Biology and Plant Molecular Biology* **40**: 503-537.

Farrar J, Pollock C, Gallagher J. 2000. Sucrose and the integration of metabolism in vascular plants. *Plant Science* **154**: 1-11.

Farrar SC, Farrar JF. 1985. Carbon fluxes in leaf blades of barley. *New Phytologist* **100**: 271-283.

Farrar SC, Farrar JF. 1986. Compartmentation and fluxes of sucrose in intact leaf blades of barley. *New Phytologist* **103**: 645-657.

Franks PJ, Adams MA, Amthor JS, Barbour MM, Berry JA, Ellsworth DS, Farquhar GD, Ghannoum O, Lloyd J, McDowell N *et al.* 2013. Sensitivity of plants to changing atmospheric CO_2 concentration: from the geological past to the next century. *New Phytologist* **197**: 1077–1094.

Gamnitzer U, Schäufele R, Schnyder H. 2009. Observing ^{13}C labelling kinetics in CO_2 respired by a temperate grassland ecosystem. *New Phytologist* **184**: 376-386.

Gebbing T, Schnyder H. 2001. ^{13}C labeling kinetics of sucrose in glumes indicates significant refixation of respiratory CO_2 in the wheat ear. *Functional Plant Biology* **28**: 1047-1053.

Gebbing T, Schnyder H, Kühbauch W. 1998. Carbon mobilization in shoot parts and roots of wheat during grain filling: assessment by $^{13}C/^{12}C$ steady-state labelling, growth analysis and balance sheets of reserves. *Plant, Cell & Environment* **21**: 301-313.

Gebbing T, Schnyder H, Kühbauch W. 1999. The utilization of pre-anthesis reserves in grain filling of wheat. Assessment by steady-state $^{13}CO_2/^{12}CO_2$ labelling. *Plant, Cell & Environment* **22**: 851-858.

Geigenberger P, Stitt M. 1991. A "futile" cycle of sucrose synthesis and degradation is involved in regulating partitioning between sucrose, starch and respiration in cotyledons of germinating *Ricinus communis* L. seedlings when phloem transport is inhibited. *Planta* **185**: 81-90.

Geiger DR, Ploeger BJ, Fox TC, Fondy BR. 1983. Sources of sucrose translocated from illuminated sugar beet source leaves. *Plant Physiology* **72**: 964-970.

Geiger DR, Swanson C. 1965a. Evaluation of selected parameters in a sugar beet translocation system. *Plant Physiology* **40**: 942.

Geiger DR, Swanson C. 1965b. Sucrose translocation in the sugar beet. *Plant Physiology* **40**: 685.

Ghashghaie J, Badeck FW. 2014. Opposite carbon isotope discrimination during dark respiration in leaves versus roots–a review. *New Phytologist* **201**: 751-769.

Ghirardo A, Gutknecht J, Zimmer I, Brüggemann N, Schnitzler J-P. 2011. Biogenic volatile organic compound and respiratory CO_2 emissions after ^{13}C-labeling: online tracing of C translocation dynamics in poplar plants. *PLoS One* **6**: e17393.

Giaquinta RT. 1979. Sucrose translocation and storage in the sugar beet. *Plant Physiology* **63**: 828-832.

Giaquinta RT. 1983. Phloem loading of sucrose. *Annual Review of Plant Physiology* **34**: 347-387.

Goldschmidt EE, Huber SC. 1992. Regulation of photosynthesis by end-product accumulation in leaves of plants storing starch, sucrose, and hexose sugars. *Plant Physiology* **99**: 1443-1448.

Gong XY, Schäufele R, Feneis W, Schnyder H. 2015. $^{13}CO_2/^{12}CO_2$ exchange fluxes in a clamp-on leaf cuvette: disentangling artefacts and flux components. *Plant Cell & Environment* **38**: 2417-2432.

Gong XY, Schäufele R, Lehmeier CA, Tcherkez G, Schnyder H. 2017. Atmospheric CO2 mole fraction affects stand-scale carbon use efficiency of sunflower by stimulating respiration in light. *Plant, Cell & Environment* **40**: 401-412.

González J, Remaud G, Jamin E, Naulet N, Martin GG. 1999. Specific natural isotope profile studied by isotope ratio mass spectrometry (SNIP− IRMS): $^{13}C/^{12}C$ ratios of

fructose, glucose, and sucrose for improved detection of sugar addition to pineapple juices and concentrates. *Journal of Agricultural and Food Chemistry* **47**: 2316-2321.

Gordon AJ, Ryle GJA, WEBB G. 1980. The relationship between sucrose and starch during 'dark'export from leaves of uniculm barley. *Journal of Experimental Botany* **31**: 845-850.

Graf A, Smith AM. 2011. Starch and the clock: the dark side of plant productivity. *Trends in Plant Science* **16**: 169-175.

Heldt HW. 2005. *Plant Biochemistry.* San Diego, USA: Elsevier Akademic Press.

Hirl RT, Schnyder H, Ostler U, Schäufele R, Schleip I, Vetter SH, Auerswald K, Baca Cabrera JC, Wingate L, Barbour MM, *et al.* 2019. The ^{18}O ecohydrology of a grassland ecosystem–predictions and observations. *Hydrology and Earth System Sciences* **23**: 2581-2600.

Högy P, Brunnbauer M, Koehler P, Schwadorf K, Breuer J, Franzaring J, Zhunusbayeva D, Fangmeier A. 2013. Grain quality characteristics of spring wheat (*Triticum aestivum*) as affected by free-air CO_2 enrichment. *Environmental and Experimental Botany* **88**: 11-18.

Högy P, Wieser H, Köhler P, Schwadorf K, Breuer J, Franzaring J, Muntifering R, Fangmeier A. 2009. Effects of elevated CO_2 on grain yield and quality of wheat: results from a 3-year free-air CO_2 enrichment experiment. *Plant Biology* **11**: 60-69.

Huber SC. 1989. Biochemical mechanism for regulation of sucrose accumulation in leaves during photosynthesis. *Plant Physiology* **91**: 656-662.

IPCC. 2007. Summary for Policymakers. In: Solomon S, Qin D, Manning M, Chen Z, Marquis M, Averyt KB, Tignor M, Miller HL, eds. *Climate Change 2007: The Physical Sciences. Contribution of Working Group 1 to the Fourth Assessment Report of the Intergovernmental Panel on Climate Change*. Cambridge, UK: Cambridge University Press

Isopp H, Frehner M, Long SP, Nösberger J. 2000. Sucrose-phosphate synthase responds differently to source-sink relations and to photosynthetic rates: *Lolium perenne* L. growing at elevated pCO_2 in the field. *Plant, Cell & Environment* **23**: 597-607.

Jacquez JA. 1972. *Compartmental Analysis in Biology and Medicine.* Ann Arbor, USA: Biomedware.

Jahnke S, Stöcklin G, Willenbrink J. 1981. Translocation profiles of ^{11}C-assimilates in the petiole of *Marsilea quadrifolia L.*. *Planta* **153**: 56-63.

Jenner CF, Rathjen AJ. 1972. Factors limiting the supply of sucrose to the developing wheat grain. *Annals of Botany* **36**: 729-741.

KavanovA M, Lattanzi FA, Schnyder H. 2008. Nitrogen deficiency inhibits leaf blade growth in *Lolium perenne* by increasing cell cycle duration and decreasing mitotic and post-mitotic growth rates. *Plant, Cell & Environment* **31**: 727-737.

Kimball BA, Kobayashi K, Bindi M. 2002. Responses of agricultural crops to free-air CO_2 enrichment. *Advances in Agronomy*: Elsevier, 293-368.

Klumpp K, Schäufele R, Lötscher M, Lattanzi FA, Feneis W, Schnyder H. 2005. C-isotope composition of CO_2 respired by shoots and roots: fractionation during dark respiration? *Plant, Cell & Environment* **28**: 241-250.

Körner C. 2000. Biosphere responses to CO_2 enrichment. *Ecological Applications* **10**: 1590-1619.

Kölling K, Müller A, Flütsch P, Zeeman SC. 2013. A device for single leaf labelling with CO_2 isotopes to study carbon allocation and partitioning in *Arabidopsis thaliana*. *Plant Methods* **9**: 1-12.

Kruger NJ, Le Lay P, Ratcliffe RG. 2007. Vacuolar compartmentation complicates the steady-state analysis of glucose metabolism and forces reappraisal of sucrose cycling in plants. *Phytochemistry* **68**: 2189-2196.

Kühbauch W, Thome U. 1989. Nonstructural carbohydrates of wheat stems as influenced by sink-source manipulations. *Journal of Plant Physiology* **134**: 243-250.

Kuptz D, Fleischmann F, Matyssek R, Grams TE. 2011. Seasonal patterns of carbon allocation to respiratory pools in 60-yr-old deciduous (*Fagus sylvatica*) and evergreen (*Picea abies*) trees assessed via whole-tree stable carbon isotope labeling. *New Phytologist* **191**: 160-172.

Lattanzi FA, Ostler U, Wild M, Morvan-Bertrand A, Decau M-L, Lehmeier CA, Meuriot F, Prud'homme M-P, Schäufele R, Schnyder H. 2012. Fluxes in central carbohydrate metabolism of source leaves in a fructan-storing C_3 grass: rapid turnover and futile cycling of sucrose in continuous light under contrasted nitrogen nutrition status. *Journal of Experimental Botany* **63**: 2363-2375.

Lattanzi FA, Schnyder H, Thornton B. 2005. The sources of carbon and nitrogen supplying leaf growth. Assessment of the role of stores with compartmental models. *Plant Physiology* **137**: 383-395.

Lea PJ, Ireland RJ. 1999. Nitrogen metabolism in higher plants. In: Singh BK, ed. *Plant amino acids.* New York, Ny, USA: Marcel Dekker, 1-47.

LeBauer DS, Treseder KK. 2008. Nitrogen limitation of net primary productivity in terrestrial ecosystems is globally distributed. *Ecology* **89**: 371-379.

Lehmeier CA, Lattanzi FA, Gamnitzer U, Schäufele R, Schnyder H. 2010a. Day-length effects on carbon stores for respiration of perennial ryegrass. *New Phytologist* **188**: 719-725.

Lehmeier CA, Lattanzi FA, Schäufele R, Schnyder H. 2010b. Nitrogen deficiency increases the residence time of respiratory carbon in the respiratory substrate supply system of perennial ryegrass. *Plant, Cell & Environment* **33**: 76-87.

Lehmeier CA, Lattanzi FA, Schäufele R, Wild M, Schnyder H. 2008. Root and shoot respiration of perennial ryegrass are supplied by the same substrate pools: assessment by dynamic ^{13}C labeling and compartmental analysis of tracer kinetics. *Plant Physiology* **148**: 1148-1158.

Lemoine R. 2000. Sucrose transporters in plants: update on function and structure. *Biochimica et Biophysica Acta (BBA)-Biomembranes* **1465**: 246-262.

Long SP, Ainsworth EA, Leakey ADB, Nösberger J, Ort DR. 2006. Food for thought: lower-than-expected crop yield stimulation with rising CO_2 concentrations. *Science* **312**: 1918-1921.

Lötscher M, Klumpp K, Schnyder H. 2004. Growth and maintenance respiration for individual plants in hierarchically structured canopies of Medicago sativa and Helianthus annuus: the contribution of current and old assimilates. *New Phytologist* 164: 305–316.

Ludwig LJ, Canvin DT. 1971. The rate of photorespiration during photosynthesis and the relationship of the substrate of light respiration to the products of photosynthesis in sunflower leaves. *Plant Physiology* **48**: 712-719.

Lunn JE, Furbank RT. 1999. Tansley Review No. 105. Sucrose biosynthesis in C_4 plants. *New Phytologist* **143**: 221-237.

Lüscher A, Daepp M, Blum H, Hartwig UA, Nösberger J. 2004. Fertile temperate grassland under elevated atmospheric CO_2 - role of feed-back mechanisms and availability of growth resources. *European Journal of Agronomy* **21**: 379-398.

Marcelis LF. 1996. Sink strength as a determinant of dry matter partitioning in the whole plant. *Journal of Experimental Botany* 47: 1281-1291.

Martínez-Vilalta J, Sala A, Asensio D, Galiano L, Hoch G, Palacio S, Piper FI, Lloret F. 2016. Dynamics of non-structural carbohydrates in terrestrial plants: a global synthesis. *Ecological Monographs* **86**: 495-516.

McGrath VB, Blakeney AB, Batten GD. 1997. Fructan to nitrogen ratio as an indicator of nutrient stress in wheat crops. *New Phytologist* **136**: 145-152.

Mendiburu F. 2020. *Agricolae: statistical procedures for agricultural research*. R package v.1.3-3. [WWW document] URL https://cran.r-project.org/web/packages/agricolae/index.html [accessed 15 July 2018].

Moore BD, Cheng SH, Sims D, Seemann JR. 1999. The biochemical and molecular basis for photosynthetic acclimation to elevated atmospheric CO_2. *Plant, Cell & Environment* **22**: 567-582.

de Moraes MG, de Carvalho MAM, Franco AC, Pollock CJ, Figueiredo-Ribeiro RDCL. 2016. Fire and drought: soluble carbohydrate storage and survival mechanisms in herbaceous plants from the Cerrado. *BioScience* **66**: 107-117.

Morvan-Bertrand A, Boucaud J, Le Saos JL, Prud'homme M-P. 2001. Roles of the fructans from leaf sheaths and from the elongating leaf bases in the regrowth following defoliation of *Lolium perenne* L.. *Planta* **213**: 109-120.

Muller B, Pantin F, Génard M, Turc O, Freixes S, Piques M, Gibon Y. 2011. Water deficits uncouple growth from photosynthesis, increase C content, and modify the relationships between C and growth in sink organs. *Journal of Experimental Botany* **62**: 1715-1729.

Nelson CJ, Spollen WG. 1987. Fructans. *Physiologia Plantarum* **71**: 512-516.

Nguyen-Quoc B, Foyer CH. 2001. A role for 'futile cycles' involving invertase and sucrose synthase in sucrose metabolism of tomato fruit. *Journal of Experimental Botany* **52**: 881-889.

Noël GM, Pontis HG. 2000. Involvement of sucrose synthase in sucrose synthesis during mobilization of fructans in dormant Jerusalem artichoke tubers. *Plant Science* **159**: 191-195.

Nogués S, Tcherkez G, Cornic G, Ghashghaie J. 2004. Respiratory carbon metabolism following illumination in intact French bean leaves using $^{13}C/^{12}C$ isotope labeling. *Plant Physiology* **136**: 3245-3254.

Ostler U, Schleip I, Lattanzi FA, Schnyder H. 2016. Carbon dynamics in aboveground biomass of co-dominant plant species in a temperate grassland ecosystem: same or different? *New Phytologist* **210**: 471-484.

Pavis N, Chatterton NJ, Harrison PA, Baumgartner S, Praznik W, Boucaud J, Prud'Homme MP. 2001. Structure of fructans in roots and leaf tissues of *Lolium perenne*. *New Phytologist* **150**: 83-95.

Pollock CJ, Cairns AJ. 1991. Fructan metabolism in grasses and cereals. *Annual Review of Plant Biology* **42**: 77-101.

Pollock CJ, Jones T. 1979. Seasonal patterns of fructan metabolism in forage grasses. *New Phytologist* **83**: 9-15.

Poorter H, Gifford RM, Kriedemann PE, Wong SC. 1992. A quantitative-analysis of dark respiration and carbon content as factors in the growth-response of plants to elevated CO_2. *Australian Journal of Botany* **40**: 501-513.

Rocher JP, Prioul JL. 1987. Compartmental analysis of assimilate export in a mature maize leaf. *Plant Physiology and Biochemistry* **25**: 531-540.

R Cor Team. 2019. *R: A language and environment for statistical computing*. Vienna, Austria: R Foundation for Statistical Computing. URL http://www.r-project.org.

RStudio Team. 2016. *RStudio: Integrated Development for R.* Boston, USA: RStudio, Inc. URL http://www.rstudio.com.

Rogers A, Ainsworth EA 2006. The response of foliar carbohydrates to elevated [CO_2]. In: Nösberger J., Long SP, Blum H., Norby RJ, Hendrey GR, Stitt M, eds. *Managed Ecosystems and CO_2 Case Studies, Processes and Perspectives*. Berlin, Germany: Springer, 298-308.

Ruan YL. 2012. Signaling role of sucrose metabolism in development. *Molecular Plant* **5**: 763-765.

Ruan YL. 2014. Sucrose metabolism: gateway to diverse carbon use and sugar signaling. *Annual Review of Plant Biology* **65**: 33-67.

Ryle GJA, Powell CE, Tewson V. 1992. Effect of elevated CO_2 on the photosynthesis, respiration and growth of perennial ryegrass. *Journal of Experimental Botany* **43**: 811-818.

Sage RF, Reid CD. 1992. Photosynthetic acclimation to sub-ambient CO_2 (20 Pa) in the C_3 annual *Phaseolus vulgaris* L. *Photosynthetica* **27**: 605-617.

Sage RF, Cowling SA. 1999. Implications of stress in low CO_2 atmospheres of the past: are today's plants too conservative for a high CO_2 world? *In*: Y Luo, HA Mooney, eds. Carbon dioxide and environmental stress. San Diego, CA, USA: Academic Press, 289– 308.

Sage RF, Coleman JR. 2001. Effects of low atmospheric CO_2 on plants: more than a thing of the past. *Trends in Plant Science* **6**: 18-24.

Savitch LV, Harney T, Huner NP. 2000. Sucrose metabolism in spring and winter wheat in response to high irradiance, cold stress and cold acclimation. *Physiologia Plantarum* **108**: 270-278.

Schleip I, Lattanzi FA, Schnyder H. 2013. Common leaf life span of co-dominant species in a continuously grazed temperate pasture. *Basic and Applied Ecology* **14**: 54-63.

Schnyder H, Nelson CJ. 1987. Growth rates and carbohydrate fluxes within the elongation zone of tall fescue leaf blades. *Plant Physiology* **85**: 548-553.

Schnyder H. 1992. Long-term steady-state labelling of wheat plants by use of natural $^{13}CO_2/^{12}CO_2$ mixtures in an open, rapidly turned-over system. *Planta* **187**: 128-135.

Schnyder H. 1993. The role of carbohydrate storage and redistribution in the source-sink relations of wheat and barley during grain filling—a review. *New Phytologist* **123**: 233-245.

Schnyder H, Schäufele R, Lötscher M, Gebbing T. 2003. Disentangling CO_2 fluxes: Direct measurements of mesocosm-scale natural abundance $^{13}CO_2/^{12}CO_2$ gas exchange, ^{13}C discrimination, and labelling of CO_2 exchange flux components in controlled environments. *Plant, Cell & Environment* **26**: 1863-1874.

Schnyder H, Lattanzi FA. 2005. Partitioning respiration of C_3-C_4 mixed communities using the natural abundance ^{13}C approach-testing assumptions in a controlled environment. *Plant Biology* **7**: 592-600.

Schnyder H, Ostler U, Lehmeier C, Wild M, Morvan-Bertrand A, Schäufele R, Lattanzi F 2012. Tracing carbon fluxes: resolving complexity using isotopes. In: Matyssek R, Schnyder H, Oßwald W, Ernst D, Munch JC, Pretzsch H, eds. *Growth and Defence in Plants.* Berlin, Heidelberg, Germany: Springer, 157–173.

Schnyder H, Ostler U, Lehmeier CA 2017. Respiratory turn-over and metabolic compartments: from the design of tracer experiments to the characterization of respiratory substrate-supply systems. In: Tcherkez G, Ghashghaie J, eds. *Plant Respiration: Metabolic Fluxes and Carbon Balance. Advances in Photosynthesis and Respiration (including Bioenergy and Related Processes), vol 43.* Cham, Switzerland: Springer, 161-179.

Simpson E, Cooke RJ, Davies DD. 1981. Measurement of protein degradation in leaves of *Zea mays* using [^{3}H] acetic anhydride and tritiated water. *Plant Physiology* **67**: 1214-1219.

Smart DR, Chatterton NJ, Bugbee B. 1994. The influence of elevated CO_2 on non-structural carbohydrate distribution and fructan accumulation in wheat canopies. *Plant, Cell & Environment* **17**: 435-442.

Smith AM, Stitt M. 2007. Coordination of carbon supply and plant growth. *Plant, Cell & Environment* **30**: 1126-1149.

Smouter H, Simpson RJ. 1991. Fructan metabolism in leaves of *Lolium rigidum* Gaudin: I. Synthesis of fructan. *New Phytologist* **119**: 509-516.

Sprenger N, Bortlik K, Brandt A, Boller T, Wiemken A. 1995. Purification, cloning, and functional expression of sucrose: fructan 6-fructosyltransferase, a key enzyme of fructan synthesis in barley. *Proceedings of the National Academy of Sciences* **92**: 11652-11656.

Stitt M. 1991. Rising CO_2 levels and their potential significance for carbon flow in photosynthetic cells. *Plant, Cell & Environment* **14**: 741-762.

Stitt M, Huber S, Kerr P 1987. Control of photosynthetic sucrose formation. In: Hatch MD, Boardman NK, eds. *The Biochemistry of Plants: a Comprehensive Treatise*. New York, USA: Academic Press, 327-409.

Stitt M, Zeeman SC. 2012. Starch turnover: pathways, regulation and role in growth. *Current Opinion in Plant Biology* **15**: 282-292.

Sulpice R, Pyl ET, Ishihara H, Trenkamp S, Steinfath M, Witucka-Wall H, Gibon Y, Usadel B, Poree F, Piques MC, *et al.* 2009. Starch as a major integrator in the regulation of plant growth. *Proceedings of the National Academy of Sciences* **106**: 10348-10353.

Tcherkez G, Boex-Fontvieille E, Mahé A, Hodges M. 2012. Respiratory carbon fluxes in leaves. *Current Opinion in Plant Biology* **15**: 308-314.

Terrer C, Vicca S, Hungate BA, Phillips RP, Prentice IC. 2016. Mycorrhizal association as a primary control of the CO_2 fertilization effect. *Science* **353**: 72– 74.

Terrer C, Jackson RB, Prentice IC, Keenan TF, Kaiser C, Vicca S, Fisher JB, Reich PB, Stocker BD, Hungate BA. 2019. Nitrogen and phosphorus constrain the CO_2 fertilization of global plant biomass. *Nature Climate Change* **9**: 684-689.

Thomas H, James AR. 1999. Partitioning of sugars in *Lolium perenne* (perennial ryegrass) during drought and on rewatering. *New Phytologist* **142**: 295-305.

Thornley JH. 2011. Plant growth and respiration re-visited: maintenance respiration defined–it is an emergent property of, not a separate process within, the system–and why the respiration: photosynthesis ratio is conservative. *Annals of Botany* **108**: 1365-1380.

Tissue DT, Griffen KL, Thomas RB, Strain BR. 1995. Effects of low and elevated CO_2 on C_3 and C_4 annuals. II. Photosynthesis and leaf biochemistry. *Oecologia* **101**: 21– 28.

Trumbore S. 2006. Carbon respired by terrestrial ecosystems–recent progress and challenges. *Global Change Biology* **12**: 141-153.

Verbančič J, Lunn JE, Stitt M, Persson S. 2018. Carbon supply and the regulation of cell wall synthesis. *Molecular Plant* **11**: 75-94.

Wagner W, Keller F, Wiemken A. 1983. Fructan metabolism in cereals: induction in leaves and compartmentation in protoplasts and vacuoles. *Zeitschrift für Pflanzenphysiologie* **112**: 359-372.

Wagner W, Wiemken A, Matile P. 1986. Regulation of fructan metabolism in leaves of barley (*Hordeum vulgare L. cv Gerbel*). *Plant Physiology* **81**: 444-447.

Ward JM, Kühn C, Tegeder M, Frommer WB. 1997. Sucrose transport in higher plants. *International Review of Cytology* **178**: 41-71.

Wickham H 2016. *ggplot2: elegant graohics for data analysis.* New York, USA: Springer.

Windt CW, Vergeldt FJ, De Jager PA, Van As H. 2006. MRI of long-distance water transport: a comparison of the phloem and xylem flow characteristics and dynamics in poplar, castor bean, tomato and tobacco. *Plant, Cell & Environment* **29**: 1715-1729.

Xu ZZ, Jiang YL, Zhou GS. 2015. Response and adaptation of photosynthesis, respiration, and antioxidant systems to elevated CO_2 with environmental stress in plants. *Frontiers in Plant Science* **6**: 701.

Yang F, Gong XY, Liu HT, Schäufele R, Schnyder H. 2016. Effects of nitrogen and vapour pressure deficit on phytomer growth and development in a C_4 grass. *AoB Plants* **8**.

Zhao HY, Sun SM, Zhang LH, Yang JJ, Wang ZY, Ma FW, Li MJ. 2020. Carbohydrate metabolism and transport in apple roots under nitrogen deficiency. *Plant Physiology and Biochemistry* **155:** 455-46.

Acknowledgements

I am sincerely grateful to my supervisor, Prof. Hans Schnyder, for all his support throughout my PhD studies. I thank him very much, first, for offering me the chance to join the Grassland group for PhD studies, for his patient guidance and beneficial support on both English and science through these 5 years. I believe I can benefit from this support not only now but also in my future career.

I want to express my sincere gratitude to Prof. Karl Auerswald for inspiring discussions and indispensable points of views on my research topic. I also would like to express my sincere gratitude to my fellow PhD students Regina and Juan. We created a happy and friendly work environment, and finally completed the research project. I really treasure our friendship. Thank you, Rudi, Christoph, and Ulli, for providing helpful discussions and precise measurements of the samples. Thank you also to all of my colleagues in the lab and office， Richard Wenzel, Anja Schmidt, Monika Michler, Wolfgang Feneis, Hans Vogl, and Cordula Hertwig.

I would like to extend my appreciation to those who have provided me with unwavering support throughout my life, including my family and friends. I want to offer a special acknowledgement to Qingxu, my partner for so many years, whose affectionate support has been indispensable in enabling me to achieve my goals.

Last but not least, I gratefully acknowledge financial support from the China Scholarship Council (CSC).

Lebenslauf

Persönliche Angaben

Name	Jianjun Zhu
Geburtstag und –ort	08. June 1989 in Shandong, China
Nationalität	Chinese
Familienstand	Ledig

Ausbildung

09/2008-07/2012	Studium Grünlandlehre, Shandong Landwirtschaftliche Universität, Taian, Shandong, China Abschluss: B.Sc
09/2013-07/2017	Studium Ökologie, Institut für Botanik, Chinesische Akademie der Wissenschaften, Beijing, China Abschluss: M.Sc
10/2017- /2022	Doktorand, Lehrstuhl für Grünlandlehre, Technische Universität München

Atmospheric CO_2 and VPD alter the diel oscillation of leaf elongation in perennial ryegrass: compensation of hydraulic limitation by stored-growth

Juan C. Baca Cabrera, Regina T. Hirl, Jianjun Zhu, Rudi Schäufele and Hans Schnyder

Lehrstuhl für Grünlandlehre, Technische Universität München, Alte Akademie 12, Freising-Weihenstephan 85354, Germany

Authors for correspondence:
Juan C. Baca Cabrera
Tel: +49 (0)8161 715021
Email: juan.baca@tum.de

Hans Schnyder
Tel: +49 (0)8161 715165
Email: schnyder@wzw.tum.de

Received: *12 February 2020*
Accepted: *26 April 2020*

New Phytologist (2020) **227:** 1776–1789
doi: 10.1111/nph.16639

Key words: CO_2, diurnal oscillation, leaf growth, leaf water potential, *Lolium perenne* (perennial ryegrass), osmotic potential, vapor pressure deficit (VPD), water-soluble carbohydrates.

Summary

- We explored the effects of atmospheric CO_2 concentration (C_a) and vapor pressure deficit (VPD) on putative mechanisms controlling leaf elongation in perennial ryegrass.
- Plants were grown in stands at a C_a of 200, 400 or 800 μmol mol^{-1} combined with high (1.17 kPa) or low (0.59 kPa) VPD during the 16 h-day in well-watered conditions with reduced nitrogen supply. We measured day : night-variation of leaf elongation rate (LER_{day} : LER_{night}), final leaf length and width, epidermal cell number and length, stomatal conductance, transpiration, leaf water potential and water-soluble carbohydrates and osmotic potential in the leaf growth-and-differentiation zone (LGDZ).
- Daily mean LER or morphometric parameters did not differ between treatments, but LER_{night} strongly exceeded LER_{day}, particularly at low C_a and high VPD. Across treatments LER_{day} was negatively related to transpiration ($R^2 = 0.75$) and leaf water potential ($R^2 = 0.81$), while LER_{night} was independent of leaf water potential or turgor. Enhancement of LER_{night} over LER_{day} was proportional to the turgor-change between day and night ($R^2 = 0.93$). LGDZ sugar concentration was high throughout diel cycles, providing no evidence of source limitation in any treatment.
- Our data indicate a mechanism of diel cycling between daytime hydraulic and night-time stored-growth controls of LER, buffering C_a and daytime VPD effects on leaf elongation.

Introduction

Leaf growth is an integrating plant process (Van Volkenburgh, 1999): leaves intercept light, transpire H_2O and assimilate CO_2 in photosynthesis, supporting the growth and maintenance requirements of all parts of the plant. Conversely, leaf growth is sensitive to plant water status, which is influenced by transpiration, and depends on adequate supplies of assimilates and nutrients. As photosynthesis and transpiration respond to changing atmospheric CO_2 concentration (C_a) and humidity, one may expect fundamental effects on leaf growth (Fig. 1). Surprisingly, however, the scientific literature does not report general strong effects of atmospheric CO_2 on leaf growth (see paragraph 3 in this section), or other morphological features, particularly in conditions with growth-limiting nitrogen fertilizer availability (Reich *et al.*, 2014), a typical situation for many terrestrial ecosystems, including grassland (LeBauer & Treseder, 2008).

Grasses provide a convenient model for studies of leaf growth, as the leaf growth-and-differentiation zone (LGDZ) is physically separated from the photosynthesizing and transpiring leaf tissues. The LGDZ is non-transpiring and entirely dependent on assimilate import, as it is enclosed within the whorl of sheaths of older fully-expanded leaves (Fig. 1). Continuous cell production, expansion and differentiation in the LGDZ generate an efflux of near-fully mature and photosynthetically competent tissue from the enclosing sheath (Fig. 1). Leaf elongation rate is equivalent to the integral of (axial) cell expansion rates within a cell file spanning the length of the leaf growth zone (Schnyder *et al.*, 1990). Cell expansion depends on a close coordination of several processes and state variables, including (1) cell turgor pressure that causes a tensional stress in the primary cell wall, which stretches irreversibly when a given yield threshold is exceeded, (2) passive water flow into the expanding cell driven by the water potential gradient between the cell and the water source, (3) maintenance of this gradient by continuous adjustment of the cell osmoticum, which – in turn – generates turgor pressure, and (4) metabolic processes involved in cell wall deposition and loosening, as well as synthesis of intracellular constituents (e.g. Lockhart, 1965; Ray *et al.*, 1972; Barlow, 1986; Passioura & Fry, 1992; Martre *et al.*, 1999; Tardieu *et al.*, 1999; Pantin *et al.*, 2012; Cosgrove, 2018).

Photosynthesis of C_3 plants is not saturated with CO_2 at sub-ambient and present-day C_a (Bowes, 1993; Ainsworth & Rogers, 2007), raising the question if leaf growth can be limited, in principle, by the availability of assimilates (Ainsworth & Rogers, 2007), at least at the C_a of the Last Glacial Maximum (≈ 200 μmol mol^{-1}; Lüthi *et al.*, 2008). In fact, increased carbon

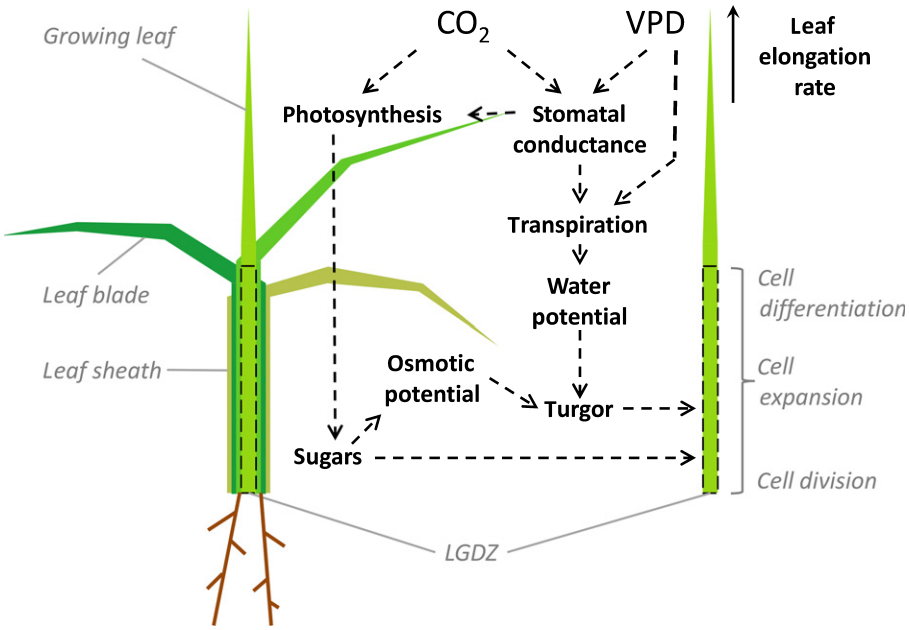

Fig. 1 Schematic illustration of source and hydraulic effects of atmospheric CO_2 concentration and vapor pressure deficit (VPD) on photosynthesis–transpiration–leaf growth physiological relationships in a vegetative grass plant (adapted from Fig. 1 in Liu *et al*., 2017). The leaf growth-and-differentiation zone (LGDZ) is fully enclosed within the sheaths of fully-expanded leaves and comprises successive zones of cell division, expansion and differentiation arranged along the longitudinal axis of the leaf. Leaf elongation is determined by (axial) cell expansion, enabled by turgor pressure-driven water uptake. Turgor pressure is the difference between osmotic potential and water potential. Stomatal conductance is sensitive to VPD and CO_2 and represents the physiological control of transpiration that affects water potential in the growth zone. Photosynthesis is influenced directly by CO_2 and indirectly by the CO_2 effect on stomatal conductance, and may act on assimilate supply to the leaf growth zone (source-limitation) as well as on the contribution of sugars (water-soluble carbohydrates) to the osmotic potential of expanding cells.

supply at elevated C_a tends to enhance leaf elongation via the stimulation of cell expansion, cell production or both (Ferris & Taylor, 1994; Ranasinghe & Taylor, 1996; Gamage *et al*., 2018). However, this response is much weaker than the effect of elevated C_a on leaf photosynthesis, stomatal conductance or water-use efficiency (Ainsworth & Long, 2005), with variability in the response linked to interactions with factors such as nutrient availability (Seneweera & Conroy, 2005), vernalization (Masle, 2000), growing season (Ferris *et al*., 1996), developmental stage (Seneweera *et al*., 1995; Masle, 2000) or genotype (Masle, 2000; Thilakarathne *et al*., 2015). Additionally, very high concentrations of carbohydrates in leaf growth zones were observed even when plants were grown at low irradiance at contemporary C_a (Schnyder & Nelson, 1989), providing no evidence of carbohydrate substrate limitation in tall fescue (*Festuca arundinacea*) in those conditions. Yet, the concentration of monosaccharides, sucrose and low-molecular weight fructans contributed up to > 0.4 MPa to the osmotic potential of leaf growth zone tissue water (Schnyder & Nelson, 1987), suggesting a possibly important role of carbohydrates in osmotic regulation in the leaf growth zone. Whether or not carbohydrate availability in the leaf growth zone can be growth-limiting (as a substrate or osmoticum) over a range of C_a remains unresolved.

Possibly, variation in leaf hydraulics is the most important factor controlling variation of leaf elongation when C_a and atmospheric vapor pressure deficit (VPD) change. A strong and rapid response of leaf elongation rate (LER) to changes in evaporative demand and leaf water status, caused by alterations in temperature, air humidity or light intensity, has been observed in several grasses (Volenec & Nelson, 1982; Parrish & Wolf, 1983; Schnyder & Nelson, 1988; Ben Haj Salah & Tardieu, 1996; Clifton-Brown & Jones, 1999; Bouchabke *et al*., 2006) in addition to effects of edaphic conditions, including drought (e.g. Passioura, 1988; Passioura, 2002). CO_2 and VPD could also indirectly influence the leaf water status of plants through their effect on stomatal conductance (g_s) (Sionit *et al*., 1981; Morrison, 1993; Tyree & Alexander, 1993; Ainsworth & Rogers, 2007; Kimball, 2016; Manderscheid *et al*., 2016; Buckley, 2019). Results from free-air CO_2 enrichment (FACE) and chamber experiments under various environmental conditions show a systematic, significant decrease of g_s in C_3 plants at elevated CO_2, producing an equivalent decrease in transpiration (Leakey *et al*., 2009). Such changes affected water potential, turgor pressure, and osmotic potential in the growing leaves of *Phaseolus vulgaris* (Ranasinghe & Taylor, 1996). However, the combined effect of atmospheric CO_2 and VPD in the growth environment on the mechanisms linking photosynthesis, transpiration and leaf growth at constant temperature have not been investigated in any detail.

One particularly conspicuous feature of leaf elongation rate is its generally strong diurnal variation, with lower rates during the day than during the night when stomata are closed and VPD is low (Bouchabke *et al*., 2006). That variation is clearly linked to hydraulic effects in the growth zone (Tardieu *et al*., 2018), but likely also involves metabolic controls, such as diurnal variation

of wall rheological properties or root hydraulic conductance connected with circadian oscillations (Ben Haj Salah & Tardieu, 1996; Pantin *et al.*, 2011; Pantin *et al.*, 2012; Caldeira *et al.*, 2014b). Possibly, such factors can give rise to a 'stored growth' effect (Pantin *et al.*, 2012), that has been defined as 'the ability of a cell to store up a potential for extension during periods of reduced turgor which can be converted into extra extension upon restoration of normal turgor' (Cleland & Rayle, 1972) and was observed for example by Hsiao *et al.* (1970) and investigated more recently by Proseus & Boyer (2008). One may predict or hypothesize that stored growth would occur at night when turgor is increased due to stomatal closure and decreased VPD. Such an effect would compensate (at least partially) the day-time depression of LER that may be caused by the effect of transpiration on plant and growth zone water potential. It is unknown, at present, if C_a modifies diurnal variation of LER and, if it does, if such variation could be explained by a stored-growth phenomenon.

To address these unknowns, we performed mesocosm experiments with three different CO_2 concentrations: 'half ambient', equivalent to the CO_2 concentration at the Last Glacial Maximum, current 'ambient', and 'double ambient', as projected for the end of this century (IPCC, 2015), combined with high or low VPD during day-time hours, to assess the effects of these environmental drivers on the photosynthesis – transpiration – leaf growth relationships in perennial ryegrass (*Lolium perenne* L.), a major forage crop in temperate climates. Specifically, we asked: (1) Do CO_2 and VPD influence daily-total LER, final leaf length and width, and epidermal cell production and expansion? (2) Does elevated CO_2 decrease the diurnal variation of LER, consistent with predictions of CO_2 effects on stomatal conductance and transpiration? In other words: are relationships between day-time transpiration and day-time LER consistent for CO_2 and VPD effects? (3) Are CO_2 and VPD effects on daytime LER consistent with the effects of these environmental drivers on leaf water potential, osmotic potential and turgor pressure in the LGDZ? (4) What is the effect of CO_2 (and VPD) on the contribution of sugars to (diurnal adjustment of) osmotic potential in the LGDZ? And, (5) do we find evidence for night-time stored-growth effects on LER compensating daytime CO_2 and VPD effects on LER? We studied these relationships with plants growing in sward-like conditions in a culture system with optimal water supply using a nutrient solution with reduced nitrogen concentration, employing previous protocols and experience (Kavanová *et al.*, 2008; Lehmeier *et al.*, 2008, 2013).

Materials and Methods

Experimental design, treatments and growth conditions

The study had a 3 × 2 factorial design with C_a and daytime VPD as factors, and air temperature controlled at 20 °C : 16 °C during the 16 h : 8 h, day : night cycle in all treatments. Three constant CO_2 concentrations (200, 400 or 800 μmol mol^{-1}), corresponding to Last Glacial Maximum (half-ambient), present-day (ambient) and end of the century projections (double-ambient, i.e. elevated) were combined with high (1.17 kPa, 50% relative humidity, RH) or low (0.59 kPa, 75% RH) VPD during the day, corresponding to dry or damp summer days in Central Europe. Night-time VPD was held constant at 0.46 kPa (75% RH) in all treatments. Light was supplied by cool-white fluorescent tubes and warm-white light-emitting diode (LED) bulbs with a photosynthetic photon flux density (PPFD) of 800 μmol m^{-2} s^{-1} at plant height. Treatments were applied 13 d after seed imbibition. Disturbance of atmospheric conditions in the chambers during handling of plants were minimized by installing air-locks in chamber doors (similar to Lehmeier *et al.*, 2008), maintenance of a small overpressure in the chambers relative to the outside atmosphere, and minimizing operations during daylight hours.

Protocols for plant growth followed closely those described by Lehmeier *et al.* (2008). In brief, individual plants of perennial ryegrass (cv. 'Acento') were grown singly in plastic tubes (350 mm height, 50 mm diameter) filled with washed quartz sand (0.3–0.8 mm grain size). Pots were arranged in plastic containers (770 mm × 560 mm × 300 mm) at a density of 383 plants m^{-2}. The close packing of pots (Supporting Information Fig. S1) resulted in a stand-like situation at harvest (leaf area index > 5.5 after canopy closure, in all treatments).

Two containers were placed in each of four growth chambers (see next paragraph). Plants were supplied with a modified 5 mM nitrate-N Hoagland nutrient solution every 6 h by briefly flooding the containers for 9 min followed by draining by gravity (Lehmeier *et al.*, 2008). The composition of the nutrient solution was the following: 1.67 mM KNO_3, 1.67 mM $Ca(NO_3)_2$, 1.0 mM $MgSO_4$, 0.5 mM KH_2PO_4, 0.5 mM NaCl, 134 μM Fe-EDTA, 46 μM H_3BO_3, 9 μM $MnSO_4$, 0.8 μM $ZnSO_4$, 0.3 μM $CuSO_4$, 0.1 μM Na_2MoO_4. This composition corresponded to a nutrient solution with 33% reduced, i.e. two-thirds-strength, nitrate-N concentration relative to normal and nominal concentrations of the other nutrients (compare with Kavanová *et al.*, 2008; Lehmeier *et al.*, 2013).

The experiments were performed inside the four plant growth chambers (PGR15; Conviron, Winnipeg, Canada) that formed part of a modernized version of the gas exchange mesocosm system described by Schnyder *et al.* (2003). Air supply to the chambers was performed by mixing dry CO_2-free air and tank CO_2 (from Linde AG, Unterschleißheim, Germany or Carbo Kohlensäurewerke, Bad Hönningen, Germany) using mass flow controllers. CO_2 and water vapor concentration in each growth chambers were measured every 30 min by an infrared gas analyzer (IRGA, Li-840; Li-Cor, Lincoln, NE, USA). Air temperature and RH in the chambers were measured continuously with the chamber control system (CMP6050, Conviron), which was calibrated before each experimental run (see next paragraph) using external sensors. Light intensity at canopy height was measured with a quantum sensor (LI-190R; Li-Cor) and adjusted periodically. RH gradients between the top and bottom of fully-developed canopies were < 5% and neglected in further analysis.

We performed five sequential experimental runs of 10 to 12 wk duration with four growth chambers, with different treatments in each run, and allocation of treatments to different chambers between sequential runs, as in Liu *et al.* (2016) (Supporting Information Table S1). We observed no chamber effect

on the parameters reported in this study. Measurements of leaf growth, leaf gas exchange and carbohydrate concentration were performed in experimental runs 1–4 and water status measurements in the last run.

Leaf elongation rate (LER)

LER was determined as in Schnyder & Nelson (1988) and Schnyder *et al.* (1990). All plants were in the vegetative stage and had 7 to 11 tillers. Briefly, leaf length was measured on the main tiller of eight randomly selected plants per chamber ($n = 16$–40 per treatment), during 14 d after canopy closure (days 49–62 after imbibition of seed). Measurements were performed every day at the end of the light period on all simultaneously growing leaves (one or two leaves) per main tiller, by recording the distance between the tip of the elongating leaf and the ligule of the youngest fully expanded leaf using a ruler. The daily rate of change in blade length was taken as the measure of the mean daily rate of leaf elongation (LER, in mm h^{-1}). For comparisons among treatments the values obtained during the phase of near-maximum, near-steady growth were used. This corresponded to the phase when the elongating leaf blade had reached ~ 40–65% of its final length (Fig. S2) and all leaf elongation was due to blade elongation. In addition, leaf length was measured at the end of the day and the end of the following night on two successive days, to obtain the LER during day (LER_{day}) and night (LER_{night}).

At the end of the 2 wk-long measurement period plants were sampled for the estimation of additional morphological parameters (leaf length, leaf area) using a similar protocol as Liu *et al.* (2016). The Image J software (Schneider *et al.*, 2012) was used for digital analysis.

Epidermal cell length and number

Two fully developed leaf blades from each of four plants per treatment were sampled at 66 d after the start of the experiment. The selected leaves were cut near the ligule and a 3 cm-long replica of the abaxial epidermis was taken in the basal region of the blade as in Schnyder *et al.* (1990) using a thin layer of 4% (w/w) polyvinylformaldehyde (Formvar 1595 E; Merck Darmstadt, Germany).

Digital images of representative sections of each replica (0.7 mm × 4 mm) were obtained with a fluorescence microscope (BX 61; Olympus Corp., Tokyo, Japan) operated with the CellSense Dimension software of the Centre for Advanced Light Microscopy (CALM, Technical University of Munich, Germany), at ×10 magnification. The ImageJ software (Schneider *et al.*, 2012) was used to measure cell length in cell files without stomata. Replicas with fewer than 50 identifiable cells were excluded from the analysis.

Epidermal cell number (in a cell file running from the base to the tip of the leaf blade) was estimated as final leaf blade length divided by epidermal cell length. Former work with perennial ryegrass demonstrated epidermal cell length was virtually constant along the leaf blade (Schnyder *et al.*, 1990). Also, we found no differences in cell length densities near the proximal and distal margins of epidermal replicas taken from the region that corresponded to the cells/tissue that expanded during the LER measurements (Fig. S3).

Stomatal conductance and leaf- and canopy-scale transpiration

Chamber-scale canopy transpiration (E_{canopy}) was measured continuously during the 2-wk interval in which LER was determined. For each chamber, canopy transpiration (in mmol H_2O m^{-2} s^{-1}) was calculated every 30 min as the difference between the H_2O fluxes at the inlet (F_{in}, in mmol H_2O s^{-1}) and outlet (F_{out}, in mmol H_2O s^{-1}) of the growth chamber, divided by the chamber ground area (s, 1.5 m^2):

$$E_{canopy} = (F_{in} - F_{out})/s \qquad \text{Eqn 1}$$

These measurements were made while the RH of the chamber atmosphere was kept near the nominal level (SD ± 0.9%) by using a high-pressure water vapor generator (FINESTFOG, Ottobrunn, Germany) that added a known amount of water vapor to the chamber air whenever the nominal RH dropped below a specified threshold (1–2% RH lower than the chamber setpoint). The chamber-based humidification system was inactivated during that period. Vapor addition rate by the vapor generator was equated with F_{in}, as the fresh air supplied to the chambers was dry (dewpoint < –70 °C). Before each experimental run, a calibration was performed to obtain the water addition rate of the nozzles. Water vapor losses due to condensation inside the chambers were quantified by collection and weighing of the condensate and accounted for in the calculations.

In parallel, leaf-level measurements of stomatal conductance and transpiration were performed with a LI-6400 (Li-Cor) portable CO_2/H_2O gas exchange system with a clamp-on leaf cuvette on 6–12 plants per treatment. That measurement system was installed in a separate plant growth chamber (E15, Conviron). For measurements, individual plants were removed from their growth chamber, and the midsection of the youngest fully developed leaf blades of four tillers was enclosed in the 2 cm × 3 cm leaf cuvette. Stomatal conductance to water vapor (g_s, in mol H_2O m^{-2} s^{-1}) and leaf transpiration (in mmol H_2O m^{-2} s^{-1}) were measured at a leaf temperature of 21 °C and a PPFD of 800 µmol m^{-2} s^{-1}. CO_2 concentration and RH in the leaf cuvette were set equal to the conditions in the growth environment. Measurements were logged once steady-state conditions for stomatal conductance and water vapor concentration were reached.

Osmotic potential, leaf water potential and turgor

Total osmotic potential in the LGDZ, leaf water potential, and turgor pressure were estimated in the treatments with C_a of 200 and 800 µmol mol^{-1} at both high and low VPD. Samples for osmotic potential measurements were collected 2 h before the end of the day and night, on two sampling days between days 61

and 74. Six plants were randomly selected from each chamber and the LGDZ of two fully developed tillers pooled into one sample, sealed in paper bags, frozen in liquid nitrogen and stored at −18°C. The frozen samples ($n = 4$ per treatment) were thawed at room temperature and sap was extracted under mechanical pressure. Osmotic potential was then measured with a vapor pressure osmometer (5100C; Wescor Inc., Logan, UT, USA). On day 76, leaf water potential of eight plants per treatment was determined with the pressure chamber technique (Scholander *et al.*, 1965): 2 h before the end of the day individual plants were taken from a growth chamber, the youngest fully expanded leaf blade of a major tiller was cut near the ligule and immediately placed in a pressure chamber (Model 1002; PMS Instrument Company, Albany, OR, USA), following the recommendations by Turner (1981). Plants were returned to the same chamber and the protocol repeated on another tiller 2 h before the end of the night. Turgor was estimated as the difference between osmotic potential and leaf water potential, neglecting (1) the water potential gradient between the youngest fully expanded leaf and the LGDZ and (2) the fraction of apoplastic water, that were assumed to be sufficiently small or similar between treatments (Passioura, 1980; Martre *et al.*, 2001). As they comprised the entire LGDZ and youngest fully-expanded leaf blade, our measurements ignored the turgor gradients between expanding and fully-expanded tissue in the LGDZ, and the water potential gradient between the expanding tissue and the water source (e.g. Nonami & Boyer, 1993; Martre *et al.*, 1999; Fricke & Peters, 2002). In detailed investigations of hydraulic conductivities in vegetative plants of tall fescue – a closely related species – Martre *et al.* (2001, Table 1) found a water potential-gradient of 0.19 MPa between the transpiring, youngest fully-expanded leaf and the leaf growth zone, a difference that corresponded to 10% to 16% of the leaf water potential of the youngest fully-expanded leaf blade in light, in our investigations.

Water-soluble carbohydrates

LGDZ tissue was excised from two mature tillers of six plants per chamber on day 62 after imbibition and pooled together into one sample, both at the end of the day and night period, during experimental runs 1–4 ($n = 4$ per treatment). Fresh weight of the samples was determined and samples were frozen in liquid nitrogen and stored in a freezer at −18 °C until freeze drying. Dry samples were ball-milled to a fine powder and stored again at −18 °C until extraction of water-soluble carbohydrates as in Schnyder & de Visser (1999). The water-soluble carbohydrates components fructose, glucose, sucrose and fructan were separated by high-performance liquid chromatography (HPLC, Shodex Sugar KS 801 and 802; Showa Denko, Tokyo, Japan) and carbohydrates detected with a refractive index detector (Shodex RI-101). Analytical grade fructose, glucose, sucrose and inulin (all from Merck) were used as standards.

To obtain the mean degree of polymerization of fructans, fructans were separated from other water-soluble carbohydrates components by HPLC, hydrolyzed by heating in 0.02 M hydrochloric acid (HCl) for 1 h (Wolf & Ellmore, 1975), and fructose and glucose in the hydrolysate separated by HPLC and quantified as earlier. The mean degree of polymerization of fructan was obtained as fructose : glucose + 1, and used to calculate the mean molecular weight of fructan in the LGZD.

The osmotic potential of water-soluble carbohydrates in the LGDZ was estimated from the molar concentration of the individual water-soluble carbohydrates per unit tissue water in the LGDZ, assuming 40 mM = 0.1 MPa (Schnyder & Nelson, 1987).

Statistics

Linear mixed models were fitted to analyze the effect of CO_2, VPD, diel period (day or night) and their interactions on LER, morphometric traits, stomatal conductance, transpiration and carbohydrate concentration. Growth chamber, experimental run and multiple measurements on individual plants were included in the models as random effects. Type III Wald test was used for determining the significance of the fixed effects and the *post hoc* Tukey's HSD test was performed for pairwise comparisons among treatments. Additionally, linear models were used to test the effect of the explanatory variables on leaf water potential, osmotic potential and turgor. Finally, treatment averages were calculated and linear regression analysis was performed to determine the relationship between the different target variables. All statistical analyses were conducted in R v.3.6.1 (R Core Team, 2019). The R-packages NLME (Pinheiro *et al.*, 2019), emmeans (Lenth, 2018) and ggplot2 (Wickham, 2016) were used for fitting linear mixed models, performing the *post hoc* tests and for data plotting, respectively. The number of replicates varied between measured parameters and treatments and is indicated in the figure legends and table captions.

Table 1 Results of a linear mixed model, testing the response of daily mean leaf elongation rate of *Lolium perenne* to atmospheric CO_2 concentration, daytime vapor pressure deficit (VPD) and their interaction ($n = 16$–40).

Factor	df	*F*-value	*P*-value
CO_2	9	1.47	0.26
VPD	9	1.12	0.32
$CO_2 \times$ VPD	9	1.87	0.21

Results

LER, final leaf length and width, and epidermal cell length and number

Daily mean LER showed no statistically significant responses to CO_2, daytime VPD or their interaction (Fig. 2a; Table 1). Likewise, morphometric traits associated with the leaf growth process, i.e. final leaf blade length and width and epidermal cell length and number (Fig. 2e–h), leaf appearance interval (Fig. S4) and the time from leaf appearance to cessation of leaf elongation (not shown) revealed no significant differences between treatments.

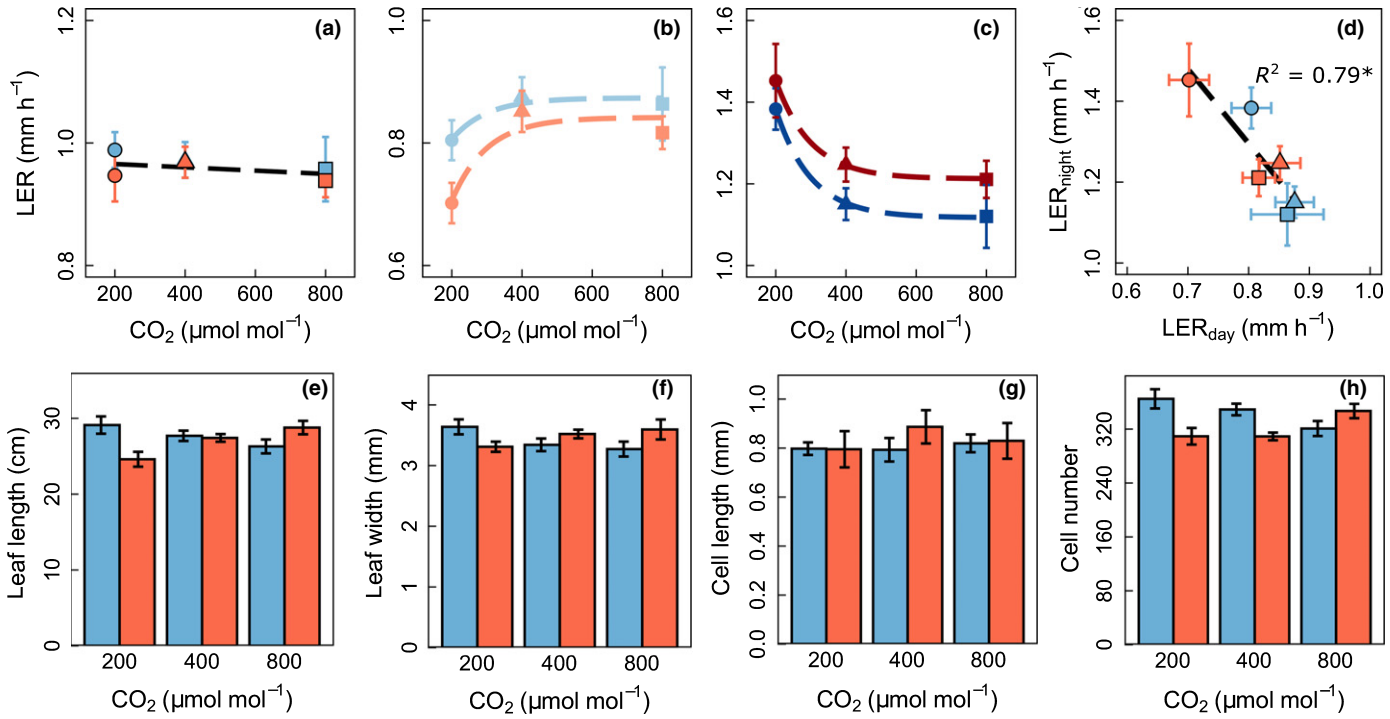

Fig. 2 Morphometric traits of *Lolium perenne* as influenced by atmospheric CO_2 concentration at low (0.59 kPa; blue color) and high daytime vapor pressure deficit (VPD) (1.17 kPa; red): daily mean leaf elongation rate (LER) (a), LER during day (b), LER during night (c), the relationship between LER during day (LER_{day}) and during night (LER_{night}) (d), final leaf length (e), mean leaf width (f), epidermal cell length (g), and epidermal cell number (h). VPD at night was kept the same in all treatments (0.46 kPa). Symbols: circles, 200 µmol mol^{-1} CO_2; triangles, 400 µmol mol^{-1} CO_2; squares, 800 µmol mol^{-1} CO_2. Significance level of the linear regression in (d): *, $P<0.05$. Data points and error bars represent the mean ± SE. For details, see the Materials and Methods section.

Conversely, LER exhibited pronounced diel variation, with higher rates at night in all treatments ($LER_{night} > LER_{day}$, $P<0.001$). The amplitude of the diel variation differed between treatments, due to a significant interaction of LER with daytime VPD (night-time VPD was the same in all treatments) and CO_2 (Table 2, $P<0.001$; Figs 2b,c, S5). LER_{day} increased and LER_{night} decreased exponentially with C_a. Even though daytime VPD had no statistically significant effect (Tables 2, S2), a systematic difference in LER between VPD levels was evident. High (relative to low) daytime VPD reduced LER_{day} (−0.04 mm h^{-1}) and enhanced LER_{night} (+0.07 mm h^{-1}, averaged over all treatments) throughout the range of CO_2 levels. The greatest divergence between LER_{day} and LER_{night} occurred at low C_a and high daytime VPD ($LER_{night} : LER_{day} = 2.0$) and the smallest at high C_a and low daytime VPD (1.3). The net result of CO_2 and daytime VPD effects was a close negative and virtually-fully compensating relationship between LER_{night} and LER_{day} across all six treatments (Fig. 2d, $R^2 = 0.79$, $P<0.05$).

Stomatal conductance, transpiration and relationship with LER_{day}

The g_s and transpiration were measured on the youngest fully-expanded leaf blade (Fig. 3a,b) under the same conditions of light intensity, C_a and daytime VPD as in the growth environment. The g_s strongly reacted to CO_2 concentration, VPD and their interaction (Table 3): g_s significantly decreased with both C_a (according to a negative exponential function, $P<0.001$) and VPD ($P<0.01$), with a VPD-sensitivity that decreased with C_a (Fig. 3a). Accordingly, g_s was highest when VPD and C_a were low, and lowest when VPD and C_a were high; but the enhancement of g_s by low VPD (relative to high VPD) was greater at a C_a of 200 µmol mol^{-1} (2.6-fold) than at 800 µmol mol^{-1} (1.5-fold) (Table S3).

Leaf transpiration decreased exponentially with increasing C_a, dropping by more than 55% between 200 and 800 µmol mol^{-1} ($P<0.001$; Table 3) at both VPD levels. We also noted a greater leaf transpiration at high relative to low VPD level (> 10% for all

Table 2 Results of a linear mixed model, testing the response of leaf elongation rate of *Lolium perenne* to diel period (leaf elongation during day or night), atmospheric CO_2 concentration (exponential function; see Fig. 2), daytime vapor pressure deficit (VPD) and two-way interactions (n = 16–40).

Factor	df	*F*-value	*P*-value
Day/night	100	47.2	< 0.001
CO_2	9	5.6	0.04
Daytime VPD	9	2.2	0.17
Day/night × CO_2	100	60.5	< 0.001
Day/night × daytime VPD	100	12.9	< 0.001

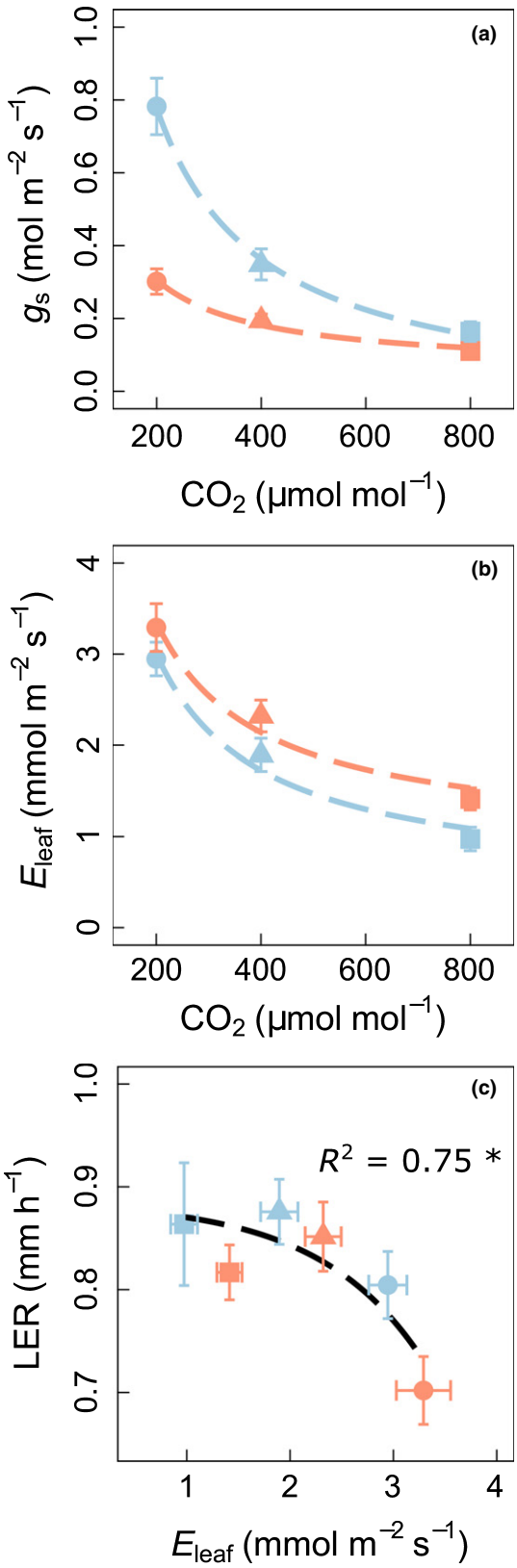

Fig. 3 Daytime stomatal conductance (g_s) (a) and leaf transpiration (E_{leaf}) (b) of the youngest fully-expanded leaf of *Lolium perenne* as affected by atmospheric CO_2 concentration and daytime vapor pressure deficit (VPD) (n = 6–12) (low VPD, 0.59 kPa, blue color; high VPD, 1.17 kPa, red) in the growth environment. Night-time VPD in the growth environment was kept the same in all treatments (0.46 kPa). Measurement conditions were the same as in the growth environment during the day (PPFD, 800 µmol m^{-2} s^{-1}; leaf temperature 21 °C, and CO_2 and VPD as indicated earlier). (c) The relationship between leaf elongation rate during day (LER_{day}) (Fig. 2b) and E_{leaf}. Significance level of the exponential function in (c): *, $P < 0.05$. Data points and error bars represent the mean ± SE.

CO_2 levels); but this effect was not statistically significant due to the variability of leaf transpiration (Fig. 3c; Table S3). Simultaneously, a significant curvilinear relationship ($R^2 = 0.75$; $P < 0.05$) existed between leaf transpiration and LER_{day}. LER_{day} decreased sharply with leaf transpiration when leaf transpiration increased above approximately 2.5–3.0 mmol m^{-2} s^{-1} in plants grown at a C_a of 200 µmol mol^{-1} (Fig. 3c).

Water-soluble carbohydrates

The concentration of the water-soluble carbohydrates components fructose, glucose, sucrose and fructan in the LGDZ was determined at the end of the day and of the night, in all treatments. Very high water-soluble carbohydrate concentrations (with total water-soluble carbohydrate > 53% of dry matter content) were observed in all treatments at the end of both day and night. Differences between treatments and throughout the diurnal cycle were generally small, however treatment effects were observed for the molar concentrations of the individual carbohydrates. This was the case for: (1) sucrose, which showed systematic diurnal variation with concentration decreasing by 25% on average between the end of the day and the end of the night (Fig. 4c, $P < 0.001$) and strongest relative decreases at low C_a; (2) a greater fructose concentration in the low C_a treatments relative to the other C_a treatments (+21% on average); (3) a greater fructan concentration at high VPD (+43% in average, due mainly to a lower degree of polymerization relative to low VPD), which determined a greater total water-soluble carbohydrate concentration at high VPD (+16%); (4) a lower fructan concentration at 200 µmol mol^{-1} compared with the other CO_2 levels (−25% on average) and (5) a small decrease of total water-soluble carbohydrate concentration during the night (−5% on average of all treatments), due mainly to decreases of sucrose and fructan concentration (Tables S4, S5). Conversely, glucose and fructose concentrations did not show signs of depletion during the night (Fig. 4a,b). Together, the monosaccharides accounted for 64 to 77% of the total contribution of all water-soluble carbohydrates to the osmotic potential in the LGDZ. The latter was 26–34% of the total osmotic potential, and did not differ systematically between treatments or diel periods, although the relative contribution was, on average, slightly higher at the end of the night (Fig. 4f).

Leaf water potential, osmotic potential, turgor and relationships with LER_{day} and LER_{night}

The water potential of the youngest fully-expanded leaf blade and the osmotic potential of tissue water in the LGDZ were

Table 3 Results of a linear mixed model, testing the response of stomatal conductance (g_s) and leaf transpiration of *Lolium perenne* to atmospheric CO_2 concentration (exponential function; see Fig. 3), daytime vapor pressure deficit (VPD) and their interaction ($n = 6$–12).

	g_s		Leaf transpiration	
Factor	*F*-value	*P*-value	*F*-value	*P*-value
CO_2	75.7	< 0.001	39.8	< 0.001
Daytime VPD	15.6	< 0.01	0.42	0.53
CO_2 × daytime VPD	13.4	< 0.01	0.04	0.84

Conditions in the leaf cuvette during measurement of g_s and leaf transpiration were the same as in the growth chamber of origin of the respective plants.

determined at the end of the day and at the end of the night in the extreme C_a treatments (200 and 800 µmol mol^{-1} CO_2) with low or high daytime VPD (Fig. 5a,b). Turgor pressure in the LGDZ (Fig. 5c) was estimated as the difference between leaf water potential and osmotic potential, neglecting possible water potential-gradients between the LGDZ and the youngest fully expanded leaf blade.

Treatments had no effect on leaf water potential, or osmotic potential or turgor at the end of the night. However, leaf water potential ($P < 0.001$), osmotic potential ($P < 0.01$) and turgor ($P < 0.001$) changed significantly between the end of the night and the end of the day in each of the four treatments (Fig. 5a–c; Table 4). These changes were inversely related to CO_2 concentration ($P < 0.001$); that is, changes of leaf water potential, osmotic potential and turgor between end of the night and end of the day were greater at low than at high C_a (Fig. 5a–c; Table 4). On the contrary, we found a statistically significant effect of VPD on leaf water potential ($P < 0.001$), but not on osmotic potential or turgor at the end of the day (Table 4).

Leaf water potential was negatively related with canopy transpiration, following a virtually identical relationship across treatments when day and night measurements were pooled (Fig. 5d; $R^2 = 0.98$; $P < 0.001$). Leaf water potential and osmotic potential exhibited a close proportionality (Fig. 5e; $R^2 = 0.89$; $P < 0.001$) that also implied a linear (and proportional) increase of turgor with leaf water potential, represented as the difference between the 1 : 1 line and the data points in Fig. 5(e). LER_{day} responded linearly to leaf water potential measured at the end of the day (Fig. 5f, $R^2 = 0.81$). That relationship was determined primarily by the effect of CO_2 on LER_{day} ($P < 0.05$).

We found no relationship between LER_{night} and leaf water potential or osmotic potential or turgor estimates obtained at the end of the night (Table S6, $P > 0.05$). But, we observed a tight relationship between the enhancement of LER_{night} relative to LER_{day} and the increase in turgor between the end of the day and the end of the night ($R^2 = 0.93$, $P < 0.05$; Fig. 6), with the intercept of this relationship not being significantly different from zero ($P > 0.05$).

Discussion

Our work demonstrates a strong diurnal oscillation of LER in *L. perenne* that was determined by (1) a variable hydraulic limitation of daytime LER driven by atmospheric CO_2 level (C_a) and

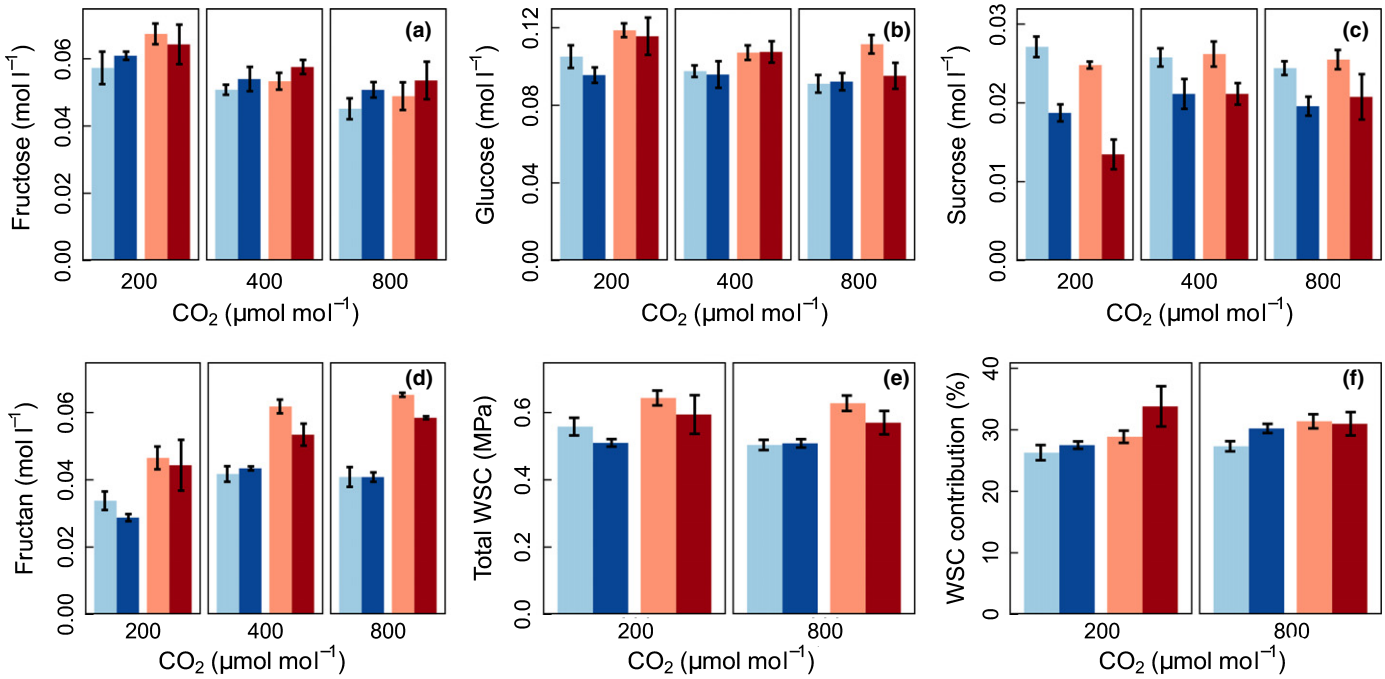

Fig. 4 Molar concentration of fructose (a), glucose (b), sucrose (c) and fructan (d) in the leaf growth-and-differentiation zone (LGDZ) of *Lolium perenne*, and osmotic potential of the total water-soluble carbohydrate (WSC) (e), and its contribution to the total osmotic potential measured in the LGDZ (f) as influenced by atmospheric CO_2 concentration at low (0.59 kPa, blue color) and high daytime vapor pressure deficit (VPD) (1.17 kPa, red), for measurements at the end of the day (light colored bars) and at the end of the night (dark colored bars). VPD at night was kept the same in all treatments (0.46 kPa). Data points and error bars represent the mean ± SE ($n = 4$). Notice the different scales in plots (a)–(d).

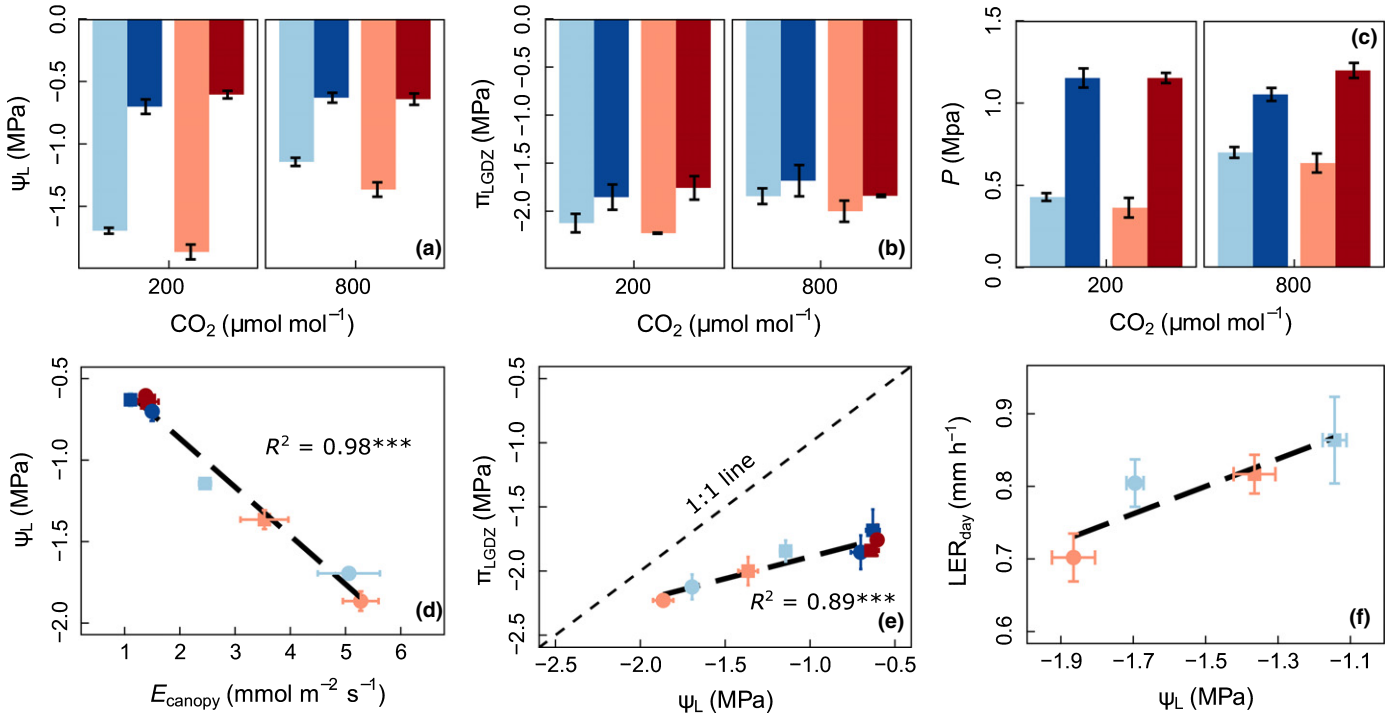

Fig. 5 Water potential of the youngest fully expanded leaf (Ψ_L) of *Lolium perenne* ($n = 8$) (a), osmotic potential of tissue water in the leaf growth-and-differentiation zone, LGDZ (π_{LGDZ}) ($n = 4$) (b), turgor pressure (P) in the LGDZ, estimated as the difference between π_{LGDZ} and Ψ_L ($n = 4$) (c), and relationship between Ψ_L and canopy transpiration (E_{canopy}) (d), between Ψ_L and π_{LGDZ} (e) and between Ψ_L and leaf elongation rate (LER) (f) for measurements at the end of the day (light colored bars or symbols) and at the end of the night (dark colored bars or symbols). In (e) the difference between the 1 : 1 line and the data points represents the estimated turgor. Plants were grown in the presence of half-ambient (200 μmol mol^{-1}, circles) and double-ambient CO_2 (800 μmol mol^{-1}, squares) with low or high daytime vapor pressure deficit (VPD) (low VPD, 0.59 kPa, blue color; high VPD, 1.17 kPa, red) in their growth environment. Night-time VPD in the growth environment was kept the same in all treatments (0.46 kPa). Significance level of the linear regression in (d) and (e): ***, $P < 0.001$. Data points and error bars represent the mean ± SE. For details, see the Materials and Methods section.

Table 4 Results of a linear model (*t*-values) testing the response of leaf water potential (Ψ_L), osmotic potential in the leaf growth-and-differentiation zone, LGDZ (π_{LGDZ}) and turgor pressure of *Lolium perenne* to growth during day or night (a); and effect of atmospheric CO_2 concentration, daytime vapor pressure deficit (VPD) and their interaction on Ψ_L, π_{LGDZ} and P during growth in the day (b).

Factor	Ψ_L	π_{LGDZ}	Turgor
(a) Day/night	12.4***	3.0**	7.4***
CO_2	126.8***	7.9*	5.6*
(b) Daytime VPD	20.1***	2.2^{ns}	0.11^{ns}
CO_2 × daytime VPD	0.3^{ns}	0.08^{ns}	0.0^{ns}

No significant effects were detected during night growth ($P > 0.05$). Significance levels: ns, not significant ($P > 0.05$); *, $P < 0.05$; **, $P < 0.01$; ***, $P < 0.001$.

(daytime) VPD, and (2) a full compensation of the daytime hydraulic limitation of elongation by a night-time enhancement of LER, that was consistent with a stored-growth effect. As a result, at daily timescale, LER and a suite of leaf morphogenetic parameters (leaf blade length and width, epidermal cell length and number) were insensitive to C_a (and daytime VPD), explaining, in part, the less-than expected growth response towards elevated CO_2. However, we did note a decrease of specific leaf area

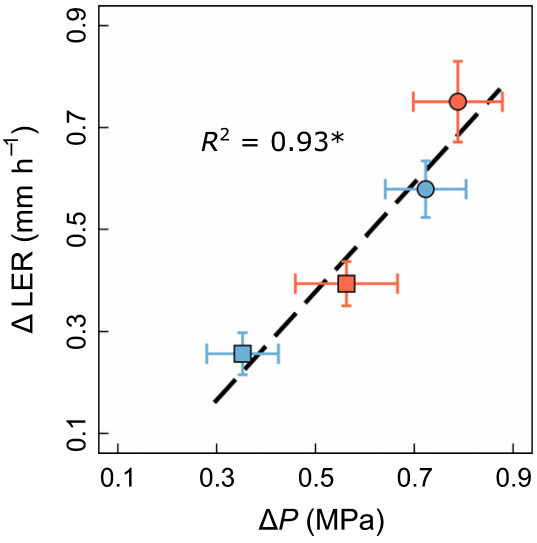

Fig. 6 Enhancement of nocturnal leaf elongation rate (LER_{night}) over diurnal leaf elongation rate (LER_{day}) ($\Delta LER = LER_{night} - LER_{day}$) of *Lolium perenne* as related to the turgor change (ΔP) between end of night and end of day. Symbols: circles, 200 μmol mol^{-1} CO_2; squares, 800 μmol mol^{-1} CO_2; blue, low vapor pressure deficit; red, high vapor pressure deficit. Significance level of the linear regression: *, $P < 0.05$. Data points and error bars represent the mean ± SE.

(SLA) with increasing CO_2 level (Fig. S4), a typical CO_2 growth-response (Poorter & Navas, 2003; Ainsworth & Long, 2005). Furthermore, notably, epidermal cell length was close to that observed by Kavanová *et al.* (2008) in nitrogen-limited conditions with the same cultivar of perennial ryegrass.

The presence of a strong hydraulic limitation of LER_{day} in all treatments in this work was supported by (1) the strong decreases of leaf water potential between the end of the night and the end of day, and low leaf water potential (< −1.0 MPa) at the end of the day, that was combined with (2) strong decreases of osmotic potential and turgor towards the end of the day, and (3) a significantly lower LER_{day} than LER_{night}, despite of the 4 °C lower air temperature at night. These relationships were unrelated to soil drying during the day as stands were watered frequently, resulting in a near-constant volumetric water content in the soil (water content > 20%, data not shown) and a virtually constant canopy transpiration throughout the light periods in all treatments (Fig. S6). Also, source-limitation was highly unlikely, as water-soluble carbohydrate concentration was greater than 53% of dry mass in the LGDZ in all treatments throughout the day–night cycle. Hydraulic limitation of LER_{day} occurring independently of soil water deficit has been observed repeatedly (Tardieu *et al.*, 2010; Pantin *et al.*, 2012; Caldeira *et al.*, 2014a) and was related to high irradiance (Gallagher & Biscoe, 1979), high air VPD (e.g. Parrish & Wolf, 1983; Table 2) or low nitrogen nutritional status (Radin & Boyer, 1982). Radin & Boyer (1982) observed greater reductions of daytime relative to night-time leaf expansion in sunflower, when nitrogen nutrition was limiting. We used a Hoagland-type nutrient solution with reduced nitrogen concentration (−33% relative to the standard solution and nominal concentrations of other elements) which could have contributed to the observed reduction of $LER_{day} : LER_{night}$. But, between-treatment variation of LER_{day} was unrelated to the effect observed by Radin & Boyer (1982) as nitrogen concentration of the LGDZ was highest (Table S7) in the treatment with the greatest disparity between LER_{day} and LER_{night}. However, we did grow plants at a high irradiance (16 h of 800 $\mu mol\ m^{-2}\ s^{-1}$ PPFD at canopy height), causing a high daytime evaporative demand particularly in the treatments with high daytime VPD. The effect of high irradiance (and high air VPD) on LER_{day} is generally associated with strong decreases of leaf water potential and turgor in the leaf growth zone (Tardieu *et al.*, 2010; Pantin *et al.*, 2012).

The C_a or its interaction with VPD strongly modified the hydraulic limitation of LER_{day}, as shown by (1) the negative relationship between LER_{day} and transpiration, principally caused by a negative response of transpiration to C_a, (2) the close negative relationship between leaf water potential and transpiration that depended mostly on variation of C_a, (3) the covariation of leaf water potential and osmotic potential that was primarily driven by variation of C_a, and finally (4) the drastic decrease in turgor and LER during daytime compared to night-time. Accordingly, the effect of C_a on LER_{day} conformed with that expected for hydraulic limitation, predicted based on its effect on stomatal conductance and transpiration during daytime (Fig. 1), although the effect did not persist at the daily level due to compensating night-time effects on leaf elongation (see 'stored growth' in the following paragraphs). Although hydraulic limitation of LER_{day} caused by low C_a has not been reported before, a strong negative relationship between (ABA mediated) stomatal conductance and leaf elongation during daytime was demonstrated earlier (Tardieu *et al.*, 2010). It is worth noting that the applied treatments did not alter the water relations in our system. The relationship between canopy transpiration and leaf water potential was extremely tight ($R^2 = 0.98$), suggesting a constant hydraulic conductivity and a lack of acclimation of this parameter to the different C_a and VPD environments. Also, the treatments followed a very similar leaf water potential vs osmotic potential relationship which remained unaltered throughout the day : night cycle. Similarly, sugar (and by difference, non-sugar) contributions to osmotic adjustment remained relatively constant in the diel cycle, and accounted for 26 to 34% (and 66 to 74%) of osmotic potential, independently of C_a or VPD.

Remarkably, none of the treatments showed diel variations in the concentration of fructose and glucose, the most important sugar osmoticum (64–77% of the total osmotic potential attributable to water-soluble carbohydrates). Night-time depletion of sucrose may have resulted (at least in part) from enhanced sucrose hydrolysis by invertase to generate fructose and glucose in the LGDZ (Koch, 2004; Lunn, 2008). Also, the night-time reduction of sucrose concentration in the LGDZ may have contributed to sustain carbohydrate import into the LGDZ (Schnyder & Nelson, 1988) as total water-soluble carbohydrate concentration did not decrease markedly during the night, despite of the greatly enhanced LER_{night} (particularly at low C_a) and associated enhanced growth-related water deposition (nocturnal decreases in water content of the LGDZ were not observed, data not shown). Again, these observations support the view that neither LER_{day} nor LER_{night} were source limited.

In contrast with daytime LER, nocturnal LER showed no evidence of hydraulic limitation, as LER_{night} was not significantly related with any of the hydraulic parameters assessed at the end of the dark period. But, we did observe a negative correlation between atmospheric CO_2 concentration and LER_{night} that was – however – non-causal, as reciprocal transfer of plants between CO_2 environments at the beginning of the night period did not alter their subsequent LER_{night} (Fig. S7; Table S8), effectively demonstrating that LER_{night} was insensitive to night-time CO_2. Clearly, therefore, differences between treatments in LER_{night} were a consequence (carryover) of daytime atmospheric conditions of CO_2 and daytime VPD. Indeed, the enhancement of LER_{night} over LER_{day} was closely related to the nocturnal recovery of turgor. This LER_{night} response conforms with the 'stored growth' phenomenon that is reflected in above-normal growth when turgor recovers after a period of turgor loss and inhibited growth (Serpe & Matthews, 1994; Proseus & Boyer, 2008; Pantin *et al.*, 2012). The mechanism of stored growth is not fully understood, but the phenomenon has been associated with adjustments in wall yielding properties (e.g. Serpe & Matthews, 1994). Studies with *Chara corallina* cells demonstrated an accumulation of unused cell wall precursors in the cytoplasm during the phase of low turgor, which were used after turgor recovery

and led to an enhancement in cell growth (Proseus & Boyer, 2006). The stored growth effect, however, may not be ubiquitous among grasses (see e.g. the independent response of LER_{night} and LER_{day} to VPD in maize, Bouchabke *et al.*, 2006) or may perhaps interact with other factors, such as source or nutritional limitation.

Although we did not analyze the kinetics of LER during the night, it is well known that abrupt changes from full light to darkness or from darkness to light (as used here and often employed in diurnal 'cycles' in growth chamber experiments), typically produce transient (< 1 h-long) enhancements or inhibitions of LER (Durand *et al.*, 1995), that are indicative of an elastic component of expansion. These short-lived transients are often followed by near constant LER during the remainder of the day or night periods, with the transient enhancements or inhibitions accounting for a relatively small portion of the overall differences between daytime and night-time elongation in well-watered conditions and constant temperature at the growth zone (Schnyder & Nelson, 1988; Durand *et al.*, 1995).

Clearly, the most remarkable result of this work was the virtually complete compensation of reduced daytime leaf expansion by night-time leaf expansion, as LER averaged over a 24 h period did not differ significantly between treatments. As the photoperiod was 16 h, a unit decrease of LER_{day} actually required a two-unit increase of LER_{night} for full compensation. These results are also consistent and indicative of a mechanism governing the daily mean or integral rate of cell wall loosening independently of the variable daytime depressions of turgor that were controlled by atmospheric conditions of CO_2 and VPD. The nocturnal enhancement of cell wall expansion must have been closely proportional to the nocturnal turgor increase, with a very similar proportionality factor (cell length increment per unit increase of turgor) for all treatments, as the enhancement of LER_{night} over LER_{day} followed the same proportionality with the nocturnal turgor increase. Although we did not observe the processes of cell division and elongation directly, our observations of virtually constant final leaf length, leaf appearance interval, leaf elongation duration post emergence, and final epidermal cell length and number must have some implications for the underlying patterns of cell division and elongation, as LER is a function of cell division (production) and elongation rate along contiguous cell files (Schnyder *et al.*, 1990; Kavanová *et al.*, 2006, 2008), also with respect to CO_2 effects (Masle, 2000). It is well established for perennial ryegrass (and related species such as tall fescue), grown in a wide range of environmental conditions, that the duration of individual epidermal cell expansion, from the emergence from the cell division zone to the time when it attains its' final length, is about 3 to 4 d in similar thermal environments (MacAdam *et al.*, 1989; Schnyder *et al.*, 1990; Kavanová *et al.*, 2006, 2008). This would imply that individual elongating epidermal cells experienced several diurnal perturbations of cell expansion rate resulting from the observed treatment-dependent diurnal variations of LER. The simplest, most parsimonious hypothesis that can explain the relationship between the diurnal LER dynamics and diurnal epidermal cell elongation dynamics is, therefore, that epidermal cell elongation rate exhibited proportionally the same diurnal perturbations as LER. We cannot rule out, however, based on our data alone, that there is perhaps a more complex mechanism, e.g. some complementary compensation between cell elongation rate and duration dynamics that could modify to some extent the exact relationship between LER and epidermal cell elongation rate dynamics (Masle, 2000). In addition, other works have found some CO_2 effect on cell division and expansion (e.g. Ferris *et al.*, 1996; Masle, 2000), and it is not clear what mechanism(s) caused divergence of those results from the present. Certainly, the diel elongation responses found in this work warrant more detailed mechanistic studies with spatio-temporal detail at the level of expanding tissue, including the kinematics of growth, cell division, expansion and associated metabolic processes (e.g. Green *et al.*, 1971; Nonami & Boyer, 1993; Martre *et al.*, 1999; Fricke & Peters, 2002; Moulia *et al.*, 2019).

In conclusion, this work demonstrated a close integration of daytime and night-time leaf elongation in an important forage grass under contrasting atmospheric CO_2 and VPD conditions in a controlled environment mesocosm. LER_{day} was under hydraulic control, in agreement with expected effects of atmospheric CO_2 and VPD on stomatal control, and ensuing effects on transpiration and hydraulic effects on cell wall expansion. Conversely, a compensatory growth mechanism (stored growth) controlled LER_{night} in such a way that daily LER remained unaffected by atmospheric conditions of CO_2 and VPD. Source limitation was not a factor under the conditions of this experiment as water-soluble carbohydrate levels in the LGDZ were high even when atmospheric CO_2 concentration was only half-ambient. Absence of source limitation may have resulted, in part, from a relatively limiting nitrogen fertilizer supply and the high radiation received by the stands. Water supply was unlimiting, thus putative feedbacks of eventual soil drying on the leaf elongation process – that would occur more readily with high transpiration at low C_a – had no effect, but are important factors to be considered. So, building on the present findings, studies of the diel oscillation of leaf elongation and underlying mechanism should be expanded to a greater range of plant functional groups, environmental conditions (including photoperiod length, irradiance, and thermal and nutritional conditions) to further improve our understanding of the plant physiology of climate change adaptation.

Acknowledgements

The authors thank Michaela Kaspar and Lea Lorentz for help with leaf elongation measurements, Anja Schmidt, Monika Michler, Angela Ernst-Schwärzli, Wolfgang Feneis and Richard Wenzel for assistance with sampling and sample processing (AS, MM, AES), maintenance of the mesocosm facility and gas exchange equipment (WF, RW) and carbohydrate analyses (AS), and Urs Schmidhalter (Chair of Plant Nutrition) for helpful methodological discussions. The Chair of Plant Nutrition is thanked for lending the vapor pressure osmometer and pressure chamber. The authors further thank the Center for Advanced Light Microscopy (CALM) for providing access to their

equipment and software for digital image analysis. This research was supported by the Deutsche Forschungsgemeinschaft (DFG SCHN 557/9-1). JZ was supported by the China Scholarship Council (CSC).

Author contributions

JCBC and HS designed the experiment. JCBC performed the research, analyzed the data and wrote the first draft. RTH, JZ and RS helped with gas exchange measurements. All authors contributed to the revision of the manuscript.

ORCID

Juan C. Baca Cabrera https://orcid.org/0000-0001-8159-3837
Hans Schnyder https://orcid.org/0000-0002-0139-7535

References

Ainsworth EA, Long SP. 2005. What have we learned from 15 years of free-air CO_2 enrichment (FACE)? A meta-analytic review of the responses of photosynthesis, canopy properties and plant production to rising CO_2. *New Phytologist* **165**: 351–372.

Ainsworth EA, Rogers A. 2007. The response of photosynthesis and stomatal conductance to rising CO_2: mechanisms and environmental interactions. *Plant, Cell & Environment* **30**: 258–270.

Barlow E. 1986. Water relations of expanding leaves. *Functional Plant Biology* **13**: 45–58.

Ben Haj Salah H, Tardieu F. 1996. Quantitative analysis of the combined effects of temperature, evaporative demand and light on leaf elongation rate in well-watered field and laboratory-grown maize plants. *Journal of Experimental Botany* **47**: 1689–1698.

Bouchabke O, Tardieu F, Simonneau T. 2006. Leaf growth and turgor in growing cells of maize (*Zea mays* L.) respond to evaporative demand under moderate irrigation but not in water-saturated soil. *Plant, Cell & Environment* **29**: 1138–1148.

Bowes G. 1993. Facing the inevitable: plants and increasing atmospheric CO_2. *Annual Review of Plant Physiology and Plant Molecular Biology* **44**: 309–332.

Buckley TN. 2019. How do stomata respond to water status? *New Phytologist* **224**: 21–36.

Caldeira CF, Bosio M, Parent B, Jeanguenin L, Chaumont F, Tardieu F. 2014a. A hydraulic model is compatible with rapid changes in leaf elongation rate under fluctuating evaporative demand and soil water status. *Plant Physiology* **164**: 1718–1730.

Caldeira CF, Jeanguenin L, Chaumont F, Tardieu F. 2014b. Circadian rhythms of hydraulic conductance and growth are enhanced by drought and improve plant performance. *Nature Communications* **5**: 5365.

Cleland R, Rayle DL. 1972. Absence of auxin-induced stored growth in *Avena* coleoptiles and its implication concerning the mechanism of wall extension. *Planta* **106**: 61–71.

Clifton-Brown JC, Jones MB. 1999. Alteration of transpiration rate, by changing air vapour pressure deficit, influences leaf extension rate transiently in *Miscanthus*. *Journal of Experimental Botany* **50**: 1393–1401.

Cosgrove DJ. 2018. Diffuse growth of plant cell walls. *Plant Physiology* **176**: 16–27.

Durand J-L, Onillon B, Schnyder H, Rademacher I. 1995. Drought effects on cellular and spatial parameters of leaf growth in tall fescue. *Journal of Experimental Botany* **46**: 1147–1155.

Ferris R, Nijs I, Behaeghe T, Impens I. 1996. Contrasting CO_2 and temperature effects on leaf growth of perennial ryegrass in spring and summer. *Journal of Experimental Botany* **47**: 1033–1043.

Ferris R, Taylor G. 1994. Elevated CO_2, water relations and biophysics of leaf extension in four chalk grassland herbs. *New Phytologist* **127**: 297–307.

Fricke W, Peters WS. 2002. The biophysics of leaf growth in salt-stressed barley. A study at the cell level. *Plant Physiology* **129**: 374–388.

Gallagher JN, Biscoe PV. 1979. Field studies of cereal leaf growth: III. Barley leaf extension in relation to temperature, irradiance and water potential. *Journal of Experimental Botany* **30**: 645–655.

Gamage D, Thompson M, Sutherland M, Hirotsu N, Makino A, Seneweera S. 2018. New insights into the cellular mechanisms of plant growth at elevated atmospheric carbon dioxide concentrations. *Plant, Cell & Environment* **41**: 1233–1246.

Green PB, Erickson RO, Buggy J. 1971. Metabolic and physical control of cell elongation rate: in vivo studies in *Nitella*. *Plant Physiology* **47**: 423–430.

Hsiao TC, Acevedo E, Henderson DW. 1970. Maize leaf elongation: continuous measurements and close dependence on plant water status. *Science* **168**: 590–591.

IPCC. 2015. Climate change 2014: synthesis report. In: Core Writing Team, Pachauri RK, Meyer LA, eds. *Contribution of working groups I, II and III to the fifth assessment report of the intergovernmental panel on climate change*. Geneva, Switzerland: IPCC.

Kavanová M, Lattanzi FA, Grimoldi AA, Schnyder H. 2006. Phosphorus deficiency decreases cell division and elongation in grass leaves. *Plant Physiology* **141**: 766–775.

Kavanová M, Lattanzi FA, Schnyder H. 2008. Nitrogen deficiency inhibits leaf blade growth in *Lolium perenne* by increasing cell cycle duration and decreasing mitotic and post-mitotic growth rates. *Plant, Cell & Environment* **31**: 727–737.

Kimball BA. 2016. Crop responses to elevated CO_2 and interactions with H_2O, N, and temperature. *Current Opinion in Plant Biology* **31**: 36–43.

Koch K. 2004. Sucrose metabolism: regulatory mechanisms and pivotal roles in sugar sensing and plant development. *Current Opinion in Plant Biology* **7**: 235–246.

Leakey ADB, Ainsworth EA, Bernacchi CJ, Rogers A, Long SP, Ort DR. 2009. Elevated CO_2 effects on plant carbon, nitrogen, and water relations: six important lessons from FACE. *Journal of Experimental Botany* **60**: 2859–2876.

LeBauer DS, Treseder KK. 2008. Nitrogen limitation of net primary productivity in terrestrial ecosystems is globally distributed. *Ecology* **89**: 371–379.

Lehmeier CA, Lattanzi FA, Schäufele R, Wild M, Schnyder H. 2008. Root and shoot respiration of perennial ryegrass are supplied by the same substrate pools: assessment by dynamic ^{13}C labeling and compartmental analysis of tracer kinetics. *Plant Physiology* **148**: 1148–1158.

Lehmeier CA, Wild M, Schnyder H. 2013. Nitrogen stress affects the turnover and size of nitrogen pools supplying leaf growth in a grass. *Plant Physiology* **162**: 2095–2105.

Lenth R. 2018. Package 'lsmeans'. *The American Statistician* **34**: 216–221.

Liu HT, Gong XY, Schäufele R, Yang F, Hirl RT, Schmidt A, Schnyder H. 2016. Nitrogen fertilization and $\delta^{18}O$ of CO_2 have no effect on ^{18}O-enrichment of leaf water and cellulose in Cleistogenes squarrosa (C_4) – is VPD the sole control? *Plant, Cell & Environment* **39**: 2701–2712.

Liu HT, Schäufele R, Gong XY, Schnyder H. 2017. The $\delta^{18}O$ and $\delta^{2}H$ of water in the leaf growth-and-differentiation zone of grasses is close to source water in both humid and dry atmospheres. *New Phytologist* **214**: 1423–1431.

Lockhart JA. 1965. An analysis of irreversible plant cell elongation. *Journal of Theoretical Biology* **8**: 264–275.

Lunn JE. 2008. Sucrose metabolism. In: Smith AM, ed. *Encyclopedia of life science (ELS)*. Chichester, UK: John Wiley & Sons, 1–9.

Lüthi D, Le Floch M, Bereiter B, Blunier T, Barnola J-M, Siegenthaler U, Raynaud D, Jouzel J, Fischer H, Kawamura K *et al.* 2008. High-resolution carbon dioxide concentration record 650,000–800,000 years before present. *Nature* **453**: 379–382.

MacAdam JW, Volenec JJ, Nelson CJ. 1989. Effects of nitrogen on mesophyll cell division and epidermal cell elongation in tall fescue leaf blades. *Plant Physiology* **89**: 549–556.

Manderscheid R, Erbs M, Burkart S, Wittich K-P, Löpmeier F-J, Weigel H-J. 2016. Effects of free-air carbon dioxide enrichment on sap flow and canopy microclimate of maize grown under different water supply. *Journal of Agronomy and Crop Science* **202**: 255–268.

Martre P, Bogeat-Triboulot M-B, Durand J-L. 1999. Measurement of a growth-induced water potential gradient in tall fescue leaves. *New Phytologist* **142**: 435–439.

Martre P, Cochard H, Durand J-L. 2001. Hydraulic architecture and water flow in growing grass tillers (*Festuca arundinacea* Schreb.). *Plant, Cell & Environment* **24**: 65–76.

Masle J. 2000. The effects of elevated CO_2 concentrations on cell division rates, growth patterns, and blade anatomy in young wheat plants are modulated by factors related to leaf position, vernalization, and genotype. *Plant Physiology* **122**: 1399–1415.

Morrison MJ. 1993. Heat stress during reproduction in summer rape. *Canadian Journal of Botany* **71**: 303–308.

Moulia B, Bastien R, Chauvet-Thiry H, Leblanc-Fournier N. 2019. Posture control in land plants: growth, position sensing, proprioception, balance, and elasticity. *Journal of Experimental Botany* **70**: 3467–3494.

Nonami H, Boyer JS. 1993. Direct demonstration of a growth-induced water potential gradient. *Plant Physiology* **102**: 13–19.

Pantin F, Simonneau T, Muller B. 2012. Coming of leaf age: control of growth by hydraulics and metabolics during leaf ontogeny. *New Phytologist* **196**: 349–366.

Pantin F, Simonneau T, Rolland G, Dauzat M, Muller B. 2011. Control of leaf expansion: a developmental switch from metabolics to hydraulics. *Plant Physiology* **156**: 803–815.

Parrish DJ, Wolf DD. 1983. Kinetics of tall fescue leaf elongation: responses to changes in illumination and vapor pressure 1. *Crop Science* **23**: 659–663.

Passioura JB. 1980. The meaning of matric potential. *Journal of Experimental Botany* **31**: 1161–1169.

Passioura JB. 1988. Root signals control leaf expansion in wheat seedlings growing in drying soil. *Functional Plant Biology* **15**: 687–693.

Passioura JB. 2002. Soil conditions and plant growth. *Plant, Cell & Environment* **25**: 311–318.

Passioura JB, Fry SC. 1992. Turgor and cell expansion: beyond the Lockhart equation. *Functional Plant Biology* **19**: 565–576.

Pinheiro J, Bates D, DebRoy S, Sarkar D, R Core Team. 2019. *nlme: Linear and Nonlinear Mixed Effects Models. R package v.3.1-141.* [WWW document] URL https://CRAN.R-project.org/package=nlme.

Poorter H, Navas M-L. 2003. Plant growth and competition at elevated CO_2: on winners, losers and functional groups. *New Phytologist* **157**: 175–198.

Proseus TE, Boyer JS. 2006. Periplasm turgor pressure controls wall deposition and assembly in growing *Chara corallina* cells. *Annals of Botany* **98**: 93–105.

Proseus TE, Boyer JS. 2008. Calcium pectate chemistry causes growth to be stored in *Chara corallina*: a test of the pectate cycle. *Plant, Cell & Environment* **31**: 1147–1155.

R Core Team. 2019. *R: A language and environment for statistical computing.* Vienna, Austria: R Foundation for Statistical Computing.

Radin JW, Boyer JS. 1982. Control of leaf expansion by nitrogen nutrition in sunflower plants. *Plant Physiology* **69**: 771–775.

Ranasinghe S, Taylor G. 1996. Mechanism for increased leaf growth in elevated CO_2. *Journal of Experimental Botany* **47**: 349–358.

Ray PM, Green PB, Cleland R. 1972. Role of turgor in plant cell growth. *Nature* **239**: 163–164.

Reich PB, Hobbie SE, Lee TD. 2014. Plant growth enhancement by elevated CO_2 eliminated by joint water and nitrogen limitation. *Nature Geoscience* **7**: 920.

Schneider CA, Rasband WS, Eliceiri KW. 2012. NIH Image to ImageJ: 25 years of image analysis. *Nature Methods* **9**: 671.

Schnyder H, de Visser R. 1999. Fluxes of reserve-derived and currently assimilated carbon and nitrogen in perennial ryegrass recovering from defoliation. The regrowing tiller and its component functionally distinct zones. *Plant Physiology* **119**: 1423–1436.

Schnyder H, Nelson CJ. 1987. Growth rates and carbohydrate fluxes within the elongation zone of tall fescue leaf blades. *Plant Physiology* **85**: 548–553.

Schnyder H, Nelson CJ. 1988. Diurnal growth of tall fescue leaf blades. I. Spatial distribution of growth, deposition of water, and assimilate import in the elongation zone. *Plant Physiology* **86**: 1070–1076.

Schnyder H, Nelson CJ. 1989. Growth rates and assimilate partitioning in the elongation zone of tall fescue leaf blades at high and low irradiance. *Plant Physiology* **90**: 1201–1206.

Schnyder H, Schäufele R, Lötscher M, Gebbing T. 2003. Disentangling CO_2 fluxes: direct measurements of mesocosm-scale natural abundance $^{13}CO_2/^{12}CO_2$ gas exchange, ^{13}C discrimination, and labelling of CO_2 exchange flux components in controlled environments. *Plant, Cell and Environment* **26**: 1863–1874.

Schnyder H, Seo S, Rademacher IF, Kühbauch W. 1990. Spatial distribution of growth rates and of epidermal cell lengths in the elongation zone during leaf development in *Lolium perenne* L. *Planta* **181**: 423–431.

Scholander PF, Hammel HT, Bradstreet ED, Hemmingsen EA. 1965. Sap pressure in vascular plants. *Science* **148**: 339–346.

Seneweera SP, Basra AS, Barlow EW, Conroy JP. 1995. Diurnal regulation of leaf blade elongation in rice by CO_2. *Plant Physiology* **108**: 1471–1477.

Seneweera SP, Conroy JP. 2005. Enhanced leaf elongation rates of wheat at elevated CO_2: is it related to carbon and nitrogen dynamics within the growing leaf blade? *Environmental and Experimental Botany* **54**: 174–181.

Serpe MD, Matthews MA. 1994. Changes in cell wall yielding and stored growth in *Begonia argenteo-guttata* L. leaves during the development of water deficits. *Plant and Cell Physiology* **35**: 619–626.

Sionit N, Strain BR, Hellmers Henry, Kramer PJ. 1981. Effects of atmospheric CO_2 concentration and water stress on water relations of wheat. *Botanical Gazette* **142**: 191–196.

Tardieu F, Granier C, Muller B. 1999. Modelling leaf expansion in a fluctuating environment: are changes in specific leaf area a consequence of changes in expansion rate? *New Phytologist* **143**: 33–43.

Tardieu F, Parent B, Simonneau T. 2010. Control of leaf growth by abscisic acid: hydraulic or non-hydraulic processes? *Plant, Cell & Environment* **33**: 636–647.

Tardieu F, Simonneau T, Muller B. 2018. The physiological basis of drought tolerance in crop plants: a scenario-dependent probabilistic approach. *Annual Review of Plant Biology* **69**: 733–759.

Thilakarathne CL, Tausz-Posch S, Cane K, Norton RM, Fitzgerald GJ, Tausz M, Seneweera S. 2015. Intraspecific variation in leaf growth of wheat (*Triticum aestivum*) under Australian Grain Free Air CO_2 Enrichment (AGFACE): is it regulated through carbon and/or nitrogen supply? *Functional Plant Biology* **42**: 299–308.

Turner NC. 1981. Techniques and experimental approaches for the measurement of plant water status. *Plant and soil* **58**: 339–366.

Tyree MT, Alexander JD. 1993. Plant water relations and the effects of elevated CO_2: a review and suggestions for future research. *Vegetatio* **104**: 47–62.

Van Volkenburgh E. 1999. Leaf expansion–an integrating plant behaviour. *Plant, Cell & Environment* **22**: 1463–1473.

Volenec JJ, Nelson CJ. 1982. Diurnal leaf elongation of contrasting tall fescue genotypes. *Crop Science* **22**: 531–535.

Wickham H. 2016. *ggplot2: elegant graphics for data analysis.* New York, NY, USA: Springer Verlag.

Wolf DD, Ellmore TL. 1975. Automated hydrolysis of nonreducing sugars and fructosans from plant tissue. *Crop Science* **15**: 775–777.

Supporting Information

Additional Supporting Information may be found online in the Supporting Information section at the end of the article.

Fig. S1 Pot arrangement in the growth chamber.

Fig. S2 Daily leaf elongation rate of *Lolium perenne* at different leaf developmental stages as influenced by atmospheric CO_2 concentration at low and high daytime VPD.

Fig. S3 Epidermal cell length density at the margins of an individual leaf blade replica in *Lolium perenne* plants grown at different atmospheric CO_2 concentrations at low or high daytime VPD.

Fig. S4 Leaf appearance interval and specific leaf area of *Lolium perenne* as influenced by atmospheric CO_2 concentration and VPD.

Fig. S5 Time course of leaf elongation rate of *Lolium perenne* as influenced by atmospheric CO_2 concentration and VPD.

Fig. S6 Canopy transpiration of *Lolium perenne* during day-light hours as influenced by atmospheric CO_2 concentration, VPD and irrigation events.

Fig. S7 Nocturnal leaf elongation rate of *Lolium perenne* as influenced by nocturnal transfers to contrasting atmospheric CO_2 concentration.

Table S1 Experimental design.

Table S2 Response of daytime and night-time leaf elongation rate of *Lolium perenne* to atmospheric CO_2 concentration, daytime VPD and their interaction.

Table S3 Stomatal conductance and leaf transpiration of *Lolium perenne* during the day at different atmospheric CO_2 concentration and daytime VPD.

Table S4 Response of water-soluble carbohydrate concentration in the leaf growth-and-differentiation zone of *Lolium perenne* to atmospheric CO_2 concentration, daytime VPD and diel period.

Table S5 Concentration of water-soluble carbohydrates in the leaf growth-and-differentiation zone of *Lolium perenne* at the end of the day and night at different atmospheric CO_2 concentration and daytime VPD.

Table S6 Response of nocturnal leaf elongation rate of *Lolium perenne* to water potential of the youngest fully-expanded leaf, osmotic potential of the leaf growth-and-differentiation zone and turgor.

Table S7 Nitrogen concentration in the leaf growth-and-differentiation zone of *Lolium perenne* for combinations of atmospheric CO_2 concentration and daytime VPD levels.

Table S8 Response of nocturnal leaf elongation rate of *Lolium perenne* to transfer/swapping of plants between contrasting CO_2 environments.

Please note: Wiley Blackwell are not responsible for the content or functionality of any Supporting Information supplied by the authors. Any queries (other than missing material) should be directed to the *New Phytologist* Central Office.

18O enrichment of leaf cellulose correlated with 18O enrichment of leaf sucrose but not bulk leaf water in a C3 grass across contrasts of atmospheric CO2 concentration and air humidity

Juan C. Baca Cabrera
Technische Universität München, Lehrstuhl für Grünlandlehre https://orcid.org/0000-0001-8159-3837

Regina T. Hirl
Technische Universität München, Lehrstuhl für Grünlandlehre

Rudi Schäufele
Technische Universität München, Lehrstuhl für Grünlandlehre

Jianjun Zhu
Technische Universität München, Lehrstuhl für Grünlandlehre

Haitao Liu
College of Resources and Environment, Henan Agricultural University

Jérôme Ogée
UMR ISPA, INRAE

Hans Schnyder (schnyder@wzw.tum.de)
Technische Universität München, Lehrstuhl für Grünlandlehre https://orcid.org/0000-0002-0139-7535

Research Article

Keywords: Lolium perenne (perennial ryegrass), Barbour-Farquhar model of 18O-enrichment in cellulose, 18O in leaf water, sucrose and cellulose, atmospheric CO2 concentration, relative humidity of air

DOI: https://doi.org/10.21203/rs.3.rs-596094/v1

^{18}O enrichment of leaf cellulose correlated with ^{18}O enrichment of leaf sucrose but not bulk leaf water in a C_3 grass across contrasts of atmospheric CO_2 concentration and air humidity

Authors

Juan C. Baca Cabrera[1], Regina T. Hirl[1], Rudi Schäufele[1], Jianjun Zhu[1], Haitao Liu[2], Jérôme Ogée[3], Hans Schnyder[1]

Addresses

[1] Technische Universität München, Lehrstuhl für Grünlandlehre, Alte Akademie 12, 85354 Freising-Weihenstephan, Germany

[2] College of Resources and Environment, Henan Agricultural University, Zhengzhou 450002, PR China

[3] UMR ISPA, INRAE, 33140 Villenave d'Ornon, France

Author for correspondence

Hans Schnyder

Tel.: +49 (0)8161-715165; Email: schnyder@wzw.tum.de

Additional information:

Total word count: 5118

Introduction: 1419

Material and Methods: 1157

Results: 676

Discussion: 1866

Number of figures: 3 (1 in color)

Number of tables: 1

Supporting information included

Summary

- The ^{18}O composition of plant cellulose is often used to reconstruct past climate and plant function. However, uncertainty remains regarding the estimation of the leaf sucrose ^{18}O signal and its subsequent attenuation by ^{18}O exchange with source water during cellulose synthesis.
- We grew *Lolium perenne* at three CO_2 concentrations (200, 400 or 800 μmol mol^{-1}) and two relative humidity (RH) levels (50% or 75%), and determined ^{18}O enrichment of leaf sucrose ($\Delta^{18}O_{Sucrose}$), bulk leaf water ($\Delta^{18}O_{LW}$), leaf cellulose ($\Delta^{18}O_{Cellulose}$) and water at the site of cellulose synthesis ($\Delta^{18}O_{CelSynW}$).
- $\Delta^{18}O_{Cellulose}$ correlated with $\Delta^{18}O_{Sucrose}$ (R^2=0.87) but not with $\Delta^{18}O_{LW}$ (R^2=0.04), due to a variable ^{18}O discrepancy (range 2.0-9.0‰) between sucrose synthesis water ($\Delta^{18}O_{SucSynW}$, estimated from $\Delta^{18}O_{Sucrose}$) and bulk leaf water. The discrepancy resulted mainly from an RH effect. The proportion of oxygen in cellulose that exchanged with medium water during cellulose formation (p_{ex}), was near-constant when referenced to $\Delta^{18}O_{SucSynW}$ ($p_{ex\text{-}SucSynW}$ = 0.52±0.02 SE), but varied when related to bulk leaf water ($p_{ex\text{-}LW}$ = –0.01 to 0.46).
- We conclude that previously reported RH-dependent variations of $p_{ex\text{-}LW}$ in grasses are related to a discrepancy between $\Delta^{18}O_{SucSynW}$ and $\Delta^{18}O_{LW}$ that may result from spatial heterogeneity in ^{18}O gradients of leaf water and photosynthetic sucrose synthesis.

Key words: *Lolium perenne* (perennial ryegrass), Barbour-Farquhar model of ^{18}O-enrichment in cellulose, ^{18}O in leaf water, sucrose and cellulose, atmospheric CO_2 concentration, relative humidity of air.

Introduction

The oxygen isotope $^{18}O/^{16}O$ ratio of plant cellulose ($\delta^{18}O_{Cellulose}$) and its enrichment above source water ($\Delta^{18}O_{Cellulose}$, with $\Delta^{18}O_{Cellulose} \approx \delta^{18}O_{Cellulose} - \delta^{18}O_{Source}$) contain important environmental and physiological information (see e.g. Roden *et al.*, 2000; Barbour, 2007; Werner *et al.*, 2012; Gessler *et al.*, 2014 for reviews). This is based on the fact that all oxygen in cellulose ultimately originates from water (DeNiro & Epstein, 1979; Liu *et al.*, 2016), and that evaporative ^{18}O enrichment of water in leaves (Dongmann *et al.*, 1974; Flanagan *et al.*, 1991; Roden & Ehleringer, 1999; Farquhar & Cernusak, 2005; Cernusak *et al.*, 2016) imprints an ^{18}O signal onto photosynthetic products (Sternberg & DeNiro, 1983; Sternberg *et al.*, 1986; Farquhar *et al.*, 1998) used for cellulose synthesis in growing sink tissues (Barbour *et al.*, 2000; Helliker & Ehleringer, 2002; Cernusak *et al.*, 2005). However, the exact isotopic identity of the water that dictates the ^{18}O signal of primary photosynthetic products is still uncertain (Lehmann *et al.*, 2017) and a variable proportion ($p_{ex}p_x$, see below) of the original ^{18}O signal in photosynthetic products appears to be subsequently lost by exchange with source water (Helliker & Ehleringer, 2002; Lehmann *et al.*, 2017; Hirl *et al.*, 2021), so that the relationship between the ^{18}O signal in cellulose and evaporative events determining the ^{18}O signal in photosynthetic products is still unsettled. The present paper is addressing these uncertainties, and explores the underlying mechanisms, using perennial ryegrass (*Lolium perenne*, C_3) grown in contrasting CO_2 and atmospheric humidity levels as a model plant.

Current mechanistic understanding of the relationship between evaporative ^{18}O enrichment of water at the site of sucrose synthesis ($\Delta^{18}O_{SucSynW}$) – the most ubiquitous primary photosynthetic product and translocated sugar – and $\Delta^{18}O_{Cellulose}$ can be summarized quantitatively for steady-state conditions (Barbour & Farquhar, 2000) as:

$$\Delta^{18}O_{Cellulose} = \Delta^{18}O_{SucSynW}\,(1 - p_{ex}p_x) + \varepsilon_{bio}, \qquad \text{Eqn 1}$$

where p_x denotes the proportion of unenriched source water at the site of cellulose synthesis, p_{ex} is the proportion of oxygen atoms in cellulose that have exchanged with medium water during cellulose formation at that site, and ε_{bio} is the average biochemical fractionation between carbonyl oxygen and water. The term $\Delta^{18}O_{SucSynW} + \varepsilon_{bio}$ represents the ^{18}O enrichment of leaf sucrose above source water. In field conditions, Eqn 1 requires consideration of non-steady-states and necessitates computation of flux-weighted signals (Cernusak *et al.*, 2005; Barbour, 2007).

When applying Eqn. 1, it is generally assumed that p_x, p_{ex} and ε_{bio} are constant parameters: p_x is often set to unity while p_{ex} is often assumed to vary within a narrow range

between 0.4 and 0.5 (Barbour, 2007; Liu *et al.*, 2016) and ε_{bio} is equal to 27‰ (Sternberg & DeNiro, 1983; Yakir & DeNiro, 1990). Another, almost general, assumption of previous works has been that $\Delta^{18}O_{SucSynW}$ equals the average ^{18}O enrichment of bulk or lamina leaf water ($\Delta^{18}O_{LW}$), so that (assimilation-weighted) $\Delta^{18}O_{SucSynW}$ can be replaced by $\Delta^{18}O_{LW}$ in Eqn 1. This assumption is practical, as measurements (and modelling) of $\Delta^{18}O_{LW}$ are relatively straightforward in comparison to $\Delta^{18}O_{SucSynW}$. However, this assumption is often hard to validate from cellulose ^{18}O data because p_{ex} cannot be measured directly, and can only be estimated as a fitted parameter in Eqn 1. Values of p_{ex} estimated in this way therefore absorb all the uncertainty in the other parameters of the equation, including any possible error in the $\Delta^{18}O_{LW} \approx \Delta^{18}O_{SucSynW}$ assumption.

The assumption that $\Delta^{18}O_{LW} \approx \Delta^{18}O_{SucSynW}$ has received direct support in only two studies that compared ^{18}O enrichment in phloem sap dry organic matter and assimilation-weighted bulk leaf water: one on *Ricinus communis* during steady-state leaf cuvette measurements (Cernusak *et al.*, 2003) and another on *Eucalyptus globulus* in the field (Cernusak *et al.*, 2005). Both studies found good agreement between the two signals, provided that the biochemical fractionation ε_{bio} was set at 27‰. However, phloem sap is not only composed of sucrose and recent work by Lehmann *et al.* (2017) with two C_3 grasses in controlled environments found that sucrose extracted from leaves was substantially more ^{18}O enriched than 27‰ relative to bulk leaf water, questioning the universal validity of the $\Delta^{18}O_{LW} \approx \Delta^{18}O_{SucSynW}$ assumption.

Several other recent studies seem to agree that most simplifying assumptions often applied to the Barbour-Farquhar model (i.e. $\Delta^{18}O_{LW} = \Delta^{18}O_{SucSynW}$; ε_{bio} = 27‰; $p_x \approx 1$; $p_{ex} \approx$ 0.4-0.5) should be questioned. First, there are good indications that the biochemical fractionation ε_{bio} decreases with increasing temperature, with a virtually identical temperature-dependence in aquatic plants and in heterotrophically grown wheat seedlings (Sternberg & Ellsworth, 2011) and a value of *ca.* 26.7‰ at 20°C. This temperature dependence of ε_{bio} was also required to explain interannual and seasonal variations of leaf $\delta^{18}O_{cellulose}$ in a temperate grassland ecosystem (Hirl *et al.*, 2021). In addition, although p_x has been shown to be close to unity in trees (Cernusak *et al.*, 2005) and in the leaf growth-and-differentiation zone of grasses (Liu *et al.*, 2017) that is protected from evaporation, p_x is less certain in dicot species because the leaves are directly exposed to evaporative conditions during their growth. Several recent studies (Song *et al.*, 2014; Liu *et al.*, 2016; Cheesman & Cernusak, 2017; Szejner *et al.*, 2020; Hirl *et al.*, 2021) also indicated large variations in p_{ex}, when p_{ex} was estimated using Eqn 1 with $\Delta^{18}O_{SucSynW}$ replaced by $\Delta^{18}O_{LW}$, measured (or well-constrained) estimates of p_x and a

temperature-dependent ε_{bio} from Sternberg & Ellsworth (2011). Thus far, variations of p_{ex} have been mainly attributed to (1) hexose phosphates going through a futile cycle with triose phosphates before cellulose synthesis (Hill *et al.*, 1995) and an increased probability for an oxygen atom derived from sucrose going through an exchangeable carbonyl group with each turn of the futile cycle (Barbour & Farquhar, 2000; Barbour, 2007), (2) unaccounted participation of non-structural carbohydrate stores in cellulose synthesis (Pfanz *et al.*, 2002; Cernusak & Cheesman, 2015) and (3) changes in turnover of non-structural carbohydrate pools (Song *et al.*, 2014).

Estimates of p_x are also affected by any error in the $\Delta^{18}O_{SucSynW} = \Delta^{18}O_{LW}$ assumption. This is because true p_x is calculated from determinations of ^{18}O-enrichment of water at the site of cellulose synthesis ($\Delta^{18}O_{CelSynW}$), source water ($\Delta^{18}O_{Source}$, with $\Delta^{18}O_{Source} = 0$ by definition) and $\Delta^{18}O_{SucSynW}$, using a two-member mixing model that has $\Delta^{18}O_{Source}$ and $\Delta^{18}O_{SucSynW}$ as its endmember:

$$p_x = 1 - \Delta^{18}O_{CelSynW}/\Delta^{18}O_{SucSynW}. \qquad \text{Eqn 2}$$

Importantly, reported variation of p_{ex} seems to follow environmental patterns across plant functional groups, particularly with respect to relative humidity of air (RH) (Offermann *et al.*, 2011; Liu *et al.*, 2016; Hirl *et al.*, 2021). Relative humidity is known to generally affect the ^{18}O enrichment of bulk leaf water but also its spatial variations in leaf blades (Cernusak *et al.*, 2016). In particular, very large variations of ^{18}O enrichment have been found in several monocot leaves, from base to tip and center to edge (Helliker & Ehleringer, 2000; Gan *et al.*, 2002; Helliker & Ehleringer, 2002; Gan *et al.*, 2003), that may underlie variation of the $\Delta^{18}O_{LW}$ versus $\Delta^{18}O_{SucSynW}$ relationship (Lehmann *et al.*, 2017).

Another environmental factor that deserves attention when applying Eqn 1 to biological archives is atmospheric CO_2 concentration, because its rise over the last century may have affected the relationship between $\Delta^{18}O_{LW}$ and $\Delta^{18}O_{SucSynW}$ and resultant estimates of p_{ex} and p_x based on the use of $\Delta^{18}O_{LW}$ (termed $p_{ex\text{-}LW}$ in the following) instead of $\Delta^{18}O_{SucSynW}$ ($p_{ex\text{-}SucSynW}$) in Eqn 1. Atmospheric CO_2 concentration has been shown to have a strong effect on stomatal conductance (Ainsworth & Rogers, 2007; Franks *et al.*, 2013) and consequently on transpiration (Leakey *et al.*, 2009), storage of non-structural carbohydrates (Poorter & Navas, 2003) and on the diurnal oscillation of leaf elongation (Baca Cabrera *et al.*, 2020). All these factors can affect, directly or indirectly, $\Delta^{18}O_{LW}$, $\Delta^{18}O_{SucSynW}$, $\Delta^{18}O_{Cellulose}$, and p_{ex} and p_x, estimated with either $\Delta^{18}O_{LW}$ or $\Delta^{18}O_{SucSynW}$.

In this study, we explored the combined effects of atmospheric CO_2 concentration (200, 400 or 800 μmol mol^{-1}), relative humidity (RH, 50% or 75% during daytime) and their

interactions on: $\Delta^{18}O_{Cellulose}$, $\Delta^{18}O_{LW}$, $\Delta^{18}O_{CelSynW}$ (estimated as the $\Delta^{18}O$ of water in the leaf growth-and-differentiation zone, $\Delta^{18}O_{LGDZ}$, Liu *et al.*, 2017), $\Delta^{18}O_{SucSynW}$ (estimated as $\Delta^{18}O_{Sucrose} - \varepsilon_{bio}$) and p_{ex} and p_x referenced to average leaf water ($p_{ex\text{-}LW}$ and $p_{x\text{-}LW}$) and sucrose synthesis water ($p_{ex\text{-}SucSynW}$ and $p_{x\text{-}SucSynW}$). In this, we asked specifically: (1) Do atmospheric CO_2 concentration and relative humidity or their interactions affect $\Delta^{18}O_{SucSynW}$ and its relationship with $\Delta^{18}O_{LW}$? (2) Do these environmental factors influence $\Delta^{18}O_{CelSynW}$? (3) How do $\Delta^{18}O_{SucSynW}$- and $\Delta^{18}O_{LW}$-based p_{ex} and p_x respond to these environmental factors? Finally, (4) do we find diurnal variation in these parameters, i.e. between light and dark periods?

Materials and Methods

Plant material and growth conditions

Perennial ryegrass (cv. 'Acento') plants were grown in four plant growth chambers (PGR15, Conviron, Winnipeg, Canada) in a 16 h : 8 h, day : night cycle (temperature 20/16°C), under a 3 × 2 factorial design: three atmospheric CO_2 concentration levels ('half-ambient' = 200, 'ambient' = 400 or 'double-ambient' = 800 µmol mol^{-1}) and two daytime relative humidity levels (low RH = 50%, high RH = 75%; nighttime RH was 75% for all treatments), as previously described in Baca Cabrera *et al.* (2020). In brief, *L. perenne* plants were grown individually in plastic tubes (350 mm height, 50 mm diameter) filled with washed quartz sand (0.3–0.8 mm grain size) and arranged in plastic containers (770 × 560 × 300 mm) at a density of 383 plants m^{-2}. Plants were supplied 4 times a day with a Hoagland type nutrient solution with reduced nitrate-N content (Baca Cabrera *et al.*, 2020). Light was supplied by cool-white fluorescent tubes and warm-white LED bulbs with a constant photosynthetic photon flux density (PPFD) of 800 µmol m^{-2} s^{-1} at plant height during the 16 h-long light period. A total of five sequential experimental runs were performed, resulting in five chamber scale replicates for the so-called 'reference treatment' (400 µmol mol^{-1} CO_2 / 50% RH) and three replicate mesocosm-scale runs for the other treatments.

CO_2 and RH treatments were installed on the 13th day after seed imbibition. For this, the air supplied to the chambers was mixed from dry CO_2-free air and tank CO_2 (from Linde AG, Unterschleißheim, Germany or CARBO Kohlensäurewerke, Bad Hönningen, Germany), using mass flow controllers. RH and temperature were controlled by the chamber control system (CMP6050, Conviron, Winnipeg, Canada). CO_2 concentration and RH were measured every 30 min by an infrared gas analyzer (IRGA; Li-840; Li-Cor) and never deviated more than ± 5 µmol mol^{-1} and ± 2.0% relative to the set nominal value, respectively.

Sampling design and extraction of tissue water, cellulose and sucrose

Plants from each chamber scale replicate were sampled when plant canopies were closed (leaf area index >5.5, at 7-9 weeks after the beginning of the experiment). Sampling took place at c. 2 h before the end of the light and dark periods. Each time, 12 plants were randomly selected, dissected and the sampled plant material of six plants pooled in one subsample (providing two subsamples per chamber and per sampling occasion).

For tissue water extraction, the two youngest fully expanded leaf blades and the leaf growth-and-differentiation zone (LGDZ, see Fig. 1 in Baca Cabrera *et al*., 2020) of three mature tillers per plant were excised, sealed in 12 mL Exetainer vials (Labco, High Wycombe, UK), capped, wrapped with Parafilm and stored at –18°C until water extraction. Tissue water was extracted for 2 h using cryogenic vacuum distillation as in Liu *et al.* (2016).

For cellulose and sucrose extraction, the two youngest fully expanded leaf blades of another two mature tillers from the same plants were excised, placed into paper bags, frozen in liquid nitrogen, stored at –18 °C until freeze-drying, milled and stored again at –18 °C until cellulose and sucrose extraction. α-cellulose was extracted from 50 mg of dry sample material by following the Brendel *et al.* (2000) protocol as modified by Gaudinski *et al.* (2005). Water-soluble carbohydrates were extracted from 50 mg aliquots of dry material from to the youngest fully-expanded leaf blade and sucrose separated from other compounds using a preparative HPLC technique similar to that described by Gebbing & Schnyder (2001).

Isotope analysis

Oxygen isotope composition was expressed in per mil (‰) as:

$$\delta^{18}\mathrm{O} = \left(\frac{R_{\mathrm{sample}}}{R_{\mathrm{standard}}} - 1\right) \times 1000, \qquad \text{Eqn 3}$$

with R_{sample} the $^{18}\mathrm{O}/^{16}\mathrm{O}$ ratio of the sample and R_{standard} that in the international standard (Vienna Standard Mean Ocean Water, V-SMOW). $\delta^{18}\mathrm{O}$ was measured in the following compartments: tissue water of leaf blades ($\delta^{18}\mathrm{O}_{\mathrm{LW}}$) and of the LGDZ (designated $\delta^{18}\mathrm{O}_{\mathrm{CelSynW}}$); and cellulose and sucrose of leaf blades ($\delta^{18}\mathrm{O}_{\mathrm{Cellulose}}$ and $\delta^{18}\mathrm{O}_{\mathrm{Sucrose}}$). Furthermore, the nutrient solution (the source water for plants, $\delta^{18}\mathrm{O}_{\mathrm{Source}}$) was sampled 1-2 times per week. $\delta^{18}\mathrm{O}_{\mathrm{Source}}$ was near constant throughout the experiment (–9.7 ± 0.2‰ standard deviation). $\delta^{18}\mathrm{O}_{\mathrm{Source}}$ was used to calculate $^{18}\mathrm{O}$-enrichment above source water ($\Delta^{18}\mathrm{O}_X$) of the different samples (X) as:

$$\Delta^{18}\mathrm{O}_{\chi} = \frac{\delta^{18}\mathrm{O}_{\chi} - \delta^{18}\mathrm{O}_{\mathrm{Source}}}{1 + \delta^{18}\mathrm{O}_{\mathrm{Source}}/1000}, \qquad \text{Eqn 4}$$

Water samples were analyzed by cavity ring-down spectroscopy as described in Liu *et al.* (2016). 1 µL of water sample was injected into a A0211 high precision vaporizer coupled to a L2110-i-CRDS (both Picarro Inc., Sunnyvale, Ca, USA). Each sample was measured five to twelve times depending on memory effects. After every 15–25 samples, heavy and light laboratory water standards, spanning the range of $\delta^{18}O$ values in the dataset and previously calibrated against V-SMOW, V-GISP and V-SLAP, were measured for SMOW-scaling and possible drift correction. Analytical uncertainty was <0.2‰.

Cellulose and sucrose samples were measured by isotope ratio mass spectrometry (IRMS) as in Baca Cabrera *et al.* (2021). Each sample (sucrose or cellulose) was measured against a laboratory working standard carbon monoxide gas, previously calibrated against a secondary isotope standard (IAEA-601, accuracy of calibration ±0.25‰ standard deviation). Solid internal laboratory standards (cotton powder) were run each time after the measurement of four samples for possible drift correction and for SMOW-scaling. The precision for the laboratory standard was <0.3‰.

Additionally, $\delta^{18}O$ of water vapor in the growth chambers ($\delta^{18}O_{Vapor}$) was measured by cavity ring-down spectroscopy as described in Liu *et al.* (2016). Here, we measured $\delta^{18}O_{Vapor}$ continuously during two weeks when canopies were closed, both during the light and the dark periods. $\delta^{18}O_{Vapor}$ was constant across experimental runs and treatments, but was c. 1‰ more enriched during the dark period (−14.2‰ ± 0.5‰ standard deviation) than during the light period (−15.2‰ ± 0.6‰ standard deviation). Interestingly, the $\delta^{18}O_{Vapor}$ and $\delta^{18}O_{Source}$ in the chambers were quite similar to the multi-season average observed in a nearby grassland ecosystem study (Hirl *et al.*, 2019).

Statistics

In a first step, linear mixed models were fitted to test the effect of the diel period (day vs. night) on $\Delta^{18}O_{CelSynW}$ (n=80), $\Delta^{18}O_{LW}$ (n=160), $\Delta^{18}O_{Sucrose}$ (n=70) and $\Delta^{18}O_{Cellulose}$ (n=76). All available subsamples (pseudo-replicates) were included in the analysis, with growth chamber and experimental run defined as the random factors. As a significant diel trend was only detected for $\Delta^{18}O_{LW}$, day and night data of $\Delta^{18}O_{CelSynW}$, $\Delta^{18}O_{Sucrose}$ and $\Delta^{18}O_{Cellulose}$ were pooled for further analysis. In the case of $\Delta^{18}O_{LW}$, only end of day data were used in further calculations, i.e. to estimate $p_{x\text{-}LW}$, $p_{ex\text{-}LW}$ or the discrepancy between $\Delta^{18}O_{SucSynW}$ and $\Delta^{18}O_{LW}$. Data from individual chamber scale replications were pooled and two-way ANOVA tests used to assess the effects of CO_2, RH and their interaction on $\Delta^{18}O_{CelSynW}$, $\Delta^{18}O_{LW}$, $\Delta^{18}O_{Sucrose}$, $\Delta^{18}O_{Cellulose}$, $p_{x\text{-}LW}$, $p_{x\text{-}SucSynW}$, $p_{ex\text{-}LW}$, $p_{ex\text{-}SucSynW}$, and the discrepancy between $\Delta^{18}O_{SucSynW}$ and

$\Delta^{18}O_{LW}$ ($\Delta^{18}O_{SucSynW} - \Delta^{18}O_{LW}$). All statistical analyses were conducted in R v.4.0.2 (R Core Team, 2020). The R packages nlme (Pinheiro *et al.*, 2019) and ggplot2 (Wickham, 2016) were used for fitting linear mixed models and data plotting, respectively.

Results

^{18}O enrichment of sucrose, bulk leaf water and the discrepancy between sucrose synthesis- and bulk leaf-water

^{18}O enrichment of sucrose in leaf blades ($\Delta^{18}O_{Sucrose}$) differed significantly between RH levels, with low RH resulting in a higher $\Delta^{18}O_{Sucrose}$ (+6.4‰ on average) ($P < 0.001$, Fig. 1a, Table 1). An effect of atmospheric CO_2 concentration was also detected: $\Delta^{18}O_{Sucrose}$ decreased significantly with increasing CO_2 from 45.7‰ to 42.9‰ at low RH and from 39.0‰ to 37.0‰ at high RH ($P = 0.03$). Across treatments, $\Delta^{18}O_{Sucrose}$ did not differ significantly between samples collected near the end of the day and the end of the night ($P > 0.05$, Fig. 1a).

Unexpectedly, the ^{18}O enrichment of bulk leaf water ($\Delta^{18}O_{LW}$) was not affected by RH or the interaction between atmospheric CO_2 concentration and RH (Fig. 1b and Table 1). However, we did observe an effect of atmospheric CO_2 concentration on $\Delta^{18}O_{LW}$. That effect involved a decrease of $\Delta^{18}O_{LW}$ with increasing atmospheric CO_2 concentration both when measured near the end of the day ($P < 0.01$) and end of the night ($P < 0.001$). On average, $\Delta^{18}O_{LW}$ decreased by 1.7‰ between the 'half ambient' and 'double ambient' CO_2 concentrations. Besides, we observed a significant diurnal trend for $\Delta^{18}O_{LW}$ ($P < 0.001$): $\Delta^{18}O_{LW}$ was higher at the end of the day (7.9-10.2‰) than at the end of the night (6.7-8.8‰). That diurnal trend was similar for all treatments.

To estimate ^{18}O enrichment of sucrose synthesis water ($\Delta^{18}O_{SucSynW}$) from $\Delta^{18}O_{Sucrose}$ ($\Delta^{18}O_{SucSynW} = \Delta^{18}O_{Sucrose} - \varepsilon_{bio}$; Barbour 2007) a constant ε_{bio} was assumed (26.7‰, as estimated from Sternberg & Ellsworth, 2011, at 20°C) for all samples collected near the end of the light period. These data indicated that sucrose synthesis water was always more ^{18}O-enriched than bulk leaf water (Fig.1c). The discrepancy, that is $\Delta^{18}O_{SucSynW} - \Delta^{18}O_{LW}$, seemed unaffected by CO_2 ($P > 0.05$), but was much higher at low than at high RH (8.5‰ vs. 2.2‰; $P < 0.001$).

^{18}O enrichment of water in the leaf growth-and-differentiation zone and p_x

255 The ^{18}O enrichment of water in the leaf growth-and-differentiation zone ($\Delta^{18}O_{LGDZ}$ taken here
256 as a proxy for $\Delta^{18}O_{CelSynW}$) was small for all treatments (0.1-0.9‰) (Fig. 1b). It decreased
257 slightly with increasing atmospheric CO_2 (P = 0.04, 0.4‰ decrease between 200 and 800 µmol
258 mol^{-1}, on average), but did not respond to RH or the interaction of CO_2 and RH (Table 1). Also,
259 we observed no significant differences in $\Delta^{18}O_{CelSynW}$ between day and night (P > 0.05).

260

261 **Table 1** Results of a two-way ANOVA testing the effect of atmospheric CO_2 concentration,
262 RH and their interaction on: $\Delta^{18}O$ of sucrose ($\Delta^{18}O_{Sucrose}$), $\Delta^{18}O$ of bulk water in the leaf
263 blades ($\Delta^{18}O_{LW}$) and in the leaf growth-and-differentiation zone ($\Delta^{18}O_{CelSynW}$), the discrepancy
264 between $\Delta^{18}O_{SucSynW}$ and $\Delta^{18}O_{LW}$ ($\Delta^{18}O_{SucSynW} - \Delta^{18}O_{LW}$), $\Delta^{18}O$ of cellulose in leaf blades
265 ($\Delta^{18}O_{cellulose}$) and p_{ex} and p_x referenced to average leaf water ($p_{ex\text{-}LW}$ and $p_{x\text{-}LW}$) and sucrose
266 synthesis water ($p_{ex\text{-}SucSynW}$ and $p_{x\text{-}SucSynW}$), determined for closed canopies of *L. perenne*.

	CO_2		RH		CO_2 : RH	
Parameter	*F*-value	*P*-value	*F*-value	*P*-value	*F*-value	*P*-value
$\Delta^{18}O_{Sucrose}$ (n=18)	5.6	**0.03**	63.3	**<0.001**	0.2	0.68
$\Delta^{18}O_{LW}$ (day) (n=20)	10.7	**<0.01**	0.4	0.55	0.6	0.47
$\Delta^{18}O_{LW}$ (night) (n=20)	21.2	**<0.001**	3.2	0.09	1.0	0.34
$\Delta^{18}O_{SucSynW} - \Delta^{18}O_{LW}$ (n=18)	0.4	0.56	74.0	**<0.001**	1.0	0.34
$\Delta^{18}O_{CelSynW}$ (n=20)	4.7	**0.04**	1.7	0.22	0.0	0.95
$p_{x\text{-}LW}$ (n=20)	3.6	0.07	2.4	0.14	0.0	0.97
$p_{x\text{-}SucSynW}$(n=18)	3.4	0.09	11.6	**<0.01**	0.4	0.55
$\Delta^{18}O_{Cellulose}$ (n=19)	0.0	0.88	79.4	**<0.001**	0.5	0.47
$p_{ex\text{-}LW}$ (n=19)	8.3	**0.01**	55.4	**<0.001**	0.1	0.72
$p_{ex\text{-}SucSynW}$ (n=18)	3.3	0.09	0.1	0.71	0.2	0.70

267 The number of total canopy scale replicates (n) is presented for each parameter, individually.
268 Significant P-values are highlighted in bold print.

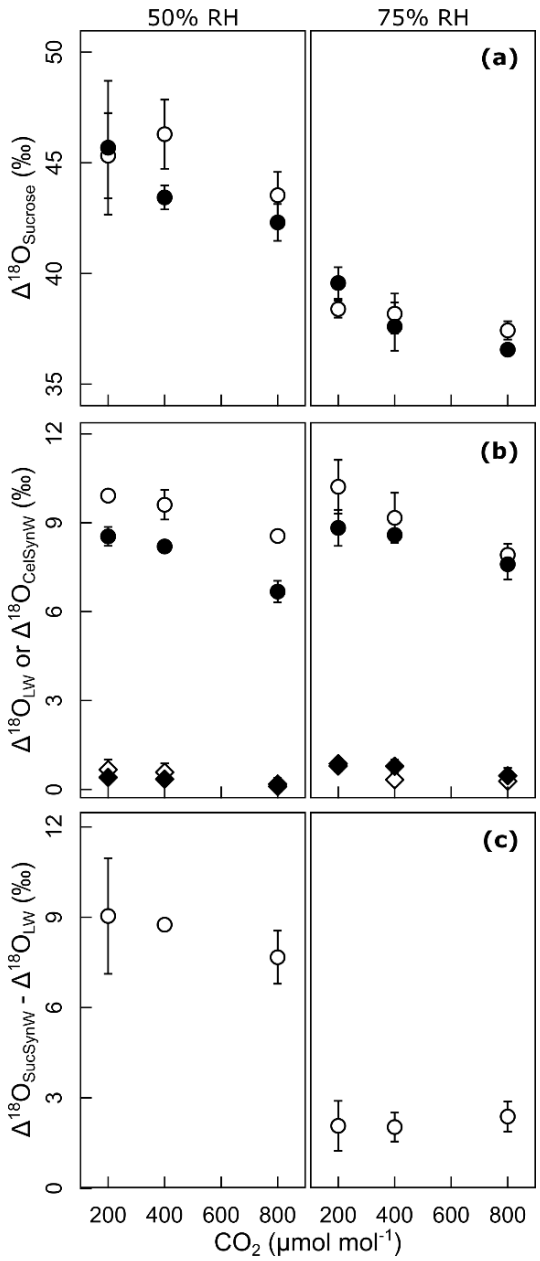

Fig. 1: $\Delta^{18}O$ of leaf blade sucrose ($\Delta^{18}O_{Sucrose}$) (a) $\Delta^{18}O$ of bulk water of leaf blades ($\Delta^{18}O_{LW}$, circles) or $\Delta^{18}O$ of water at the site of cellulose synthesis ($\Delta^{18}O_{CelSynW}$, diamonds) (b), and difference between $\Delta^{18}O$ of sucrose synthesis water and $\Delta^{18}O$ of bulk leaf water ($\Delta^{18}O_{SucSynW} - \Delta^{18}O_{LW}$) in the light period (c), as influenced by atmospheric CO_2 concentration at low RH and high RH. Full symbols represent values near the end of the dark period and empty symbols near the end of the light period. Measurements were performed in closed canopies of *L. perenne*. Data points and error bars represent the mean ± SE (n = 3-5).

The proportion of source water in the leaf growth-and-differentiation zone (p_x) was calculated using Eqn 2, with either $\Delta^{18}O_{Sucrose} - \varepsilon_{bio}$ ($p_{x\text{-}SucSynW}$) or $\Delta^{18}O_{LW}$ ($p_{x\text{-}LW}$) as alternative proxies for $\Delta^{18}O_{SucSynW}$. $p_{x\text{-}LW}$ varied in a narrow range between 0.92-0.98, but was not significantly affected by CO_2, RH or their interaction (Table 1). In comparison, $p_{x\text{-}SucSynW}$ was slightly higher, but also varied in a narrow range (0.93-0.99) that was also not affected by CO_2 or its interaction with RH, but was slightly smaller at low RH compared to high RH (0.95 vs. 0.98, $P < 0.01$, Table 1).

^{18}O enrichment of leaf cellulose and p_{ex}

279 ^{18}O enrichment of cellulose in leaf blades ($\Delta^{18}O_{Cellulose}$) was significantly affected by RH
280 (+3.1‰ at low RH relative to high RH, $P < 0.001$), but effects of CO_2 concentration or the
281 interaction of CO_2 concentration and RH were not significant (Fig. 2a, Table 1).
282 Using the data presented above and Eqn 1, we calculated p_{ex} alternatively as p_{ex}
283 referenced to sucrose synthesis water ($p_{ex\text{-}SucSynW}$) or leaf water ($p_{ex\text{-}LW}$). This showed that $p_{ex\text{-}SucSynW}$
284 was not significantly affected by CO_2 concentration, RH or their interaction and
285 averaged 0.52 (±0.02 SE) (Fig. 2b). In contrast, $p_{ex\text{-}LW}$ varied strongly between treatments from
286 −0.01 at 800 µmol CO_2 mol^{-1} and 50% RH to 0.46 at 200 µmol CO_2 mol^{-1} and 75% RH. $p_{ex\text{-}LW}$
287 was significantly affected by both RH ($P < 0.001$) and CO_2 concentration ($P = 0.01$) (Fig. 2c).
288 Across all treatments, $\Delta^{18}O_{cellulose}$ was closely related to $\Delta^{18}O_{SucSynW}$ ($R^2 = 0.87$, $P <$
289 0.01, Fig. 3), but a relationship with $\Delta^{18}O_{LW}$ was not evident ($R^2 = 0.04$, $P > 0.05$).
290

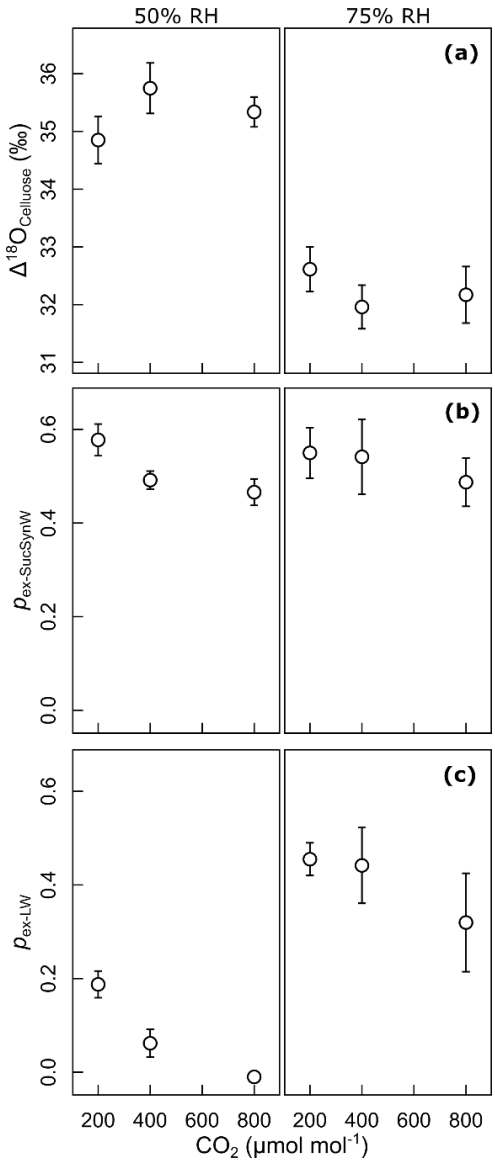

Fig. 2: $\Delta^{18}O$ of leaf blade cellulose ($\Delta^{18}O_{Cellulose}$) (a) and p_{ex}, calculated based on $\Delta^{18}O$ of sucrose synthesis water ($p_{ex\text{-}SucSynW}$) (b) or $\Delta^{18}O$ of bulk leaf water ($p_{ex\text{-}LW}$) (c), as influenced by atmospheric CO_2 concentration at low and high relative humidity. $\Delta^{18}O$ measurements were performed in closed canopies of *L. perenne*. Data points and error bars represent the mean ± SE (n = 3-5).

291

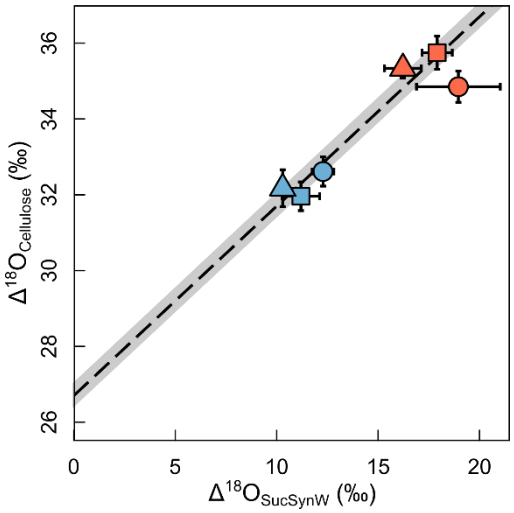

Fig. 3 Relationship between $\Delta^{18}O$ of sucrose synthesis water ($\Delta^{18}O_{SucSynW}$) and ^{18}O-enrichment of cellulose ($\Delta^{18}O_{Cellulose}$) as influenced by atmospheric CO_2 concentration (circles, 200 µmol mol^{-1}; squares, 400 µmol mol^{-1}; triangles, 800 µmol mol^{-1}), at high (blue symbols) and low relative humidity (red symbols). The dashed line and the shadowed area indicate the values predicted with the Barbour-Farquhar model with $p_{ex}p_x$ = 0.5 ($p_{x\text{-}SucSynW}$ = 0.96 and $p_{ex\text{-}SucSynW}$ = 0.52) and ε_{bio} at 18 °C (upper limit, ε_{bio} = 27.0‰), 20°C (dashed line, ε_{bio} = 26.7‰) or 22°C (lower limit, ε_{bio} = 26.4‰). Data points and error bars represent the mean ± SE.

Discussion

Isotopic discrepancy between average leaf water and sucrose synthesis water

This work found no negative effect of RH on ^{18}O enrichment of bulk leaf water ($\Delta^{18}O_{LW}$), which was unexpected (Helliker & Ehleringer, 2002; Gan *et al.*, 2003; Xiao *et al.*, 2012; Cernusak *et al.*, 2016; Liu *et al.*, 2016; Liu *et al.*, 2017; Hirl *et al.*, 2019). However, that result was highly reproducible in replicate (*n*=3-5) mesocosm-scale experiments with different CO_2 concentrations. Also, the result was not a peculiarity of the experimental equipment, as we previously found more typical, negative RH-effects on $\Delta^{18}O_{LW}$ in a range of C_3 and C_4 grasses, including a *Lolium* sp., in the same system (Liu *et al.*, 2016; Liu *et al.*, 2017). Although we are not aware of previous reports noting complete absence of an RH effect on $\Delta^{18}O_{LW}$, the effect is notoriously variable, with significant variation between plant species and stands, including in grasses (Helliker & Ehleringer, 2002; Xiao *et al.*, 2012; Liu *et al.*, 2017). Also, we note that the treatments affected canopy and leaf morphophysiological properties, that may have indirectly influenced $\Delta^{18}O_{LW}$, affecting the apparent RH sensitivity of $\Delta^{18}O_{LW}$. For instance, the high RH

317 treatments led to a significantly smaller leaf area index (LAI) and lower nitrogen content per
318 unit leaf area (both $P<0.01$; Table S1). Both these differences could reduce the apparent RH
319 sensitivity of $\Delta^{18}O_{LW}$ as noted in previous investigations with an isotope-enabled, process-
320 based soil-plant-atmosphere model of a grassland ecosystem (Hirl *et al.*, 2019). In those
321 investigations, sensitivity analysis indicated that both a decrease of photosynthetic capacity –
322 which correlates with nitrogen content per unit leaf area (Kattge *et al.*, 2009) – and LAI generate
323 an increase of $\Delta^{18}O_{LW}$, elevating $\Delta^{18}O_{LW}$ of the stands grown at high RH relative to low RH
324 (Hirl *et al.*, 2019). Although we cannot prove that these indirect mechanisms explained the
325 absence of an RH effect on $\Delta^{18}O_{LW}$ observed here, we note that such an absence was not a
326 necessary condition for the discrepancy between $\Delta^{18}O_{SucSynW}$ and $\Delta^{18}O_{LW}$ as a similar
327 discrepancy was also noted by Lehmann *et al.* (2017) in conditions with a more common
328 (negative) RH response of $\Delta^{18}O_{LW}$.

329 The negative effect of atmospheric CO_2 on $\Delta^{18}O_{LW}$ was similarly non-intuitive, since
330 leaf transpiration decreased with increasing CO_2 (Baca Cabrera *et al.*, 2020), a factor that could
331 drive an increase of $\Delta^{18}O_{LW}$ due notably to a Péclet effect (Farquhar & Lloyd, 1993; Barbour
332 *et al.*, 2000; Farquhar *et al.*, 2007). However, Hirl *et al.* (2019) found no evidence of a Péclet
333 effect in mixed species leaf samples from a temperate grassland ecosystem and in *L. perenne*
334 and *Dactylis glomerata* in controlled conditions. Also, Cooper & Norby (1994) did not find
335 consistent effects of atmospheric CO_2 on $\Delta^{18}O_{LW}$ of two deciduous tree species. Besides, we
336 know of no other studies of the effect of growth under different atmospheric CO_2 levels on
337 $\Delta^{18}O_{LW}$, which also limits opportunities for discussion. Importantly, effects of atmospheric CO_2
338 on $\Delta^{18}O_{LW}$ and associated mechanisms at stand scale, including interactive effects of nutrient
339 limitation (as observed here; Table S1), have not been investigated in any detail.

340 In contrast to $\Delta^{18}O_{LW}$, ^{18}O enrichment of sucrose ($\Delta^{18}O_{Sucrose}$) reflected very closely the
341 anticipated negative RH effect on ^{18}O enrichment of water at the site of photosynthetic sucrose
342 synthesis, i.e. $\Delta^{18}O_{SucSynW}$. That RH sensitivity was –0.25‰ per %RH on average of all
343 treatments. The effect appeared to be stable throughout diurnal cycles as we found no
344 significant difference between $\Delta^{18}O_{Sucrose}$ sampled near the end of the light and dark periods.
345 Near-constancy of $\Delta^{18}O_{Sucrose}$ and assimilation-weighted $\Delta^{18}O_{SucSynW}$ was likely related to (1)
346 the constant environmental conditions that led to virtually constant daytime stand-scale CO_2
347 assimilation (Fig. S1) and transpiration rates (Fig. S6 in Baca *et al.*, 2020) and (2) the small
348 day-night variation of $\Delta^{18}O_{LW}$ in all treatment combinations. Additionally, (3) we observed
349 diurnal variation of sucrose contents in leaf blades (Fig. S2), suggesting presence of a diurnal

sucrose store (Sicher *et al.*, 1984; Schnyder, 1993) but no starch, which may have also helped to maintain a near-constant $\Delta^{18}O_{Sucrose}$.

The fact that $\Delta^{18}O_{SucSynW}$ was significantly higher than bulk leaf $\Delta^{18}O_{LW}$ must have resulted from sucrose synthesis being closer to the evaporative sites or a greater proportion of sucrose synthesis in the distal half of the leaf blades, where ^{18}O enrichment of leaf water is much greater (Helliker & Ehleringer, 2000; Helliker & Ehleringer, 2002; Gan *et al.*, 2003; Affek *et al.*, 2006; Ogée *et al.*, 2007). Indeed, all plants grew in a dense canopy situation (with a LAI >5.5), which must have determined a significant decrease of incident radiation and probably also of photosynthetic sucrose synthesis rate between the tip and the base of leaf blades.

p_x, the proportion of source water at the site of cellulose synthesis, was close to 1

When expressed relative to irrigation water, i.e. nutrient solution, ^{18}O enrichment of water at the site of cellulose synthesis in the leaf growth-and-differentiation zone ($\Delta^{18}O_{CelSynW}$) was very low in all treatments. This implied that p_x, the proportion of source water at the site of cellulose synthesis, was close to 1, consistent with prior findings of Liu *et al.* (2017) for several C_3 and C_4 grasses. Referencing p_x to $\Delta^{18}O_{LW}$ ($p_{x\text{-}LW}$) instead of $\Delta^{18}O_{SucSynW}$ ($p_{x\text{-}SucSynW}$) caused only a small underestimation of $p_{x\text{-}LW}$ (–0.013 ±0.004 SE), due to the small leverage effect of any discrepancy between $\Delta^{18}O_{SucSynW}$ and $\Delta^{18}O_{LW}$ on estimates of p_x when $\Delta^{18}O_{CelSynW}$ is small. However, if $\Delta^{18}O_{CelSynW}$ were higher, as may be expected for leaves of dicot species (Kahmen *et al.*, 2011; Song *et al.*, 2014), any difference between $\Delta^{18}O_{SucSynW}$ and $\Delta^{18}O_{LW}$ should exert a greater effect on the difference between $p_{x\text{-}SucSynW}$ and $p_{x\text{-}LW}$.

Is true p_{ex} a constant?

This work found a near-constant $p_{ex\text{-}SucSynW}$ of 0.52 (± 0.02 SE) across contrasting environmental conditions. This near-constancy of $p_{ex\text{-}SucSynW}$ was also conserved when we altered temperature-dependent ε_{bio} (Sternberg & Ellsworth, 2011) within the limits of uncertainty for leaf temperature in our controlled environment experiments (Table S2) and contrasted sharply with estimates of $p_{ex\text{-}LW}$ in the different treatments which varied between −0.01 and 0.46. Clearly, the error made in replacing $\Delta^{18}O_{SucSynW}$ with $\Delta^{18}O_{LW}$ in Eqn 1 was the principal (if not the only) cause of variation of $p_{ex\text{-}LW}$. This indicates that the treatment-related variation of $p_{ex\text{-}LW}$ was virtually fully-independent of actual variation of substrate-oxygen exchange with medium water during transport to and at the site of cellulose synthesis as its

variation was eliminated almost entirely when the discrepancy between $\Delta^{18}O_{SucSynW}$ and $\Delta^{18}O_{LW}$ was accounted for in the analysis. So, the principal mechanism underlying variation of $p_{ex\text{-}LW}$ resided in the (source) leaf and not in the growing sink tissue. The primary data of Lehmann *et al.* (2017) are also consistent with that conclusion. However, Lehmann *et al.* (2017) made a mistake in the estimation of $p_{ex}p_x$ (their p_{sc}), due to an error in Eqn 2 of their paper (compare Eqn 1 with their Eqn 2). If we calculate $p_{ex\text{-}SucSynW}$ from their primary data using our Eqn 1, taking tap water instead of crown water as the source water $\delta^{18}O$ (–10.9‰), a temperature-dependent ε_{bio} (Sternberg & Ellsworth, 2011) of 26‰ for 28 °C, the temperature in their growth chamber, and a $p_{x\text{-}SucSynW}$ of 0.96 as observed here – Lehmann *et al.* (2017) did not determine $p_{x\text{-}LW}$ or $p_{x\text{-}SucSynW}$ –, then we obtain a mean $p_{ex\text{-}SucSynW}$ for *Dactylis glomerata* and *Lolium perenne* of *ca.* 0.55, close to our observation. Interestingly, our estimate of $p_{ex\text{-}SucSynW}$ also matches closely the mean p_{ex} estimate (0.53) calculated by Barbour & Farquhar (2000) from the data of Hill *et al.* (1995). That estimate was based on an alternative approach, that is measurements of randomization of ^{14}C-labelled hexose phosphates during cellulose synthesis in oak stem tissue.

The virtual constancy of $p_{ex\text{-}SucSynW}$ in contrasting environmental conditions is also remarkable given its theoretical range of 0.2-1.0 (Barbour & Farquhar, 2000). Clearly, the $p_{ex\text{-}LW}$ <0.2 observed at 400 and 800 μmol mol^{-1} CO_2 at a RH of 50% are outside that theoretical expectation. Although many studies have converged to a p_{ex} estimate of 0.4-0.5, if the original substrate for cellulose synthesis is carbohydrates (see compilation in Cernusak *et al.*, 2005), Song *et al.* (2014) suggested that true p_{ex} may vary significantly depending on turnover time of non-structural carbohydrates. When using the same approach as Song *et al.* (2014), we found only minor variation of turnover time of non-structural carbohydrates in our data set (Fig. S3), perhaps also contributing to the near constancy of $p_{ex\text{-}SucSynW}$. Moreover, *L. perenne* uses different fructan series, including mixed-linkage fructans, as the primary non-structural carbohydrate store (Pavis *et al.*, 2001) and all plants had very high fructan contents (>35% of dry wt) in both the leaf growth-and-differentiation zone (Baca Cabrera *et al.*, 2020) and leaf blades of fully-expanded leaves in all treatments (Fig. S2). Futile cycling of sucrose appears to be very active in *L. perenne* (Lattanzi *et al.*, 2012), and a high fraction of the substrate used for leaf structural biomass synthesis likely first passes through the fructan pool in the growth-and-differentiation zones of leaves (Schnyder *et al.*, 1988). These factors may have also contributed to the magnitude and relative constancy of $p_{ex\text{-}SucSynW}$ in this study.

Both RH and atmospheric CO_2 concentration were strong determinants of $p_{ex\text{-}LW}$ variation in our experiments. While effects of atmospheric CO_2 concentration during

plant/stand growth have not been studied previously, a very similar effect of RH on $p_{ex\text{-}LW}$ was also observed in a multi-seasonal, ecosystem-scale study of modelled and observed $\Delta^{18}O_{LW}$ and $\Delta^{18}O_{Cellulose}$ in a temperate grassland (Hirl *et al.*, 2021), showing that the same effect can also occur in natural conditions. A similar RH effect on $p_{ex\text{-}LW}$ in the C_4 grass *Cleistogenes squarrosa* (Liu *et al.*, 2016) and in several C_3 and C_4 species (Helliker & Ehleringer, 2002) was discussed by Liu *et al.* (2017). Moreover, a tendency for a similar RH effect on $p_{ex\text{-}LW}$ is also apparent in the data from *R. communis* presented by Song *et al.* (2014). It is tempting to also interpret these effects in terms of a disagreement between $\Delta^{18}O_{LW}$ and $\Delta^{18}O_{SucSynW}$. The present analysis shows that the divergence between $p_{ex\text{-}LW}$ and $p_{ex\text{-}SucSynW}$ was essentially a direct result of the discrepancy between $\Delta^{18}O_{LW}$ and $\Delta^{18}O_{SucSynW}$, with $\Delta^{18}O_{SucSynW}$ well approximated by:

$$\Delta^{18}O_{SucSynW} \approx \Delta^{18}O_{LW}\,(1 - p_{ex\text{-}LW})/\,(1 - 0.52), \text{ since} \qquad \text{Eqn 5a}$$

$$\Delta^{18}O_{SucSynW}\,(1 - p_{ex\text{-}SucSynW}\,p_{x\text{-}SucSynW}) = \Delta^{18}O_{LW}\,(1 - p_{ex\text{-}LW}\,p_{x\text{-}LW}). \qquad \text{Eqn 5b}$$

Such a rough calculation only requires knowledge of (assimilation-weighted) $\Delta^{18}O_{LW}$, ε_{bio}, p_x, $\Delta^{18}O_{Cellulose}$ (to estimate $p_{ex\text{-}LW}$) and a theoretically- or empirically-based estimate of $p_{ex\text{-}SucSynW}$ and can provide a quantitative guess for the magnitude of the discrepancy between $\Delta^{18}O_{LW}$ and $\Delta^{18}O_{SucSynW}$. We suggest that this hypothetical interpretation (Eqn 5a, b) should be tested more widely across plant functional groups and environmental conditions to evaluate the magnitude of eventual discrepancies between $\Delta^{18}O_{LW}$ and $\Delta^{18}O_{SucSynW}$ and on their implication in the interpretation of the relationship between (assimilation-weighted) leaf water ^{18}O enrichment and ^{18}O enrichment of cellulose. Most certainly, a better understanding of the relationship between $\Delta^{18}O_{LW}$ and $\Delta^{18}O_{SucSynW}$ will require a better knowledge of the spatio-temporal dynamics of convective and diffusive water fluxes and associated patterns of ^{18}O-enrichment in leaves – both at subcellular and tissue level – and corresponding spatio-temporal patterns of (photosynthetic) sucrose synthesis rates in the different parts of leaves.

Acknowledgements

We thank Anja Schmidt, Monika Michler, Angela Ernst-Schwärzli, Laura Dorn, Wolfgang Feneis, Richard Wenzel and Hans Vogl for skillful assistance in the sampling and sample processing (AS, MM, AES, HV), maintenance of the mesocosm facility and gas exchange equipment (WF, RW) and carbohydrate analyses (AS, LD). This research was supported by the Deutsche Forschungsgemeinschaft (DFG SCHN 557/9-1). JZ was supported by the China Scholarship Council (CSC).

Author contributions

452 HS, JCBC and RTH designed the study. JCBC, RTH and JZ performed the experiments,
453 sampling, and sample processing, with technical assistance (see above). RS performed the
454 isotope analyses. JCBC analyzed the data and wrote the first draft. JCBC, HS, JO, RTH, RS,
455 JZ and HL contributed to the discussion and revision of the manuscript.
456

457 **Competing interests**

458 The authors declare that they have no competing interests

References

Affek HP, Krisch MJ, Yakir D. 2006. Effects of intraleaf variations in carbonic anhydrase activity and gas exchange on leaf $C^{18}OO$ isoflux in *Zea mays*. *New Phytologist* **169**: 321-329.

Ainsworth EA, Rogers A. 2007. The response of photosynthesis and stomatal conductance to rising [CO_2]: mechanisms and environmental interactions. *Plant, Cell and Environment* **30**: 258-270.

Baca Cabrera JC, Hirl RT, Schäufele R, Macdonald A, Schnyder H. 2021. Stomatal conductance limited the CO_2 response of grassland in the last century. *BMC Biology* **19**: https://doi.org/10.1186/s12915-021-00988-4.

Baca Cabrera JC, Hirl RT, Zhu J, Schäufele R, Schnyder H. 2020. Atmospheric CO_2 and VPD alter the diel oscillation of leaf elongation in perennial ryegrass: compensation of hydraulic limitation by stored-growth. *New Phytologist* **227**: 1776-1789.

Barbour MM. 2007. Stable oxygen isotope composition of plant tissue: a review. *Functional Plant Biology* **34**: 83-94.

Barbour MM, Farquhar GD. 2000. Relative humidity- and ABA-induced variation in carbon and oxygen isotope ratios of cotton leaves. *Plant, Cell & Environment* **23**: 473-485.

Barbour MM, Fischer RA, Sayre KD, Farquhar GD. 2000. Oxygen isotope ratio of leaf and grain material correlates with stomatal conductance and grain yield in irrigated wheat. *Functional Plant Biology* **27**: 625-637.

Brendel O, Iannetta PPM, Stewart D. 2000. A rapid and simple method to isolate pure alpha-cellulose. *Phytochemical Analysis* **11**: 7-10.

Cernusak LA, Barbour MM, Arndt SK, Cheesman AW, English NB, Feild TS, Helliker BR, Holloway-Phillips MM, Holtum JA, Kahmen A. 2016. Stable isotopes in leaf water of terrestrial plants. *Plant, Cell & Environment* **39**: 1087-1102.

Cernusak LA, Cheesman AW. 2015. The benefits of recycling: how photosynthetic bark can increase drought tolerance. *New Phytologist* **208**: 995-997.

Cernusak LA, Farquhar GD, Pate JS. 2005. Environmental and physiological controls over oxygen and carbon isotope composition of Tasmanian blue gum, *Eucalyptus globulus*. *Tree Physiology* **25**: 129-146.

Cernusak LA, Wong SC, Farquhar GD. 2003. Oxygen isotope composition of phloem sap in relation to leaf water in *Ricinus communis*. *Functional Plant Biology* **30**: 1059-1070.

491 **Cheesman AW, Cernusak LA. 2017.** Infidelity in the outback: climate signal recorded in $\Delta^{18}O$
492 of leaf but not branch cellulose of eucalypts across an Australian aridity gradient. *Tree*
493 *Physiology* **37**: 554-564.
494 **Cooper LW, Norby RJ. 1994.** Atmospheric CO_2 enrichment can increase the ^{18}O content of
495 leaf water and cellulose: paleoclimatic and ecophysiological implications. *Climate*
496 *Research* **4**: 1-11.
497 **DeNiro MJ, Epstein S. 1979.** Relationship between the oxygen isotope ratios of terrestrial
498 plant cellulose, carbon dioxide, and water. *Science* **204**: 51-53.
499 **Dongmann G, Nürnberg HW, Förstel H, Wagener K. 1974.** On the enrichment of $H_2{}^{18}O$ in
500 the leaves of transpiring plants. *Radiation and Environmental Biophysics* **11**: 41-52.
501 **Farquhar GD, Barbour MM, Henry BK 1998.** Interpretation of oxygen isotope composition
502 of leaf material. In: Griffiths H ed. *Stable isotopes: integration of biological, ecological*
503 *and geochemical processes*. Oxford, UK: BIOS Scientific Publishers, 27-61.
504 **Farquhar GD, Cernusak LA. 2005.** On the isotopic composition of leaf water in the non-
505 steady state. *Functional Plant Biology* **32**: 293-303.
506 **Farquhar GD, Cernusak LA, Barnes B. 2007.** Heavy water fractionation during
507 transpiration. *Plant Physiology* **143**: 11-18.
508 **Farquhar GD, Lloyd J 1993.** Carbon and oxygen isotope effects in the exchange of carbon
509 dioxide between terrestrial plants and the atmosphere. In: Ehleringer JR, Hall AE,
510 Farquhar GD eds. *Stable isotopes and plant carbon-water relations*. San Diego:
511 Academic Press, 47-70.
512 **Flanagan LB, Comstock JP, Ehleringer JR. 1991.** Comparison of modeled and observed
513 environmental influences on the stable oxygen and hydrogen isotope composition of
514 leaf water in *Phaseolus vulgaris* L. *Plant Physiology* **96**: 588-596.
515 **Franks PJ, Adams MA, Amthor JS, Barbour MM, Berry JA, Ellsworth DS, Farquhar**
516 **GD, Ghannoum O, Lloyd J, McDowell N, et al. 2013.** Sensitivity of plants to changing
517 atmospheric CO_2 concentration: from the geological past to the next century. *New*
518 *Phytologist* **197**: 1077-1094.
519 **Gan KS, Wong SC, Yong JWH, Farquhar GD. 2002.** ^{18}O spatial patterns of vein xylem
520 water, leaf water, and dry matter in cotton leaves. *Plant Physiology* **130**: 1008-1021.
521 **Gan KS, Wong SC, Yong JWH, Farquhar GD. 2003.** Evaluation of models of leaf water ^{18}O
522 enrichment using measurements of spatial patterns of vein xylem water, leaf water and
523 dry matter in maize leaves. *Plant, Cell & Environment* **26**: 1479-1495.

Gaudinski JB, Dawson TE, Quideau S, Schuur EAG, Roden JS, Trumbore SE, Sandquist DR, Oh S-W, Wasylishen RE. 2005. Comparative analysis of cellulose preparation techniques for use with ^{13}C, ^{14}C, and ^{18}O isotopic measurements. *Analytical Chemistry* **77**: 7212-7224.

Gebbing T, Schnyder H. 2001. ^{13}C labeling kinetics of sucrose in glumes indicates significant refixation of respiratory CO_2 in the wheat ear. *Functional Plant Biology* **28**: 1047-1053.

Gessler A, Ferrio JP, Hommel R, Treydte K, Werner RA, Monson RK. 2014. Stable isotopes in tree rings: towards a mechanistic understanding of isotope fractionation and mixing processes from the leaves to the wood. *Tree Physiology* **34**: 796-818.

Helliker BR, Ehleringer JR. 2000. Establishing a grassland signature in veins: ^{18}O in the leaf water of C_3 and C_4 grasses. *Proceedings of the National Academy of Science* **97**: 7894-7898.

Helliker BR, Ehleringer JR. 2002. Differential ^{18}O enrichment of leaf cellulose in C_3 versus C_4 grasses. *Functional Plant Biology* **29**: 435-442.

Hill SA, Waterhouse JS, Field EM, Switsur VR, Ap Rees T. 1995. Rapid recycling of triose phosphates in oak stem tissue. *Plant, Cell & Environment* **18**: 931-936.

Hirl RT, Ogée J, Ostler U, Schäufele R, Baca Cabrera JC, Zhu J, Schleip I, Wingate L, Schnyder H. 2021. Temperature-sensitive biochemical ^{18}O-fractionation and humidity-dependent attenuation factor are needed to predict $\delta^{18}O$ of cellulose from leaf water in a grassland ecosystem. *New Phytologist* **229**: 3156-3171.

Hirl RT, Schnyder H, Ostler U, Schäufele R, Schleip I, Vetter SH, Auerswald K, Baca Cabrera JC, Wingate L, Barbour MM, et al. 2019. The ^{18}O ecohydrology of a grassland ecosystem – predictions and observations. *Hydrology and Earth System Sciences* **23**: 2581-2600.

Kahmen A, Sachse D, Arndt SK, Tu KP, Farrington H, Vitousek PM, Dawson TE. 2011. Cellulose $\delta^{18}O$ is an index of leaf-to-air vapor pressure difference (VPD) in tropical plants. *Proceedings of the National Academy of Sciences* **108**: 1981-1986.

Kattge J, Knorr W, Raddatz T, Wirth C. 2009. Quantifying photosynthetic capacity and its relationship to leaf nitrogen content for global-scale terrestrial biosphere models. *Global Change Biology* **15**: 976-991.

Lattanzi FA, Ostler U, Wild M, Morvan-Bertrand A, Decau M-L, Lehmeier CA, Meuriot F, Prud'homme M-P, Schäufele R, Schnyder H. 2012. Fluxes in central carbohydrate metabolism of source leaves in a fructan-storing C_3 grass: rapid turnover and futile

557 cycling of sucrose in continuous light under contrasted nitrogen nutrition status. *Journal*
558 *of Experimental Botany* **63**: 2363-2375.
559 **Leakey ADB, Bernacchi CJ, Ainsworth EA, Ort DR, Long SP, Rogers A. 2009.** Elevated
560 CO_2 effects on plant carbon, nitrogen, and water relations: six important lessons from
561 FACE. *Journal of Experimental Botany* **60**: 2859-2876.
562 **Lehmann MM, Gamarra B, Kahmen A, Siegwolf RT, Saurer M. 2017.** Oxygen isotope
563 fractionations across individual leaf carbohydrates in grass and tree species. *Plant, Cell*
564 *& Environment* **40**: 1658-1670.
565 **Liu HT, Gong XY, Schäufele R, Yang F, Hirl RT, Schmidt A, Schnyder H. 2016.** Nitrogen
566 fertilization and $\delta^{18}O$ of CO_2 have no effect on ^{18}O-enrichment of leaf water and
567 cellulose in *Cleistogenes squarrosa* (C_4) – is VPD the sole control? *Plant, Cell &*
568 *Environment* **39**: 2701-2712.
569 **Liu HT, Schäufele R, Gong XY, Schnyder H. 2017.** The $\delta^{18}O$ and $\delta^{2}H$ of water in the leaf
570 growth-and-differentiation zone of grasses is close to source water in both humid and
571 dry atmospheres. *New Phytologist* **214**: 1423-1431.
572 **Offermann C, Ferrio JP, Holst J, Grote R, Siegwolf R, Kayler Z, Gessler A. 2011.** The long
573 way down—are carbon and oxygen isotope signals in the tree ring uncoupled from
574 canopy physiological processes? *Tree Physiology* **31**: 1088-1102.
575 **Ogée J, Cuntz M, Peylin P, Bariac T. 2007.** Non-steady-state, non-uniform transpiration rate
576 and leaf anatomy effects on the progressive stable isotope enrichment of leaf water
577 along monocot leaves. *Plant, Cell and Environment* **30**: 367-387.
578 **Pavis N, Boucaud J, Prud'homme MP. 2001.** Fructans and fructan-metabolizing enzymes in
579 leaves of *Lolium perenne*. *New Phytologist* **150**: 97-109.
580 **Pfanz H, Aschan G, Langenfeld-Heyser R, Wittmann C, Loose M. 2002.** Ecology and
581 ecophysiology of tree stems: corticular and wood photosynthesis. *Naturwissenschaften*
582 **89**: 147-162.
583 **Pinheiro J, Bates D, DebRoy S, Sarkar D, R Core Team. 2019.** *nlme: linear and nonlinear*
584 *mixed effects models. R package v.3.1*-141. https://CRAN.R-project.org/package=nlme.
585 **Poorter H, Navas M-L. 2003.** Plant growth and competition at elevated CO_2: on winners,
586 losers and functional groups. *New Phytologist* **157**: 175-198.
587 **R Core Team. 2020**. *R: A language and environment for statistical computing*.
588 Vienna, Austria: R Foundation for Statistical Computing

589 **Roden JS, Ehleringer JR. 1999.** Observations of hydrogen and oxygen isotopes in leaf water
590 confirm the Craig-Gordon model under wide-ranging environmental conditions. *Plant*
591 *Physiology* **120**: 1165-1174.
592 **Roden JS, Lin G, Ehleringer JR. 2000.** A mechanistic model for interpretation of hydrogen
593 and oxygen isotope ratios in tree-ring cellulose. *Geochimica et Cosmochimica Acta* **64**:
594 21-35.
595 **Schnyder H. 1993.** The role of carbohydrate storage and redistribution in the source-sink
596 relations of wheat and barley during grain filling – a review. *New Phytologist* **123**: 233-
597 245.
598 **Schnyder H, Nelson CJ, Spollen WG. 1988.** Diurnal growth of tall fescue leaf blades. II. Dry
599 matter partitioning and carbohydrate metabolism in the elongation zone and adjacent
600 expanded tissue. *Plant Physiology* **86**: 1077-1083.
601 **Sicher RC, Kremer DF, Harris WG. 1984.** Diurnal carbohydrate metabolism of barley
602 primary leaves. *Plant Physiology* **76**: 165-169.
603 **Song X, Farquhar GD, Gessler A, Barbour MM. 2014.** Turnover time of the non-structural
604 carbohydrate pool influences $\delta^{18}O$ of leaf cellulose. *Plant, Cell & Environment* **37**:
605 2500-2507.
606 **Sternberg L, Ellsworth PFV. 2011.** Divergent biochemical fractionation, not convergent
607 temperature, explains cellulose oxygen isotope enrichment across latitudes. *PLoS ONE*
608 **6**: e28040.
609 **Sternberg LDSL, DeNiro MJ, Savidge RA. 1986.** Oxygen isotope exchange between
610 metabolites and water during biochemical reactions leading to cellulose synthesis. *Plant*
611 *Physiology* **82**: 423-427.
612 **Sternberg LDSL, DeNiro MJD. 1983.** Biogeochemical implications of the isotopic
613 equilibrium fractionation factor between the oxygen atoms of acetone and water.
614 *Geochimica et Cosmochimica Acta* **47**: 2271-2274.
615 **Szejner P, Clute T, Anderson E, Evans MN, Hu J. 2020.** Reduction in lumen area is
616 associated with the $\delta^{18}O$ exchange between sugars and source water during cellulose
617 synthesis. *New Phytologist* **226**: 1583-1593.
618 **Werner C, Schnyder H, Cuntz M, Keitel C, Zeeman MJ, Dawson TE, Badeck FW,**
619 **Brugnoli E, Ghashghaie J, Grams TEE, et al. 2012.** Progress and challenges in using
620 stable isotopes to trace plant carbon and water relations across scales. *Biogeosciences*
621 **9**: 3083-3111.

Wickham H. 2016. *ggplot2: elegant graphics for data analysis*. New York, NY, USA: Springer Verlag.

Xiao W, Lee X, Wen X, Sun X, Zhang S. 2012. Modeling biophysical controls on canopy foliage water ^{18}O enrichment in wheat and corn. *Global Change Biology* **18**: 1769-1780.

Yakir D, DeNiro MJ. 1990. Oxygen and hydrogen isotope fractionation during cellulose metabolism in *Lemna gibba* L. *Plant Physiology* **93**: 325-332.